

ON-SITE TESTING OF CROP DRYING FANS

by

Paul M. Winkelman

Thesis submitted to the Faculty of the
Virginia Polytechnic Institute and State University
in partial fulfillment of the requirements for the degree of

MASTER OF SCIENCE

in

Agricultural Engineering

APPROVED:

D. H. Vaughan, Chairman

J. S. Cundiff, Co-Chairman

T. E. Diller

September, 1988

Blacksburg, Virginia

ON-SITE TESTING OF CROP DRYING FANS

by

Paul M. Winkelman

D. H. Vaughan, Chairman

Agricultural Engineering

(ABSTRACT)

The commercial peanut dryers used today were first conceived when energy was relatively inexpensive. Since then, energy costs have increased significantly, and more efficient peanuts dryers are desirable. To evaluate dryer efficiency, a mobile fan test facility was designed, built and calibrated for on-site fan airflow and energy measurements. Four-, six-, and eight-trailer peanut dryers were tested for performance. The characteristics observed were delivery of fan airflow as compared to manufacturers' ratings, air distribution to each of the trailer supply ports, plenum leaks, and energy savings achieved by the use of flow controls. For testing, air to the dryer fan was provided by a centrifugal supply fan, where the flowrate was determined by measuring the pressure drop across a calibrated perforated plate positioned between the two fans. Airflow through each of the trailer supply ports was determined in a similar manner by measuring the pressure drop across calibrated resistance plates. Measured airflow to the trailers from dryer fans was found to be 75 to 100% of the airflow given by the manufacturers' ratings. Air distribution was poor in dryers with no baffle. However, the installation of a baffle resulted in significant improvement in air distribution. The baffle a pressure rise which reduced total airflow up to 5%. Based on a recommended airflow of $0.167 \text{ m}^3/\text{s}$ per m^3 of peanuts, fan inlets were restricted to reduce airflow, and energy savings as high as 35% were achieved. Repairs on poorly maintained dryers increased flowrate from 3 to 7%.

Acknowledgements

I would like to express my appreciation to Dr. D. H. Vaughan for his advice and support, not only as my adviser, but also as a friend. I would also like to extend my gratitude to Dr. J. S. Cundiff for his assistance, and for always finding someone to help me accomplish the task. Many thanks to Dr. T. E. Diller, for his help on the research, particularly with fluid flow, and to Dr. W. F. Wilcke, for his advice and review of the manuscripts. I am grateful to all those who assisted in the dryer testing, especially _____, _____, _____, and _____.

Appreciation is expressed to the North Carolina Alternative Energy Corporation for support of this project, with special gratitude to _____ for his assistance. Finally, I would like to thank my many fans who were always willing to work whenever I flipped a switch.

Table of Contents

Introduction	1
Objectives	6
Literature Review	7
Basic Airflow Principles	7
Airflow through Peanuts	10
Airflow Measurement	13
Shaped Nozzles	13
Pitot-Static Tube	18
Perforated Plates	26
Axial Flow Fans	28
Error Measurement	33
Experimental Materials and Procedures	37
Total Flow Measurement	37
Flow Measurement through Individual Dryer Ports	46

Power Measurements	50
Field Test Setup	52
Field Test Procedures	54
Fan Balancing	54
Data Collection	55
Description of Dryers Tested	56
Results and Discussion	65
Performance of Field Testing Equipment	65
Perforated Plate Calibration	65
Resistance Plate Calibration	76
Error Analysis of Flow Measurement Devices	83
Total Flow Measurement Error	86
Resistance Plate Flow Measurement Error	89
Resistance Plate and Perforated Plate Correlation	91
Supply Fan Effects on Dryer Fan	92
Dryer Performance	93
Effects of Repairs	93
Measured Ratings versus Manufacturers' Ratings	95
Air Distribution within the Plenum	110
Power Consumption	134
Summary and Conclusions	139
References	142
Appendix A. CUBIC FORTRAN	144

Appendix B. FANPER1 FORTRAN	148
Appendix C. PERF FORTRAN	151
Appendix D. FIELD FORTRAN	164
Vita	171

List of Illustrations

Figure 1. Typical four-trailer commercial peanut dryer unit.	3
Figure 2. Standard nozzle	15
Figure 3. Static orifice distance from tip base or stem centerline, diameters	19
Figure 4. Reference pressure coefficient as a function of porosity	23
Figure 5. Pressure drop coefficient correction factor for $Re > 2000$	24
Figure 6. Pressure drop coefficient correction factor for $M > 0$	25
Figure 7. Inlet chamber setup - ducted nozzle on chamber	30
Figure 8. Typical fan performance curves	31
Figure 9. Unrotated and rotated axes, with cubic equation.	40
Figure 10. Profile of nozzle used for calibration of perforated plate.	43
Figure 11. Experimental setup for calibration of perforated plate.	45
Figure 12. Rectangular collar with piezometer ring	47
Figure 13. Experimental setup for calibration of resistance plates.	51
Figure 14. Experimental configuration for on-site testing of peanut dryer fans.	53
Figure 15. Manufacturer's fan rating curve for 11.2-kW Aerovent	58
Figure 16. Manufacturer's fan rating curve for 7.46-kW Aerovent	59
Figure 17. Manufacturer's fan rating curve for 5.60-kW Long	60
Figure 18. Manufacturer's fan rating curve for 7.46-kW Long	61
Figure 19. Baffle dimensions and position in dryer plenum	63
Figure 20. Measured flowrates, and measured and adjusted pressure drops on two separate days.	68

Figure 21. Pressure coefficient vs. Reynolds number for perforated plate.	72
Figure 22. Pressure coefficient vs. Mach number for perforated plate.	73
Figure 23. Pressure drop-flowrate for Resistance Plate No. 7, with resistance of a trailer filled with peanuts.	77
Figure 24. Pressure coefficient and Reynolds number for Resistance Plate No. 7.	80
Figure 25. Pressure drop vs. flowrate for an eight-trailer unit equipped with an 11.2-kW Aerovent fan (Lewiston, NC).	98
Figure 26. Pressure drop vs. flowrate for a six-trailer unit equipped with an 11.2-kW Aerovent fan (Lewiston, NC).	99
Figure 27. Pressure drop vs. flowrate for a six-trailer unit equipped with a 7.46-kW Aerovent fan (Holland, VA).	101
Figure 28. Pressure drop vs. flowrate for a six-trailer unit equipped with a 7.46-kW Long fan (Blacksburg, VA).	102
Figure 29. Pressure drop vs. flowrate for a six-trailer unit equipped with a 5.60-kW Long fan (Blacksburg, VA).	103
Figure 30. Pressure drop vs. flowrate for a six-trailer unit equipped with a 7.46-kW Long fan, with baffle (Blacksburg, VA).	106
Figure 31. Pressure drop vs. flowrate for a six-trailer unit equipped with a 5.60-kW Long fan, with baffle (Blacksburg, VA).	107
Figure 32. Pressure drop vs. flowrate for an eight-trailer unit equipped with a 7.46-kW Long fan, with baffle (Blacksburg, VA).	108
Figure 33. Pressure drop vs. flowrate for a four-trailer unit equipped with a 5.60-kW Long fan, with baffle (Blacksburg, VA).	109
Figure 34. Deviation of measured from balanced flowrate with all ports open in an eight-trailer unit, 11.2-kW Aerovent fan (Lewiston, NC).	112
Figure 35. Deviation of measured from balanced flowrate with all ports open in a six-trailer unit, 11.2-kW Aerovent fan (Lewiston, NC).	113
Figure 36. Deviation of measured from balanced flowrate with all ports open in a six-trailer unit, 7.46-kW Aerovent fan (Holland, VA).	114
Figure 37. Deviation of measured from balanced flowrate with all ports open in a six-trailer unit, 5.60-kW Long fan (Blacksburg, VA).	115
Figure 38. Deviation of measured from balanced flowrate with all ports open in a six-trailer unit, 7.46-kW Long fan (Blacksburg, VA).	116
Figure 39. Deviation of measured from balanced flowrate with all ports open in a six-trailer unit, 5.60-kW Long fan, with baffle (Blacksbrug, VA).	117
Figure 40. Deviation of measured from balanced flowrate with all ports open in a six-trailer unit, 7.46-kW Long fan, with baffle (Blacksburg, VA).	118

Figure 41. Deviation of measured from balanced flowrate with all ports open in a four-trailer unit, 5.60-kW Long fan, with baffle (Blacksburg, VA).	119
Figure 42. Deviation of measured from balanced flowrate with all ports open in an eight-trailer unit, 7.46-kW Long fan, with baffle (Blacksburg, VA).	120
Figure 43. Deviation of measured from balanced flowrate with four ports open in an eight-trailer unit, 11.2-kW Aerovent fan (Lewiston, NC).	122
Figure 44. Deviation of measured from balanced flowrate with six ports open in an eight-trailer unit, 11.2-kW Aerovent fan (Lewiston, NC).	123
Figure 45. Deviation of measured from balanced flowrate with seven ports open in an eight-trailer unit, 11.2-kW Aerovent fan (Lewiston, NC).	124
Figure 46. Deviation of measured from balanced flowrate, all combinations in an eight-trailer unit, 11.2-kW Aerovent fan (Lewiston, NC).	125
Figure 47. Deviation of measured from balanced flowrate, all combinations in a six-trailer unit, 11.2-kW Aerovent fan (Lewiston, NC).	126
Figure 48. Deviation of measured from balanced flowrate, all combinations in a six-trailer unit, 7.46-kW Aerovent fan (Holland, VA).	127
Figure 49. Deviation of measured from balanced flowrate, all combinations in a six-trailer unit, 5.60-kW Long fan (Blacksburg, VA).	128
Figure 50. Deviation of measured from balanced flowrate, all combinations in a six-trailer unit, 7.46-kW Long fan (Blacksburg, VA).	129
Figure 51. Deviation of measured from balanced flowrate, all combinations in a six-trailer unit, 5.60-kW Long fan, with baffle (Blacksburg, VA).	130
Figure 52. Deviation of measured from balanced flowrate, all combinations in a six-trailer unit, 7.46-kW Long fan, with baffle (Blacksburg, VA).	131
Figure 53. Deviation of measured from balanced flowrate, all combinations in a four-trailer unit, 5.60-kW Long fan, with baffle (Blacksburg, VA).	132
Figure 54. Deviation of measured from balanced flowrate, all combinations in an eight-trailer unit, 7.46-kW Long fan, with baffle (Blacksburg, VA).	133
Figure 55. Flow reduction with inlet restrictions.	137

List of Tables

Table 1. Input and output parameters for CUBIC FORTRAN.	42
Table 2. Description of fan configurations tested.	57
Table 3. Pressure drop-flowrate equations for the 8 resistance plates.	79
Table 4. Pressure drop-flowrate equations for the 8 resistance plates, recalibration.	82
Table 5. Pressure drop as a function of Reynolds number for the 8 resistance plates, recalibration.	84
Table 6. Pressure coefficient and Reynolds number for the 8 resistance plates.	85
Table 7. Average airflow for configurations tested.	105
Table 8. Total flowrate with and without inlet restrictions.	135

Introduction

Commercial peanut drying equipment has remained relatively unchanged for many years. Although some are constructed of wood, peanut dryer plenums are normally horizontal steel cylinders 1.82 m in diameter. A typical commercial peanut dryer is depicted in Figure 1. Air is normally supplied by axial fans powered by three-phase electric motors, ranging from 5.60 to 11.2 kW. These fans, having 4 to 9 blades, are mounted in housings 0.91 to 1.22 m in diameter. Flow vanes are installed around the periphery of the housing downstream of the fan blades to remove the rotational component of the airflow. A propane burner is installed just downstream from the fan motor. The fan housing is either mounted directly to the plenum, or on a wooden frame and connected to the plenum by a canvas duct. Since the dryer plenum is larger than the fan housing, air entering the plenum must pass through an abrupt expansion. Air enters the trailers through four to eight supply ports, one for each trailer. These ports, equipped with sliding gates to reduce or shut off the air, are located on both sides of the plenum. The port openings are approximately 0.74 m square and spaced 3.05 m on center. A wooden frame is placed around the port by nailing through the metal surrounding the opening. A canvas duct is installed around this frame and kept in place by nailing other wood strips on top of it. In order to attach the canvas duct to the trailer, another wooden frame is constructed so that it fits inside the trailer plenum, which is normally 0.34 by 1.16 m. The

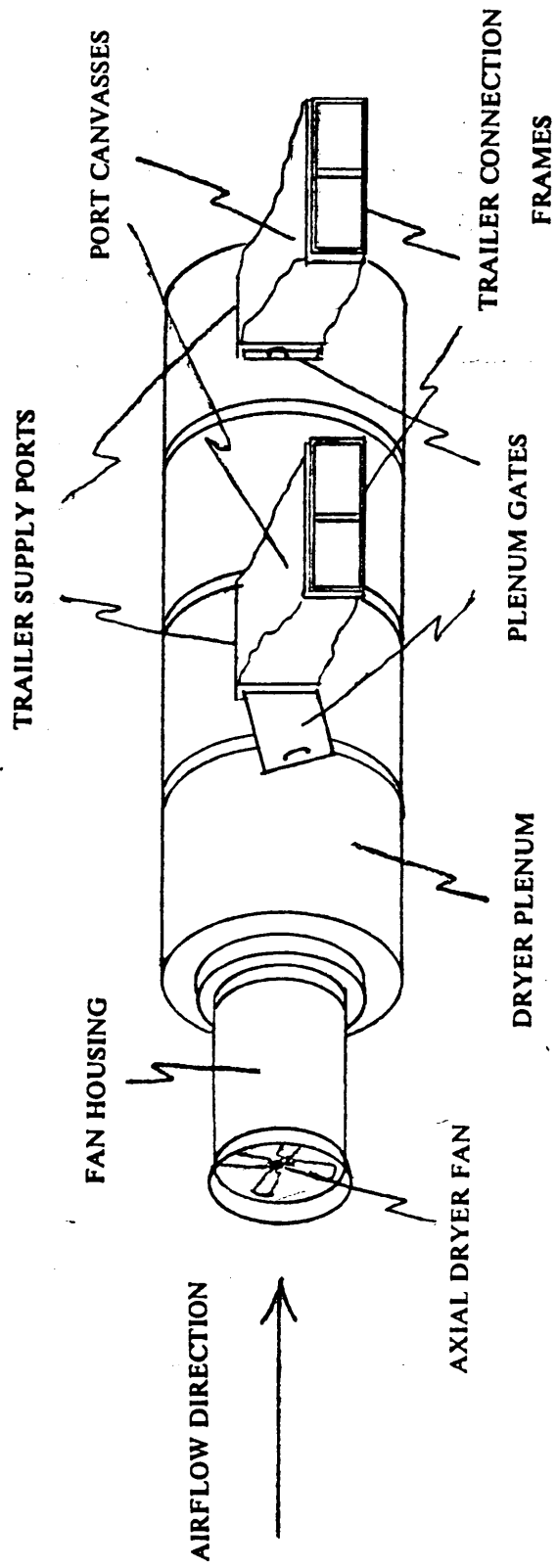


Figure 1. Typical four-trailer commercial peanut dryer unit.

canvas is clamped to this frame by wood strips nailed over it. In some cases, rubber weatherstripping is added to improve the seal between the trailer plenum and the frame. Spring loaded clips, bolted to the back of the trailer, hold the canvas duct frame to the trailer plenum. The trailers have floors made of perforated metal, which allows air to pass through from the plenum below.

Typically, peanuts are left to dry in the field for several days after digging. Depending on weather conditions, the moisture content is reduced to 25 percent wet basis, or lower, after which they are loaded into trailers. These trailers are then taken to a peanut dryer, where the peanuts are dried before they are unloaded. The peanuts are considered dry once they have reached a moisture content of 10 percent wet basis. With the air heated to 35 °C, and a recommended airflow rate of 0.167 m³/s per m³ of peanuts (Beasley and Dickens, 1963), this will take from two to three days. Since aflatoxin may be produced in as little as 24 hours in peanuts above 10 percent moisture content (Mirocha and Christensen, 1982), an insufficient drying rate increases the potential for aflatoxin production.

Since the plenum diameter remains constant, the average air velocity decreases towards the downstream end as air exits through the ports. This drop in velocity results in an increase in static pressure. The highest velocity and therefore lowest static pressure occurs just as the air enters the dryer plenum. Hence, with no device to direct airflow inside the plenum, the two opposing ports closest to the fan receive much less air than the others, often resulting in underdrying of these trailers, while the other trailers are overdried. For this reason, farmers often do not use the first two supply ports, so that dryer capacity is wasted, which means that the farmer is paying for a longer dryer plenum and a longer shed with no return on his investment. Peanuts that could otherwise be drying have to wait and risk spoilage. Flow vanes or baffles within the plenum would help to redistribute the air, and provide the same airflow to each of the trailers. Drying times would be more easily predicted if all trailers received approximately the same amount of air, whereby reducing

the risk of under- or overdrying the peanuts. In addition, trailers would not have to be shuffled around to ensure proper drying. These factors would increase drying production through the dryer.

Many of the dryers used today are old and poorly maintained. Wooden frames resting on the ground usually support the dryer, but these eventually rot, and if not replaced, the plenum rusts where it touches the soil. The sheds covering the dryers often leak, and water falls onto the joints of the plenum. If these joints are not sealed, water collects there and promotes rust. The canvas from the dryer plenum to the trailer slowly weathers and cracks. After continual removal and insertion, the wood on the trailer plenum frames wears away, and the joints become loose. The spring clips which hold them in place often break or are rendered useless by rust. With a loose seal to the trailer, air leaks out. All of these factors allow air to escape unused, adding to the farmer's cost of production. Although not covered in this research, the trailers often fall into disrepair, and if left unattended, can cause additional losses.

Towards the end of the drying season, the dryers are not always loaded to capacity. This means that some of the ports must be closed, forcing more air into those ports left open. Restricting the fan inlet would reduce airflow. A control to provide optimum airflow would save the farmer money by reducing energy consumption by the fan and burner.

In order to determine the improvements of any dryer modification, a suitable method of testing peanut dryer performance is desired. Performance can be defined in many ways. Two important aspects are the fan performance and the dryer performance. Fan performance can be determined by comparing the amount of air the fan delivers to its manufacturer's rating. Dryer performance is related to how air is distributed to each of the trailer supply ports and to losses incurred between the fan and trailers.

Measuring the air that exits each of the supply ports can be used to determine air distribution. The measured total flowrate exiting the ports indicates the fan delivery to the trailers, but is of no use in determining the leakage. If the leakage is unknown, fan performance cannot be accurately measured, since some of the delivered air is taken into account. Thus, a means of measuring total air supplied to the fan is desired. The difference between the airflow supplied to the fan and the amount exiting the supply ports is the leakage. However, to properly evaluate the fan performance, the pressure drop across the fan must be measured in addition to measuring the total flow. Due to disturbances caused by the propane burner and air entry into the plenum, accurate measurements are difficult. Some other means of estimating the pressure drop across the fan is required.

Objectives

1. To develop an on-site field test procedure to determine peanut dryer performance by:
 - a. Measuring total flow into a peanut dryer.
 - b. Measuring airflow rate from each dryer plenum port to determine air leakage and air distribution.
2. To compare fan airflow ratings acquired from field tests with those supplied by the manufacturers.
3. To determine the increased dryer performance after repairs were made to the plenum, ports, and ducts to trailers.
4. To determine a method of uniformly distributing the air through each of the ports.
5. To determine energy savings achieved by retrofitting inlet restrictions on the fan.

Literature Review

Basic Airflow Principles

Fluid flow is generally divided into two main types, turbulent and laminar. With turbulent flow, the most common in engineering practice, fluid particles move in irregular patterns (Streeter and Wylie, 1979). When laminar, fluid particles flow in layers. This phenomenon is due to the viscous effects of the fluid dampening out the turbulent tendencies. The type of flow is determined by a dimensionless factor called the Reynolds number,

$$Re = \frac{\mu DV}{\rho} \quad [1]$$

where Re = Reynolds number

μ = fluid viscosity [$N s/m^2$]

D = characteristic diameter or length [m]

V = fluid velocity [m/s]

ρ = fluid density [kg/m^3]

Units are chosen such that the Reynolds number is dimensionless. Laminar flow occurs when the Reynolds number is low, typically below 2000, and changes to turbulent flow as the Reynolds number increases. Between these two types of flow, the fluid flow passes through a critical zone and a transition zone.

Since fluid flow is not frictionless, losses occur, and these losses depend on whether the flow is laminar or turbulent. This effect is best typified in the Moody diagram for pipe flow (Streeter and Wylie, 1979). Pressure, or head, loss is given in terms of a non-dimensional variable called the friction factor,

$$f = \frac{h_f}{\frac{L}{D} \frac{V^2}{2g}} \quad [2]$$

where f = friction factor

L = pipe length [m]

D = pipe diameter [m]

V = average fluid velocity in pipe [m/s]

g = gravitational constant [$kg m/s^2$]

On the Moody diagram, the friction factor is plotted against the Reynolds number, both on logarithmic axes. Laminar flow produces a straight line with a slope of -1, and the relationship between the friction factor and the Reynolds number is,

$$f = \frac{64}{Re} \quad [3]$$

Combining Equations [2] and [3],

$$h_f = \frac{64}{Re} \frac{L}{D} \frac{V^2}{2g} \quad [4]$$

Combining Equations [1] and [4],

$$\begin{aligned} h_f &= \frac{64\rho}{\mu DV} \frac{L}{D} \frac{V^2}{2g} \\ &= \frac{32\rho LV}{\mu D^2 g} \end{aligned} \quad [5]$$

This equation demonstrates that, for laminar flow, head loss due to frictional flow is proportional to the velocity of the fluid.

At high Reynolds numbers, the friction factor approaches a constant value,

$$K = \frac{h_f}{\frac{L}{D} \frac{V^2}{2g}} \quad [6]$$

where $K = \text{constant}$

In this case, head loss is proportional to the square of the velocity.

The relationship between the friction factor and the Reynolds number is more complicated in the critical and transition zones, and is not discussed here.

One can consider a fluid flowing through several parallel pipes of varying diameters. The total head loss would be the sum of the head losses in each of the individual pipes. Some flow may be laminar, and some may be turbulent. In addition, some flow may be in the transition zone. Using a characteristic diameter to determine an apparent velocity based on the total flowrate, the head losses can be described as,

$$h_f = k_1 V_a + k_2 V_a^2 \quad [7]$$

where $k_1, k_2 = \text{constants}$

$V_a = \text{apparent velocity}$

Airflow through Peanuts

Pressure losses of air flowing through an agricultural crop for drying behaves in a fashion similar to Equation [7], since the spaces between the crop material has varying cross-sectional areas for airflow. For a given flowrate of air through a crop, the actual velocity varies throughout the crop, while the apparent velocity is constant for a constant cross-sectional area.

Much research has been done on the pressure drop of air flowing through agricultural crops. To describe the relationship between the flowrate and the associated pressure drop, Equation [7] is not generally used. Noting that the exponent of V varies between 1 and 2, it can be written as,

$$\Delta P = a V_a^n \quad [8]$$

where ΔP = pressure drop

a, n = constants, $1 \leq n \leq 2$

Shedd (1953) determined the airflow resistance of several grains and seeds. He used grain depths of 1.22 or 2.74 m in a bin, 2.13 by 2.13 m, and 3.96 m deep with a false, perforated floor. Air flowrate was determined using a displacement method. He plotted flowrate per unit area of air through the grains and seeds against the pressure drop per unit depth on logarithmic axes. If the lines were straight, he described the pressure-flow relationship using a form of Equation [8],

$$Q = a P^b \quad [9]$$

where Q = flowrate per unit floor area

P = pressure drop per unit grain depth

a = value of Q when P is unity

b = slope of curve on logarithmic axes

Shedd discovered that the lines produced were not very linear, but slightly convex upward. Brooker (1969) broke the line into several sections, determining values for a and b for each section. Shedd's work also included the flow of air through peanuts, but did not show the effect of moisture content or foreign material.

Steele (1974) did extensive research on the resistance of peanuts to airflow. He used peanut depths of 1.22 m and measured the static pressure at depths of 0.30, 0.61, 0.92 and 1.22 m. Airflow ranged

from 0.025 to 0.51 m³/s per m² of floor area. His work included the effects of foreign material, loose shelled kernels, as well as moisture content. Resistance was lower at higher moisture contents. When plotted on logarithmic axes, the pressure-flow relationship was more linear than in Shedd's case, and consequently, Equation [9] could be used to describe it. Steele also included a correction factor based on moisture content, and obtained the following equation,

$$V_a = 0.0184 \left(\frac{\Delta P}{RL} \right)^n \quad [10]$$

where V_a = apparent velocity [m/s]

ΔP = pressure drop across peanuts [Pa]

L = peanut depth [m]

R = moisture correction factor

$n = 0.618$

R was determined from,

$$R = 0.962 + 0.00392 M_{db} \quad [11]$$

where R = moisture correction factor

M_{db} = moisture content, dry basis [%]

The airflow rates used for drying peanuts vary considerably. Beasley and Dickens (1963) recommended a minimum rate of 0.167 m³/s per m³ of peanuts, and higher rates for peanuts with initial moisture contents exceeding 30 percent, wet basis. Lambert (1969) recommended flowrates ranging from 0.125 to 0.417 m³/s per m³ of peanuts for initial moisture contents ranging from 20 to 40 percent, wet basis, and 0.167 m³/s per m³ of peanuts at 25 percent moisture content. The higher flowrates were for the shallower peanut depths.

Troeger and Butler (1980) used two flowrates, 0.208 and 0.417 m³/s per m³ of peanuts in their experiments. The former was referred to as the recommended minimum, and the latter as the rate frequently used by peanut producers. They found that the higher flowrate significantly reduced the difference in moisture content between the top and bottom of the peanut bed, particularly for peanuts with high initial moisture contents. However, this higher rate increased the heat-energy consumption by 74 percent, while reducing the drying time by only 20 percent. It caused no noticeable differences in milling quality. Lower flowrates may result in non-uniform drying between the top and bottom, causing split kernels in the bottom, and mold growth on the top. The additional cost associated with the higher flowrates may be partly compensated for by increased peanut quality.

Airflow Measurement

Many methods of airflow measurement have been developed and standardized. Some methods are well-suited to certain situations.

Shaped Nozzles

Shaped nozzles, which come in various sizes, can be used for airflow measurements. The size range allows a size to be chosen for a particular range of flowrates. A standard nozzle is given by AMCA (1985) and is shown in Figure 2. The convergence profile is based on an ellipse, whose minor axis

is 0.667 times the major axis. Air pressure is measured at the inlet duct to the nozzle, and at the nozzle throat. This measurement is taken by installing 4 pressure taps, 90° apart, around the circumference of the upstream duct and the nozzle throat. The 4 pressure taps are used to determine the average static pressure, and are connected using a piezometer ring. Flowrate is determined based on the nozzle size, the pressure differential across it, and the physical properties of the air. The governing equations are given in AMCA (1985).

The volumetric flowrate through the nozzle, at the nozzle throat is,

$$Q_t = \frac{C A_t Y \sqrt{2 \Delta P / \rho_t}}{\sqrt{1 - E \beta^4}} \quad [12]$$

where Q_t = flowrate through nozzle throat [m^3/s]

A_t = area of nozzle throat [m^2]

ΔP = pressure drop across nozzle [Pa]

ρ_t = air density at nozzle throat [kg/m^3]

E = energy factor

= 1.043 for duct approach

β = ratio of nozzle throat diameter to approach duct diameter

Y = expansion factor

C = nozzle discharge coefficient

The discharge coefficient varies according to the Reynolds number. However, the Reynolds number depends on the air velocity, which cannot be determined without the discharge coefficient. The Reynolds number is approximated using the following equation,

$$Re = 70,900 D_t \sqrt{\frac{\Delta P \rho_x}{1 - \beta^4}} \quad [13]$$

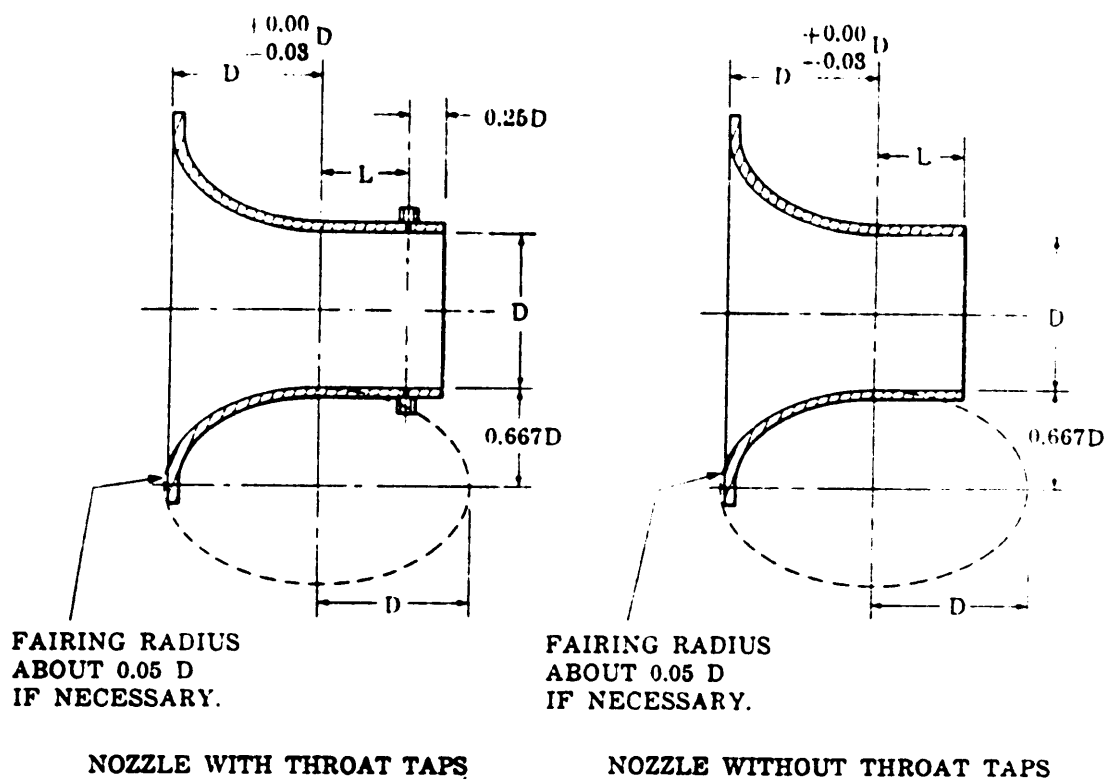


Figure 2. Standard nozzle (Reprinted from AMCA, 1985).

where D_t = diameter of nozzle throat [m]

ρ_x = air density at approach duct to nozzle [kg/m^3]

For L/D of 0.6 (refer to Figure 2), the discharge coefficient can be determined as follows,

$$C = 0.9986 - \frac{7.006}{\sqrt{Re}} + \frac{134.6}{Re} \quad [14]$$

The expansion factor, Y , is calculated from,

$$Y = 1 - (0.548 + 0.71 \beta^4)(1 - \alpha) \quad [15]$$

where α = alpha ratio

The alpha ratio is defined as the ratio of nozzle throat pressure to the absolute approach pressure, and is determined from,

$$\alpha = 1 - \frac{\Delta P}{\rho_a R (T_{du} + 273.15)} \quad [16]$$

where ρ_a = air density upstream from nozzle [kg/m^3]

T_{du} = dry bulb temperature upstream from nozzle [$^{\circ}C$]

R = universal gas constant [$N m/kg K$]

= 287.0

To determine air density, the saturated vapor pressure must first be calculated,

$$p_e = 3.24T_{wo} - 18.6T_{wo} + 692 \quad [17]$$

where p_e = saturated vapor pressure [Pa]

T_{wo} = wet bulb temperature [$^{\circ}C$]

The subscript o denotes the general test area.

The partial vapor pressure is determined from the saturated vapor pressure,

$$p_p = p_e - 2.26 p_b (T_{do} - T_{wo}) \quad [18]$$

where p_p = partial vapor pressure [Pa]

where p_b = barometric pressure [Pa]

T_{do} = dry bulb temperature [$^{\circ}$ C]

The air density is calculated from,

$$\rho_o = \frac{(p_b - 0.378 p_p)}{R} (T_{do} + 273.15) \quad [19]$$

where ρ_o = air density [kg/m^3]

For density corrections at a plane x having a different temperature and pressure,

$$\rho_x = \rho_o \left(\frac{T_{do} + 273.15}{T_{dx} + 273.15} \right) \left(\frac{p_{sx} + 13.63 p_b}{13.63 p_b} \right) \quad [20]$$

where ρ_x = air density at plane x [kg/m^3]

T_{dx} = dry bulb temperature at plane x [$^{\circ}$ C]

p_{sx} = static pressure at plane x [Pa]

When p_{sx} is less than 1000 Pa, ρ_x can be taken as being equal to ρ_o .

The flowrate of air at ambient conditions is,

$$Q = Q_t \frac{\rho_t}{\rho} \quad [21]$$

where Q = air flowrate at ambient air conditions [m^3/s]
 ρ = air density at ambient conditions [kg/m^3]

Pitot-Static Tube

Volumetric flowrate of air can also be measured by measuring the air velocity over a known area. A pitot-static tube, as described by AMCA (1985), can be used for this purpose. This method gives the velocity head in terms of pressure, which is then converted to a velocity.

$$V_p = \sqrt{\frac{2 P_{vp}}{\rho_p}} \quad [22]$$

where V_p = air velocity at pitot tube [m/s]
 P_{vp} = velocity pressure at pitot tube [Pa]
 ρ_p = air density at pitot tube [kg/m^3]

According to Pope and Harper (1966), the true reading of the dynamic head on a pitot tube can be obtained with an error of less than 0.1 percent. The error associated with the inclination of the pitot tube to the airflow is negligible if the angle of inclination is less than 3 degrees. Alignment can be done with sufficient accuracy by simply lining the pitot tube by eye (Ower and Pankhurst, 1977). If the center of the pitot tube is closer than 2 diameters to the wall, the measured velocity must be corrected. Further errors are associated with the static holes in the tube. The crowding of the streamlines near the tip produces a measured static pressure value lower than actual value. On the other hand, the measured static pressure may be higher than the actual value due to the high pressure region that exists ahead of the stem. Corrections are given in Figure 3. Static pressure correction for the stem is indicated by $(\Delta p)_s$, and $(\Delta p)_t$, for the tip.

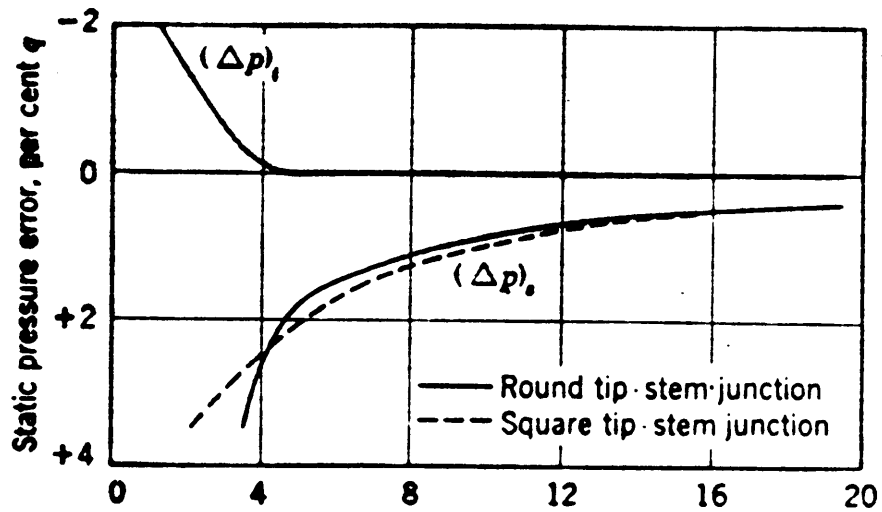


Figure 3. Static orifice distance from tip base or stem centerline, diameters (Reprinted from Pope and Harper, 1966).

Instead of a single point reading, a traverse is taken to calculate the average flowrate across the plane of interest. Rectangular openings are divided into equal areas, with the velocity reading taken at the center of each area (ASHRAE, 1981). The traverse must contain at least 16 points, and no more than 64 are necessary. If using less than 64 areas, the distance from area centers should not exceed 150 mm. The velocities, rather than the velocity heads, are averaged to determine the average velocity across the traverse plane.

These methods can be used to calibrate other devices where, which would be used where nozzle or traverse may not be practical, such as on-site field measurements. The calibration would result in an equation similar to [7] or [8]. Field measurements are often taken under different conditions than the calibration, so that some adjustments to the readings must be made. These differences are taken into account by adjusting the pressure drops by the ratio of the densities (Osbourne, 1966).

Engineering Sciences Data Unit (1972) presented a more elaborate method to account for conditions affecting pressure drops across round-wire gauzes (screens). A procedure was compiled, based on several references, so that pressure drop across screens normal to fluid flow could be determined. The pressure drop calculation is based on screen porosity and wire diameter, Reynolds number, and Mach number. From these, the pressure coefficient is determined, so that the problem is non-dimensionalized. Although both total and static pressure drops were discussed, only the static pressure drop will be considered.

The static pressure drop is determined from,

$$\Delta P = C_p \left(\frac{1}{2} \rho V_s^2 \right) \quad [23]$$

where C_p = pressure coefficient

V_s = velocity of air through screen [m/s]

The pressure coefficient is corrected for Reynolds numbers greater than 2000, or if the Mach number is much more than 0,

$$C_p = C_r \lambda_1 \lambda_2 \quad [24]$$

where C_r = reference pressure drop coefficient

λ_1 = correction factor for Reynolds number

= 1 for Reynolds number > 2000

λ_2 = correction factor for Mach number

= 1 for Mach number ≈ 0

To determine the value of λ_1 , only the Reynolds number is needed, whereas both the Mach number and the porosity of the screen is needed for λ_2 . The reference pressure drop coefficient is a function of porosity.

The Reynolds number is based on the wire diameter,

$$Re_s = \frac{\rho V_s D_s}{\mu} \quad [25]$$

where Re_s = screen Reynolds number

D_s = diameter of screen wire [m]

μ = absolute viscosity [$N s/m^2$]

The viscosity is essentially independent of pressure (Wallis, 1983). Variation in viscosity is temperature dependent and is can be determined from (AMCA, 1985),

$$\mu = (17.23 + 0.048 T_d) \times 10^{-6} \quad [26]$$

A value of $1.819 \times 10^{-6} N s/m^2$ may be used for temperatures ranging from 4 to 38 °C.

The Mach number is calculated from

$$M = \frac{V_s}{\sqrt{\gamma P/\rho}} \quad [27]$$

where M = screen Mach number

P = absolute upstream pressure [Pa]

γ = ratio of specific heats for air

= 1.400

The porosity is based on wire size and mesh density,

$$\alpha_s = (1 - N D_s)^2 \quad [28]$$

where α_s = screen porosity

N = mesh density [$meshes/m$]

In the case where the mesh is rectangular, with mesh densities of N_1 and N_2 , Equation [28] is modified,

$$\alpha_s = (1 - N_1 D_s)(1 - N_2 D_s) \quad [29]$$

Once Re , M , and α_s are known, C_r , λ_1 , and λ_2 can be determined from Figure 4 through Figure 6

This method is used to determine the pressure drop across a screen when the flowrate through it is known. Without modification, this method can also be used to determine the flowrate when the pressure drop is known, but requires a trial and error solution. However, it demonstrates the use of four dimensionless parameters, the Reynolds number, Mach number, pressure coefficient, and the porosity. These factors must each be considered for the calibration of screens for use as flow-measuring devices.

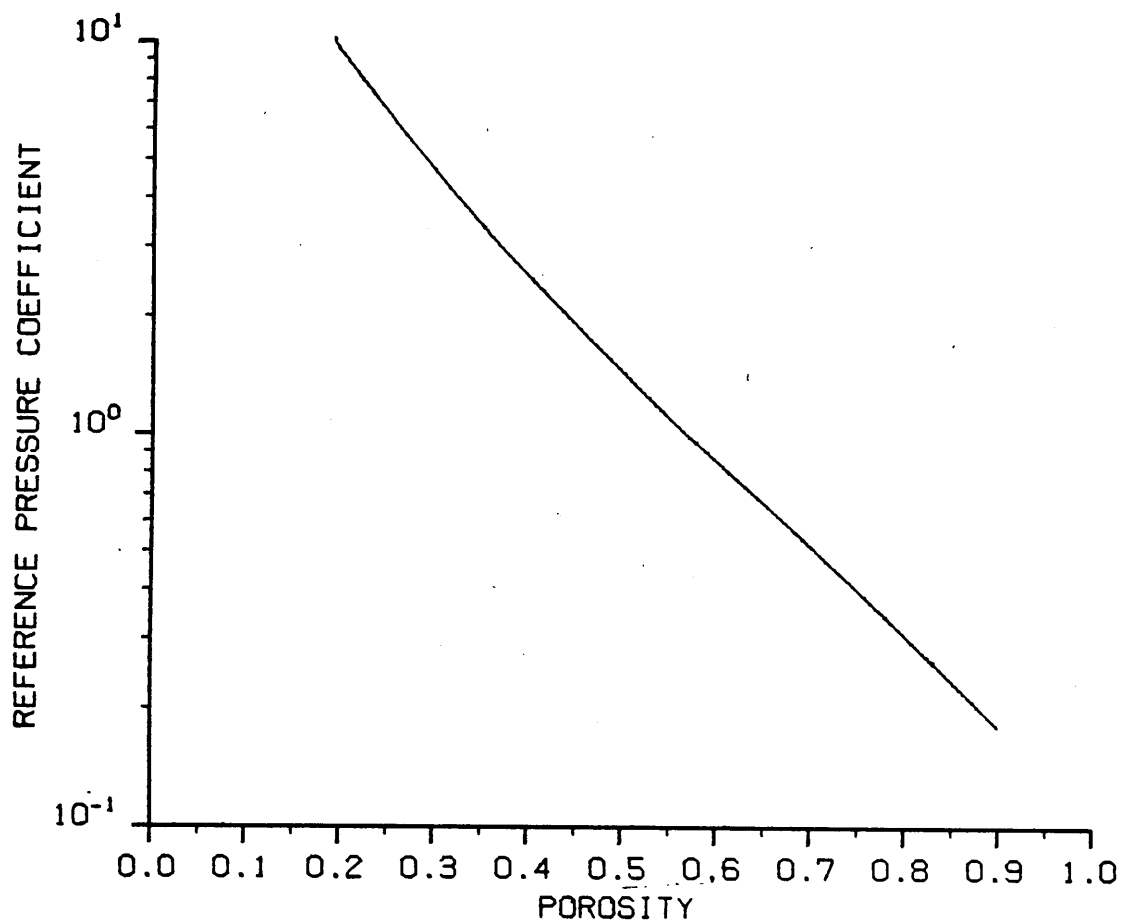


Figure 4. Reference pressure coefficient as a function of porosity (Adapted from Engineering Sciences Data Unit, 1972).

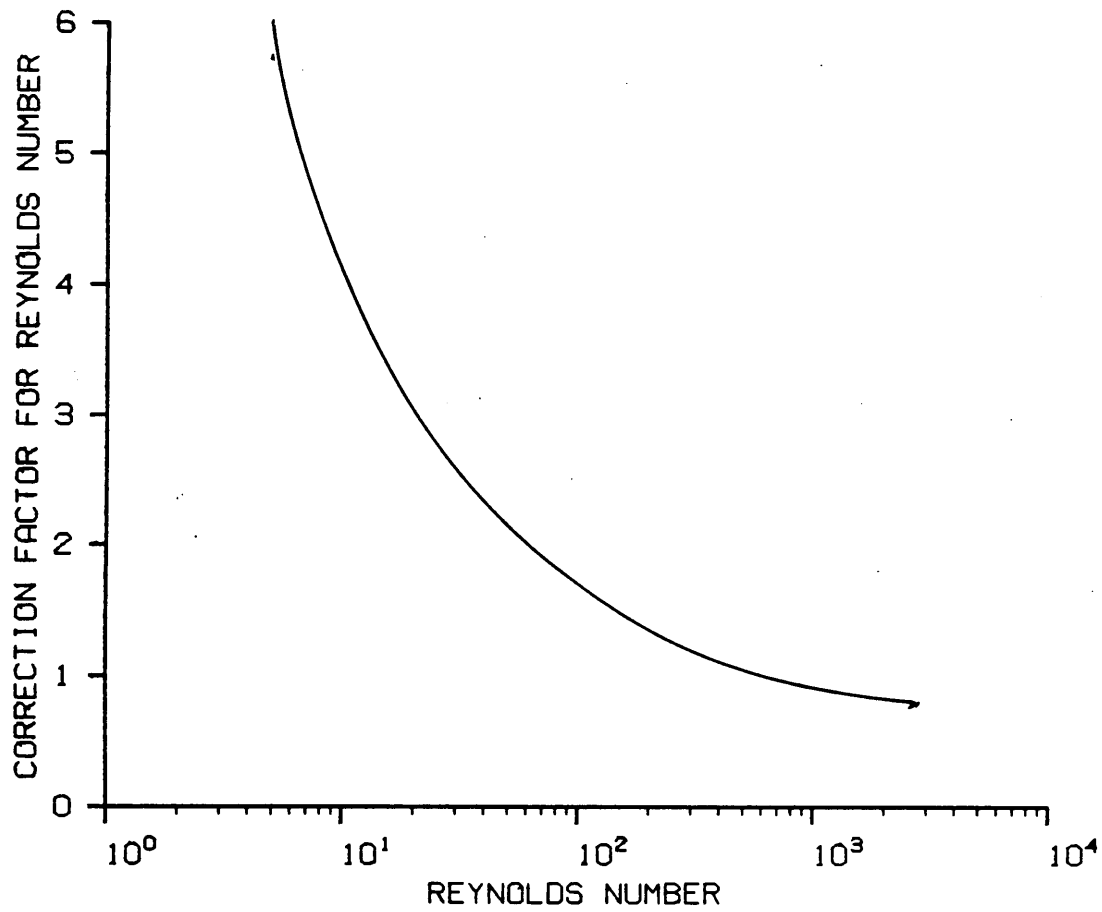


Figure 5. Pressure drop coefficient correction factor for $Re > 2000$ (Adapted from Engineering Sciences Data Unit, 1972).

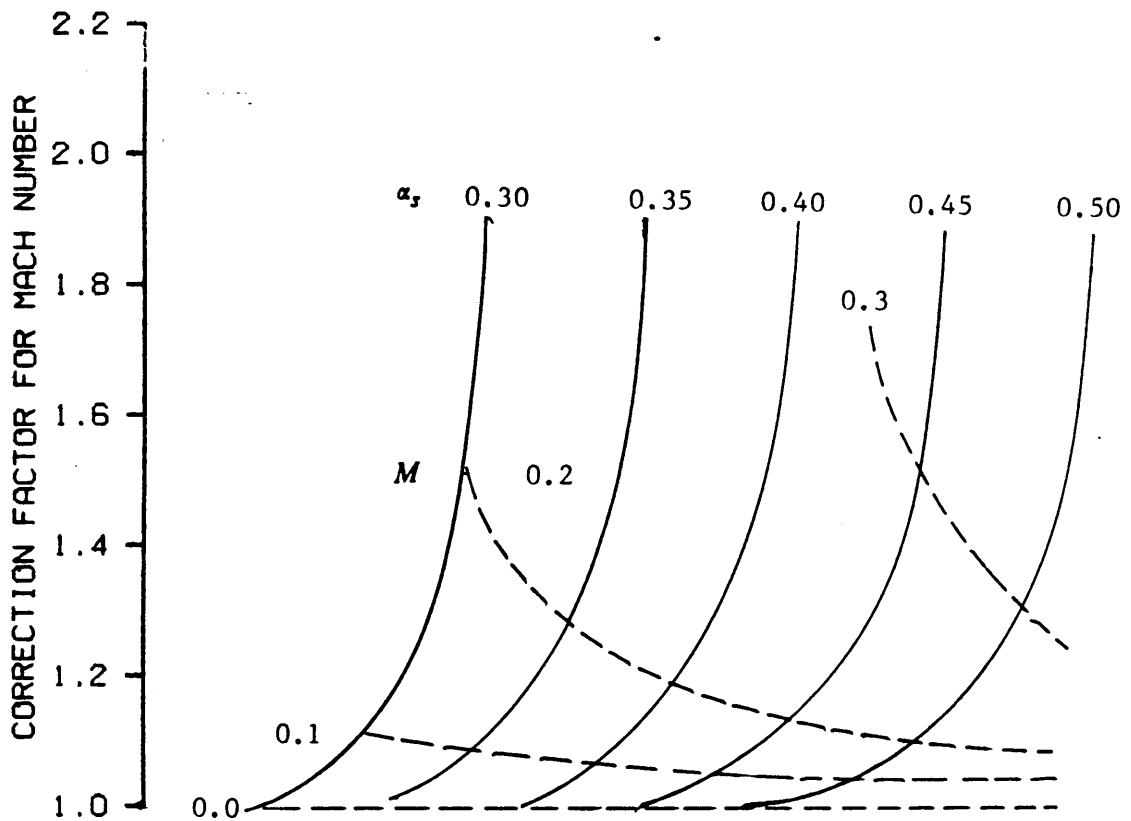


Figure 6. Pressure drop coefficient correction factor for $M > 0$ (Adapted from Engineering Sciences Data Unit, 1972).

Perforated Plates

Another method of measuring flow is by the use of orifice plates (ASHRAE, 1981). The pressure drop of air flowing through a pipe across an orifice is used to determine the flowrate, based on specifications of the orifice. This idea can be extended to the use of perforated plates, where air blows simultaneously through many holes drilled or punched in a plate. The characteristic flow through the plate, whether laminar or turbulent, depends on the Reynolds number, as represented in Equation [6]. The Reynolds number will be large if the hole diameter, and the air velocity through the hole are both high. With holes of equal diameter and air velocity (i.e., uniform flow across the plate), one would expect identical flow types for all the holes. Using Equation [7], one would expect a value of 2 for n for turbulent flow, and 1 for laminar flow.

Shedd (1954) measured pressure drop and airflow across a perforated metal sheet, and plotted the values on a log-log scale. He did not present his data in the form of Equation [7], but the slopes calculated from the lines in the graph give a value of n of 1.93, which is close to the expected value of 2. Differences may be due to experimental error, or flow that is not purely turbulent. In addition, some adjustments may have to be made to account for effects of the Reynolds number, Mach number and pressure coefficient.

Although a velocity traverse is normally done to determine volumetric flowrate, it may not be necessary if flows are sufficiently uniform. Mehta and Bradshaw (1979) state that a contraction reduces both mean and fluctuating velocity variations to a smaller fraction of the average velocity. A satisfactory contraction will typically have velocity variation of ± 0.5 percent outside the boundary layer. Short contraction lengths may result in separation of air from the wall. Longer contractions reduce the risk of separation, but adds to the construction costs, and the thickness of

the boundary layer. For smaller contractions, contraction ratios from 6 to 9 are normally used. (The contraction ratio is the ratio of inlet area to outlet area.)

When a contraction has a non-circular cross-section, the flow near the wall tends to migrate laterally. However, problems do not usually occur if a square contraction is well designed. For the same uniformity as an axisymmetric contraction, two-dimensional contractions require about 25 percent more length.

Analytical solutions to the Stokes-Beltrami equation or the Laplace equation have been derived (Mehta and Bradshaw, 1979). It is difficult, though, to derive a satisfactory wall shape design. One method is to design by eye. Shape is not as important as smoothness in contour shape. At least the first and second derivatives of the contour shape should be zero or very small. A contraction is followed by a working section. It should be at least 0.5 diameters long to bring the flow non-uniformities to an acceptable level.

Mikhail (1979) described a method for determining the optimum contraction, i.e., the shortest one that satisfies the flow quality requirements in the test section. Boundary layer separation must be avoided, and the flow must have a specified uniformity. Non-uniformity of flow is due largely to the wall contour of the contraction exit.

For an axisymmetric contraction, the contraction length is typically 2 to 2.5 times the inlet radius, and the test section, downstream of the contraction, is 4 to 5 times the exit radius.

Rather than define the contour shape directly, Mikhail defined the contraction radius in terms of its second derivative. The inlet and exit sections were separated by the inflection point of the contour, and were given by two different equations. For the inlet radius,

$$R'' = -A_1 (1 + B_i Z_1) [\sin(\pi Z_1)]^{N_i} \quad 0 < Z_1 < 1 \quad [30]$$

Similarly, for the exit section

$$R'' = A_2 (1 + B_e Z_2) [\sin(\pi Z_2)]^{N_e} \quad 0 < Z_2 < 1 \quad [31]$$

Z_1 and Z_2 are the non-dimensionalized forms of the distance along the nozzle axis, in the inlet and outlet sections, respectively. A_1 and A_2 are chosen to give the desired contraction ratio. B_i and B_e control the location of the distribution peak, and N_i and N_e determine the squareness or pointedness of the distribution shape. The contraction shape was determined to be optimum when $N_i = 0.01$, $B_i = 1.5$, $N_e = 3$, and $B_e = 0.0$. For a contraction ratio of 8, the optimum length of the inlet section was 0.60 times the inlet radius, and the optimum length of the exit section was 0.45 times the length of the inlet radius. This ratio produced a flow uniformity of ± 0.25 percent. When the contraction ratio is between 4 and 12, the required length decreases as the contraction ratio increases.

Axial Flow Fans

An axial fan is a fan in which the flow of air is largely parallel to the axis of the impeller. Air approaches the fan in an axial direction, but leaves with a rotational component caused by the impeller torque (Osbourne, 1966). This component can be removed and converted to useful static pressure by the addition of guide vanes downstream of the fan, or pre-rotational vanes upstream, rotating the air in the opposite direction to the impeller direction. Two impellers can be used, ro-

tating in opposite directions, so that the rotational components cancel each other out. This type of setup is called a contrarotating fan.

Fan characteristics are typically given in terms of flowrate and pressure drops. Fan total pressure is the total pressure drop across the fan. Fan velocity pressure is measured at the fan outlet, based on the volumetric flow divided by the outlet area. Fan static pressure is the difference between the fan total pressure and the fan velocity pressure. Many setups for testing fans are given by AMCA (1985), one of which is shown in Figure 7.

Fan total pressure as well as fan static pressure are plotted against flowrate, as shown in Figure 8. The pressure-flowrate curve often dips as the shutoff pressure is approached (Jorgensen, 1970). This dip may be in the form of a discontinuity, and is referred to as "stall". This phenomenon results from the separation of the flow at the back of the blades (Eck, 1973).

Fan curves allow fans to be matched to the pressure-flowrate conditions they will encounter once installed. However, fan performance can be affected by the specific location and design of the ductwork (Clarke et al., 1978), which affects flowrate, static pressure and fan brake horsepower. Lack of sufficient outlet duct length results in fan performance differences between field and laboratory. These effects may cause a gain or a loss, depending on the length of the outlet duct.

As shown in Figure 8, fan performance can also be measured in terms of total fan efficiency, and is the ratio of fan output power to fan input power. It is defined as (AMCA, 1985),

$$\eta_t = \frac{Q P_t K_p}{H} \quad [32]$$

where η_t = fan total efficiency

H = fan input power [W]

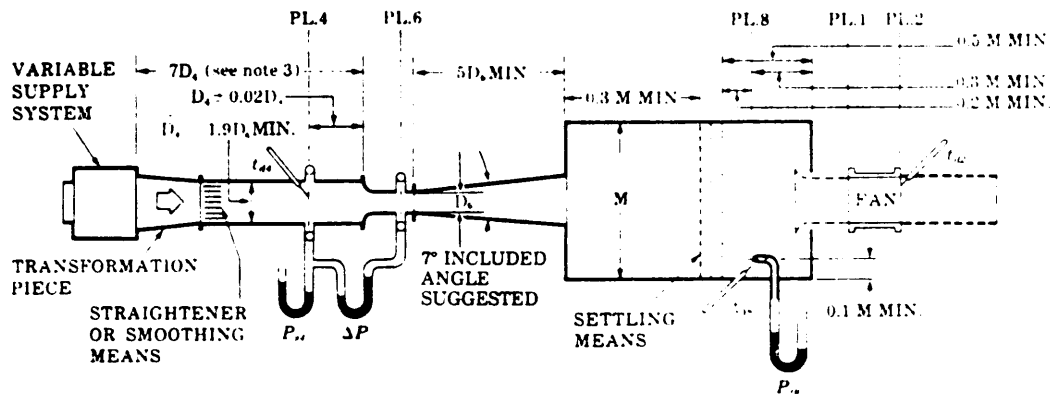


Figure 7. Inlet chamber setup - ducted nozzle on chamber (Reprinted from AMCA, 1985).

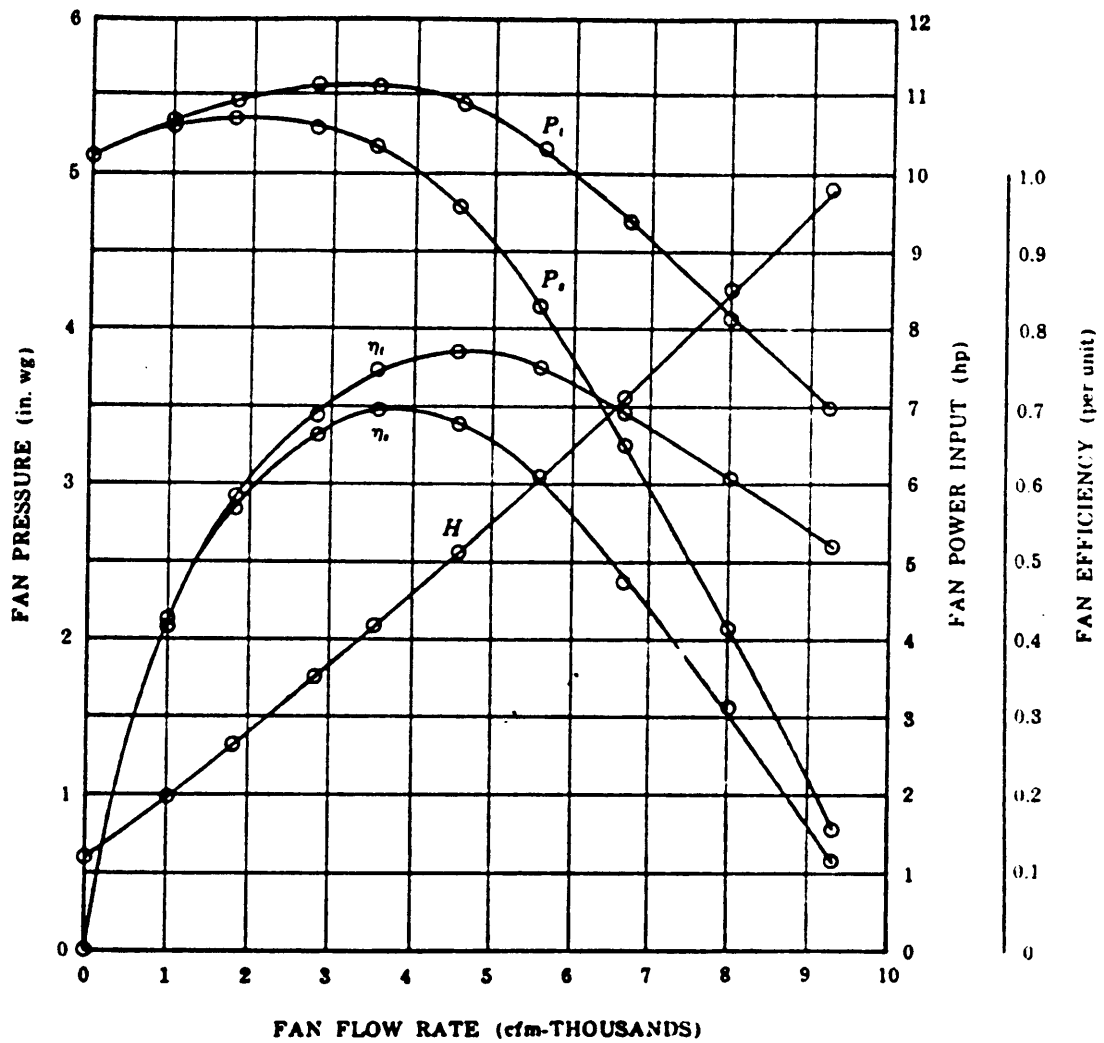


Figure 8. Typical fan performance curves (Reprinted from AMCA, 1985).

Fan static efficiency is also commonly used,

$$\eta_s = \eta_t \left(\frac{P_s}{P_t} \right) \quad [33]$$

where η_s = fan static efficiency

P_s = fan static pressure [Pa]

To design an axial fan, the first consideration is speed of operation (Jorgensen, 1970). Reynolds number effects favor low speed fans, whereas high speed fans are more economical due to size reduction. The rotative speed is also useful in determining hub-tip ratio, as well as the number, chord length, and angles of the blades. These factors also affect required size. The hub-tip ratio is based on the specific speed (Wallis, 1983),

$$N_s = N_f Q^{0.5} \Delta P^{-0.75} \quad [34]$$

where: N_s = specific speed

N_f = fan rpm

The number of blades is also a function of the specific speed. The capacity of the fan per revolution at a given blade angle determines the solidity of the blades (ratio of chord length to blade spacing). As the incidence angle of the blade increases, a higher pressure may be obtained. However, drag also increases, so blade angle should be carefully applied to the design (Wallis, 1983). Since linear velocity decreases toward the hub, the incidence angle of the fan blade must increase accordingly to maintain a constant fluid angle (Jorgensen, 1970).

Error Measurement

Every measurement has associated error. In order to determine the true value of a measured quantity, some estimate of the error is required. Errors may be either dependent or independent. Independent errors are the most probable, so that, when depicted as vectors, the error is at a right angle to the resultant of the previous errors (Rabinowicz, 1970). The worst case is when the errors are dependent and all point in the same direction. Suppose there exists a variable, F , which is a function of four independent variables,

$$F = f(a,b,c,d) \quad [35]$$

The total error can be determined from,

$$e_F^2 = \sum_{i=a}^d \left(\frac{\partial f}{\partial i} \right)^2 e_i^2 \quad [36]$$

where e_F = absolute error in F

e_i = absolute error for each dependent variable

Error can also be expressed as a fraction of the variable,

$$\epsilon_F = \frac{e_F}{F} \quad [37]$$

To demonstrate the difference between independent and dependent variables, let f be assigned a specific function,

$$F = abcd \quad [38]$$

Equation [36] reduces to

$$\varepsilon_F = \sqrt{\sum_{l=a}^d \varepsilon_l^2} \quad [39]$$

In this case, total error will be at a minimum. However, if the errors are dependent,

$$\varepsilon_F = \sum_{l=a}^d \varepsilon_l \quad [40]$$

If a and b are independent and c and d are dependent, then error is calculated from,

$$\varepsilon_F = \sqrt{\varepsilon_a^2 + \varepsilon_b^2 + (\varepsilon_c + \varepsilon_d)^2} \quad [41]$$

Abernethy and Thompson (1980) divided the error into two general categories: precision, or random error, and bias, or fixed error. Precision error results from repeated measurements which do not agree exactly. This approach produces a scatter of values, so that the precision index can be measured using the standard deviation,

$$S = \sqrt{\frac{\sum_{i=1}^N (x_i - \bar{x})^2}{N - 1}} \quad [42]$$

where S = standard deviation

N = number of data points

x_i = individual measurement

\bar{x} = average of individual measurements

Bias results when the average of the measured values is shifted from the true value. Large biases must be known to properly determine the error.

The total uncertainty in a measurement is determined from these two errors. For symmetrical bias,

$$U = \pm (B + t_{95} S) \quad [43]$$

where U = uncertainty of measurement

B = bias

t_{95} = 95th percentile of the two-tailed t-test

However, since biases may not be symmetrical, the upper and lower bounds on the uncertainty must be determined separately,

$$U_{LB} = B_{LB} - t_{95} S \quad [44]$$

$$U_{UB} = B_{UB} + t_{95} S \quad [45]$$

where U_{LB} = lower bound of uncertainty

U_{UB} = upper bound of uncertainty

B_{LB} = lower bound of bias

B_{UB} = upper bound of bias

When the degrees of freedom are greater than 30, t_{95} is approximately 2.

The biases and precision indices must be combined separately before a total uncertainty value can be determined,

$$U = \sqrt{\sum B_i^2} + 2\sqrt{\sum S_i^2} \quad [46]$$

The precision index for F in Equation [35] is determined from,

$$S_F = \sqrt{\frac{\partial f}{\partial a} S_a^2 + \frac{\partial f}{\partial b} S_b^2 + \frac{\partial f}{\partial c} S_c^2 + \frac{\partial f}{\partial d} S_d^2} \quad [47]$$

where S_F = precision index for F

S_a = precision index for a

S_b = precision index for b

S_c = precision index for c

S_d = precision index for d

The bias limits are calculated in a similar fashion,

$$B_F = \sqrt{\frac{\partial f}{\partial a} B_a^2 + \frac{\partial f}{\partial b} B_b^2 + \frac{\partial f}{\partial c} B_c^2 + \frac{\partial f}{\partial d} B_d^2} \quad [48]$$

where B_F = bias limit for F

B_a = bias limit for a

B_b = bias limit for b

B_c = bias limit for c

B_d = bias limit for d

Experimental Materials and Procedures

Total Flow Measurement

In order to measure total flow into the dryer fan, a variable air supply was constructed during the summer of 1986. This supply consisted of a four-cylinder diesel engine which drove a back inclined centrifugal fan, 0.900 m in diameter, through a hydrostatic transmission. The outlet of the fan was connected to a settling chamber, 2.40 by 2.40 m. The settling chamber contained three layers of wire mesh to create a uniform flow. On the outlet end of the settling chamber, a perforated plate was installed. This plate was calibrated so that the flow through it could be determined by measuring the pressure drop across it. Piezometer rings with four measuring points, one at the center of each side wall, were installed on both sides of the plate.

A canvas duct, approximately 2.4 by 2.4 m and 3.7 m long, stretched from the perforated plate to an end plate. This duct will be referred to as the connecting canvas. The end plate, 2.4 m wide

and 2.7 m high, contained a circular opening which fit over the dryer fan inlet. An additional piece of canvas was tied around the fan inlet, and clamped into the opening by a steel ring.

To calibrate the perforated plate, a reliable means of determining volumetric flow was needed. No nozzles as described by AMCA (1985) were available which could handle such a large flowrate. A pitot traverse was considered to be too tedious for calibration over a large area for a wide range of flowrates. It was decided that the best method would be to construct a square converging nozzle, similar to those used in wind tunnels. With a proper design, the velocity profile would be sufficiently uniform so that a pitot traverse would not be necessary.

A good nozzle design requires a smooth nozzle profile. Both mathematical and graphical methods of determining nozzle profiles were considered. Since space and cost were not critical, the nozzle was designed to be sufficiently long to ensure flow separation would not occur. Although increasing length increases the boundary layer thickness, and hence decreases the effective outlet area of the nozzle, it is considered acceptable compared to the risk of separation. Mikhail (1979) presented a method which calculates the shortest nozzle, but this method was not used. A method was desired which could easily be modified for design changes, and provide a quick generation of numbers for construction purposes. For this reason, a mathematical method was preferred to a graphical one. To further simplify the design, an equation was needed with an inflection point so that both the inlet and exit sections of the nozzle could be described by the same equation. In addition, it needed first and second derivatives that were close to zero at the inlet and exit.

A cubic equation was chosen since it contains an inflection point. The general form of the equation is,

$$y = ax^3 \quad [49]$$

where $a = \text{constant}$

This equation contains both the inflection point and zero first and second derivatives at $x = 0$, and cannot be used in this form to describe a nozzle profile. To overcome this problem, the axes were rotated such that the nozzle of the desired length would have slopes of zero at the inlet and exit. Figure 9 shows the unrotated and rotated sets of axes, represented by x and y , and x' and y' , respectively. The inflection point, where inlet and exit sections meet, is located at the origin. The x and y axes are rotated an amount θ to produce x' and y' . The exit section of the nozzle has a length x_L' , and a depth, measured from the point of inflection, y_L' . The slope at the point (x_L', y_L') is

$$\left. \frac{dy'}{dx'} \right|_{x'=x_L'} = 0 \quad [50]$$

In terms of the unrotated axes, the slope is

$$\left. \frac{dy}{dx} \right|_{x=x_L} = 3 a x_L^2 = \tan \theta \quad [51]$$

Combining Equations [49] and [51],

$$y_L = a x_L^3 = \frac{x_L (\tan \theta)}{3} \quad [52]$$

The unrotated and rotated axes are related as follows,

$$x = x' \cos \theta - y' \sin \theta \quad [53]$$

$$y = x' \sin \theta + y' \cos \theta \quad [54]$$

Replacing Equations [53] and [54] in [52],

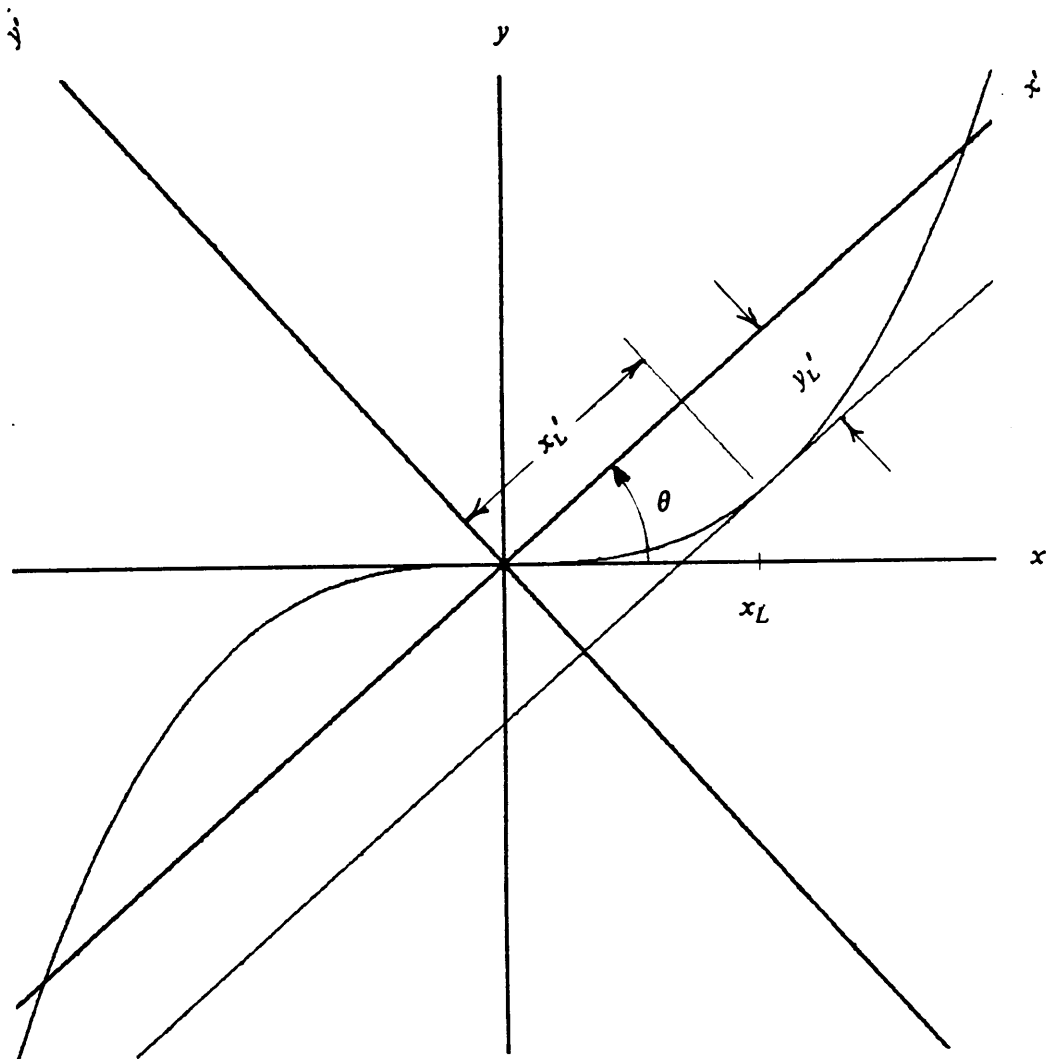


Figure 9. Unrotated and rotated axes, with cubic equation.

$$y_L' = - \frac{2 x_L' \sin \theta}{3 \cos \theta + \sin \theta \tan \theta} \quad [55]$$

Selection of an exit length, x_L' and an angle of rotation, θ , determined a value of y_L' , the depth of the nozzle, as well as the value of a . Once a was determined, values of x and y could be generated using Equation [49], and plotted after converting the values to x' and y' using transposed versions of Equations [53], and [54]. The calculations were performed by CUBIC FORTRAN, listed in Appendix A.

A nozzle exit length of 1.80 m was selected. Since the same equation was used for both inlet and exit sections with no modifications, inlet length equalled exit length, resulting in a total length of 3.60 m. Values of θ were chosen to produce a profile with a smooth curve and small second derivatives. With the inlet dimensions set at 2.421 by 2.421 m, the value of y_L' determined the contraction ratio. Since the same equation was used for both the inlet and outlet sections of the nozzle, the inlet depth was equal to the outlet depth. Hence, the total convergence is equal to $2y_L'$. A scaling factor was used to adjust the values of y' to change the contraction ratio, if desired. The chosen contraction ratio was 7.55, which was within the usual range of 6 to 9 (Mehta and Bradshaw, 1979). To create a square nozzle, a mirror image of the profile obtained was generated. The input parameters, as well as some of the output values, are shown in Table 1.

For construction purposes, the length along the profile, rather than the axis, was needed. Using a fourth order Runge-Kutta integration method, the arc length was numerically determined by CUBIC FORTRAN.

A nozzle was constructed based on the values in Table 1, whose profile is shown in Figure 10. It was built of galvanized iron in three sections. To install the nozzle on the supply fan, the canvas duct and end plate were removed. Once the nozzle was mounted, a short piece of straight duct

Table 1. Input and output parameters for CUBIC FORTRAN.

INPUT	
Exit length, x_L'	1.800 m
Exit depth	0.385 m
Inlet length	1.800 m
Inlet depth	0.385 m
Angle of rotation, θ	18.4°
Nozzle inlet height	2.421 m
Nozzle inlet width	2.421 m
OUTPUT	
Equation constant, a	0.0331
Unrotated outlet length, x_L	1.8295
Exit depth, y_L'	0.3850
Exit depth, scaled, y_L'	0.3850
Contraction ratio	7.5516

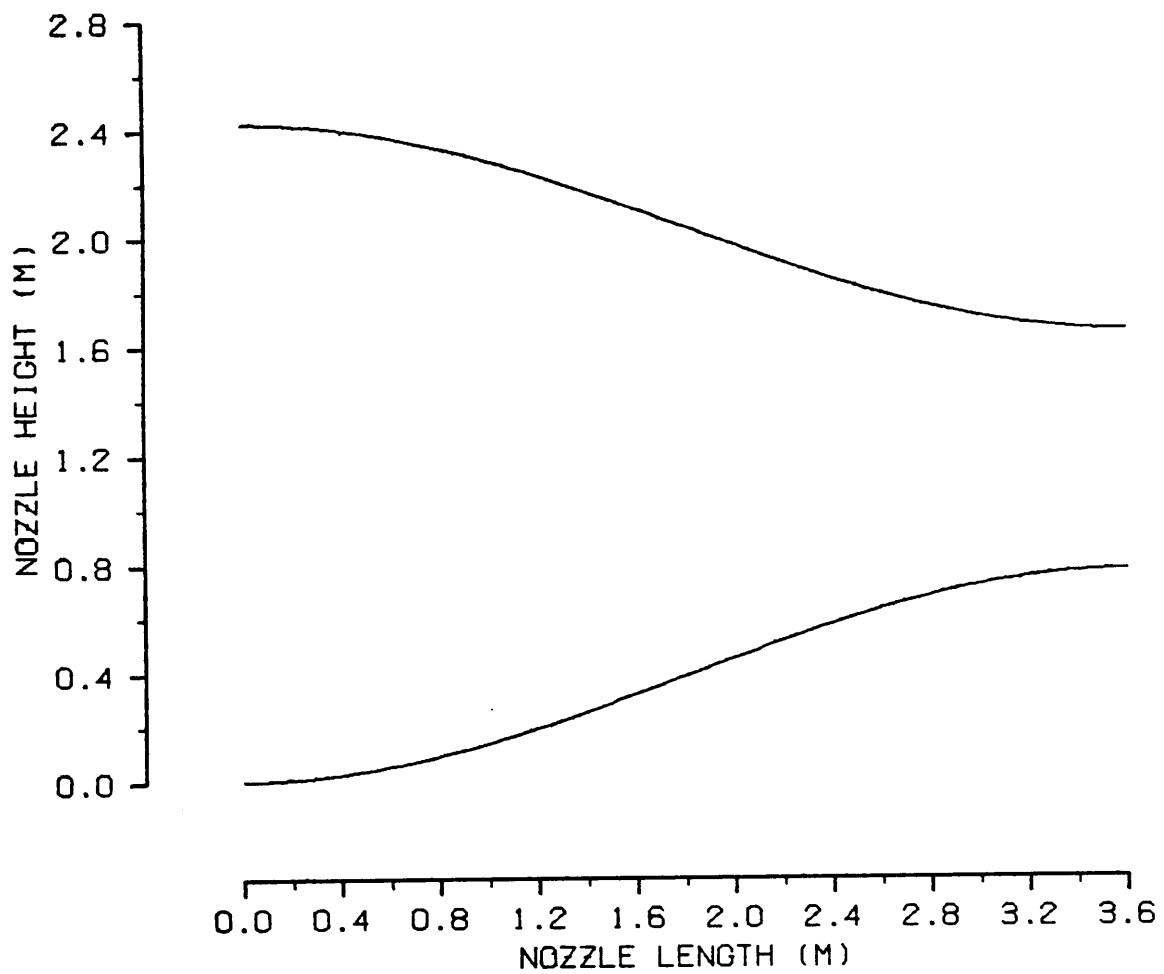


Figure 10. Profile of nozzle used for calibration of perforated plate.

was attached to it (Figure 11). This extension helped to ensure a straight flow for velocity measurement (Mehta and Bradshaw, 1979).

Velocity was measured using a standard pitot tube and micromanometer (Dwyer Microtector). The pitot tube was held in place by a ring stand. The pressure drop across the perforated plate was measured using an inclined manometer filled with 0.826 specific gravity oil. Wet and dry bulb temperatures were taken by measuring the resistance of thermistors. Barometric pressure was also measured.

In order to verify flow uniformity, a traverse was taken on a six-by-six grid in the duct extension mounted on the nozzle. The velocity pressure was measured at the center of each grid area. The six-by-six grid gave a spacing of slightly less than 0.150 m, which conforms to recommendations given by ASHRAE (1981).

Two perforated plates were calibrated. The first had 516 holes, each 0.0254 m in diameter, punched at equidistant spacing in an 2.4 m by 2.4 m sheet of 10-gauge metal. With the supply fan set near its highest speed, a pressure drop of 1000 Pa was developed, delivering 6.6 m³/s. This amount was insufficient to supply an average peanut dryer fan, which may deliver as much as 19.0 m³/s. A new plate was designed based on a flowrate of 21.0 m³/s at a pressure drop of 1000 Pa. Using the same size holes, the amount of air that passes through each is approximately equal, so that the number of holes required was $516 \times 21.0/6.6$, or 1642 holes. This number was changed slightly to 1628 holes to allow easy spacing within the given area. The second perforated plate was calibrated by measuring only the center-line velocity at the outlet of the extension mounted on the nozzle. The supply fan was set at ten different speeds, with the velocity pressure and pressure drop across the perforated plate measured for each setting.

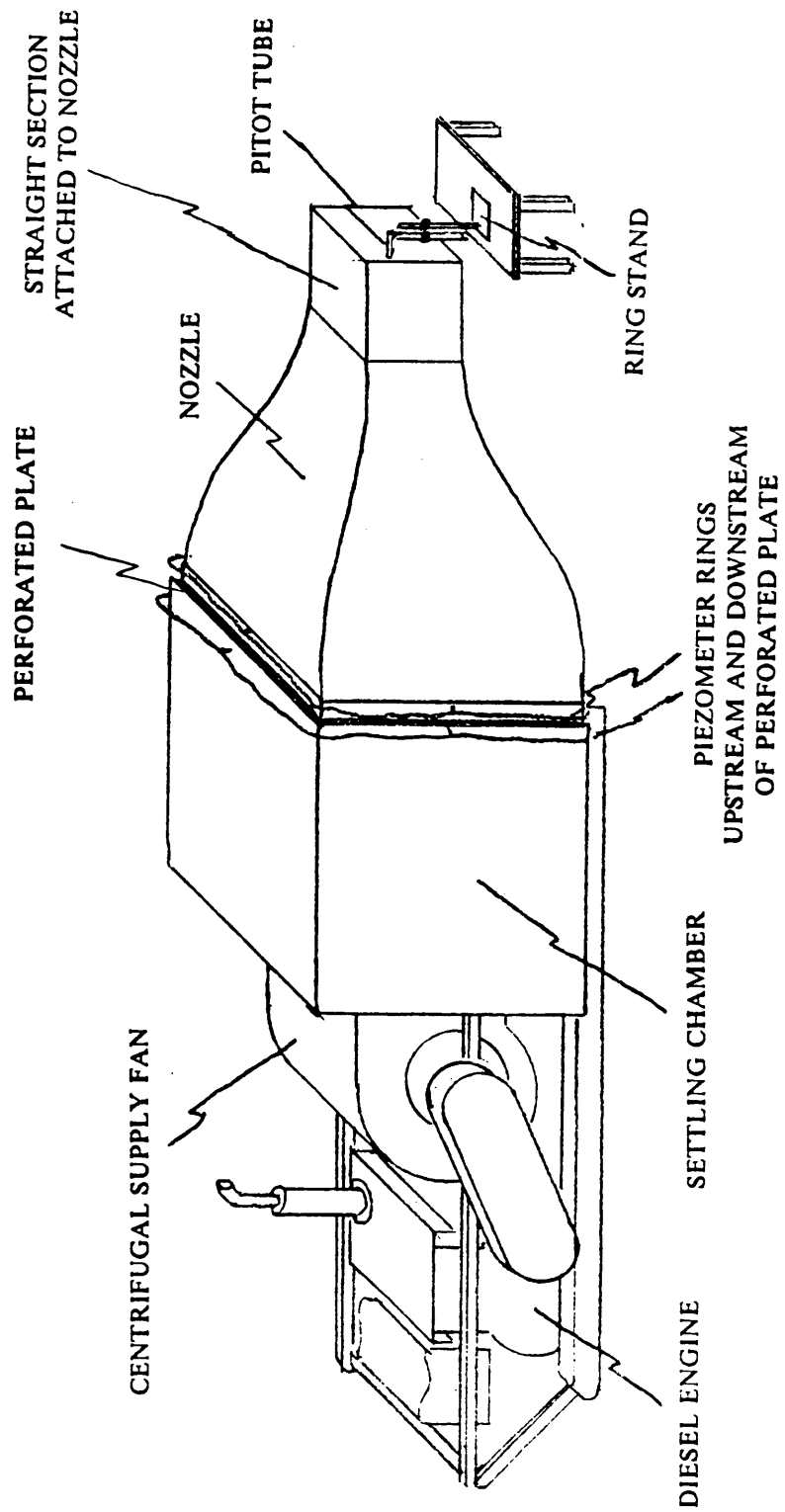


Figure 11. Experimental setup for calibration of perforated plate.

Flow Measurement through Individual Dryer Ports

The amount of air exiting each of the ports in the dryer plenum is an important part of testing dryer performance. Initially, rectangular collars equipped with piezometer rings were constructed (Figure 12). These were bolted to the trailer plenums, and the wooden frames with the canvas ducts attached were clamped to the upstream side. With the trailers filled with peanuts, the pressure at each of the piezometer rings was measured. Initial plans were to use this pressure measurement, and determine flowrate based on a value given by Steele (1974) for the resistance of a 1.3 m depth of peanuts.

Preliminary testing was conducted in Lewiston, North Carolina, in October, 1986. It was quickly discovered that trailer conditions adversely affect the readings. Pressure measurements would increase as much as 25 percent by simply patching some of the holes in the trailers with duct tape. Noticeable changes in pressure drop at a given port also occurred if trailers were interchanged. Because of this, it was impossible to determine if the flow distribution was due to the dryer plenum or the trailers. Initial testing in one particular dryer showed that the trailers on the left side of the plenum had consistently lower pressure drops than those on the right. However, upon closer inspection, it was found that the trailers on the left were considerably older and in greater disrepair than those on the right. This difference resulted in greater leakage, which reduced resistance and the pressure drop. In order to more accurately test the dryer, a better method of flow measurement through the plenum ports was needed.

A more accurate flow measurement could be obtained by thoroughly repairing the trailers, and having these trailers filled with peanuts. They would then be used to test the peanut dryer. This method had numerous drawbacks. First, many hours of labor would be required to carry out the

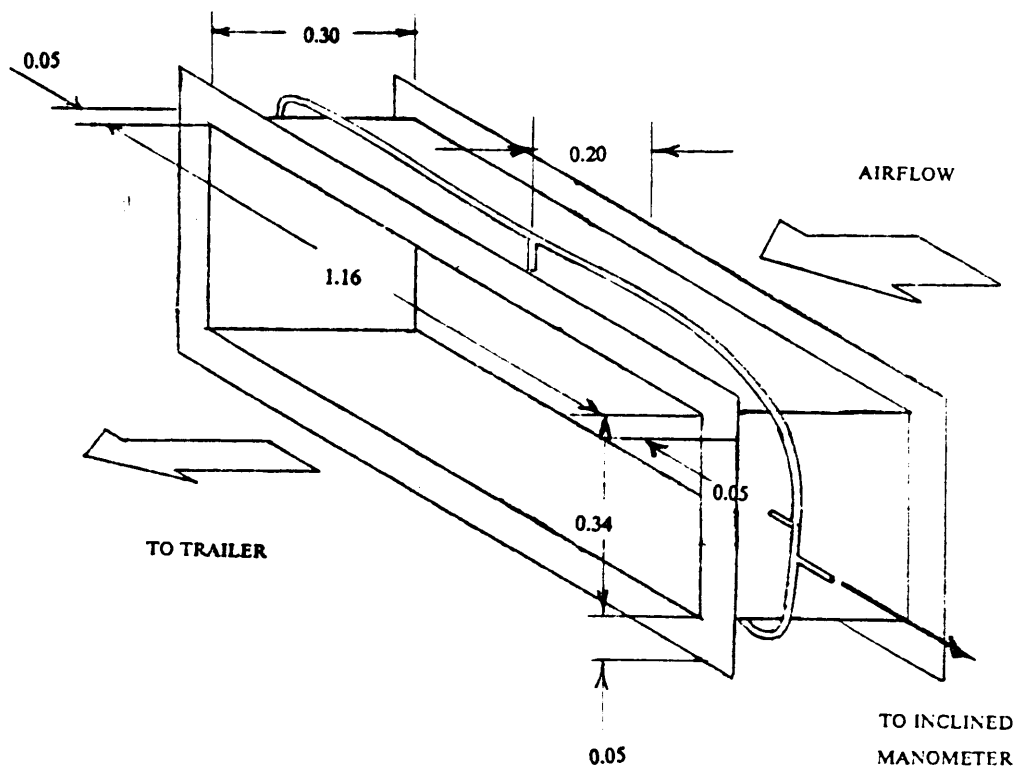


Figure 12. Rectangular collar with piezometer ring (All dimensions in meters).

repairs. Second, it would require the cooperation of the peanut producer during the drying season. Peanut producers are anxious to get their peanuts dried, and do not have the time to ensure that all repaired trailers are placed at the proper dryer after filling in the field. Finally, testing must be carried out in a short period of time during the drying season.

This method was abandoned in favor of using calibrated devices at the dryer supply ports. These devices would have a known resistance so that the flowrate could be determined by measuring the pressure drop across them. Testing could be done throughout the year without interfering in the peanut producer's drying schedule.

The first attempt to simulate peanuts consisted of two aluminum plates, each with 42 holes, 0.051 m in diameter, fitted to the rectangular collars. These plates were designed so that they could slide relative to one another, thus altering the amount of open area. In this way, the resistance could easily be changed so that the dryer could be tested over a range of flowrates.

However, if the dryer is to be realistically tested, the resistances should be similar to a load of peanuts in a trailer. Similarity means their pressure drop - flowrate curve should closely follow that of peanuts. The similarity was checked by calibrating the aluminum plates and comparing the results to the equation developed for peanuts by Steele (1974), Equation [10]. Converting velocity to volumetric flowrate, Steele's equation becomes,

$$Q = VA = 0.0184 A \left(\frac{\Delta P}{RL} \right)^{0.618} \quad [56]$$

where Q = volumetric flowrate through peanuts [m^3/s]

A = cross-sectional area of peanuts [m^2]

The cross-sectional areas and depths of several trailers at Lewiston were measured and averaged. An average depth of 1.3 m and an area of 8.4 m² were computed. Assigning these values, and re-arranging so that pressure drop is a function of flowrate,

$$\Delta p = 26.67 R Q^{1.618} \quad [57]$$

Using a recommended flowrate of 0.167 m³/s per m³ of peanuts, a typical Lewiston trailer required 1.82 m³/s, which gave a pressure drop of about 70 Pa, depending on the value of R . (Although the resistance from the peanut trailer itself is unknown, it was assumed to be negligible compared to the peanuts.) The actual pressure drop measured during the 1986 testing at Lewiston ranged from 2 to 60 Pa on an eight-trailer unit with trailers connected to all eight ports.

Upon calibration, it was quickly realized that the aluminum plates had resistances much higher than that of peanuts. More holes reduced the resistance of the plates, but did not adequately simulate peanuts, since the flow characteristics were different. The flow through the holes in the aluminum plate was turbulent, so that, with a constant area, the pressure drop across it was proportional to the square of the flowrate. The pressure drop across peanuts is proportional to the power of 1.618 of the flowrate. Therefore, the aluminum plates could not be used to determine dryer performance as it would behave in actual drying conditions.

In a second attempt to simulate the resistance of peanuts, several kinds of cloth in different combinations were tried. These were placed on wooden frames which were then bolted to the collars. These frames with material attached are hereafter referred to as "resistance plates".

To calibrate the resistance plates, the test setup shown in Figure 13 was used. It was based on the fan test setup defined by AMCA (1985) in Figure 7. A centrifugal fan was driven by a 7.46-kW, three-phase electric motor equipped with a variable sheave. Air passed through a standard nozzle,

with 0.61 m inlet and 0.305 m outlet. A diverging, tapered, round duct connected the nozzle outlet to a settling chamber. A rectangular opening, 0.34 by 1.16 m was cut in the downstream end of the chamber. The collar shown in Figure 12 was bolted over the opening, the joint was taped to eliminate leaks, and then the resistance plate was bolted to the collar.

After numerous tests, a combination of one layer of fiberglass window screen (6.17 by 7.00 meshes/cm), four layers of cotton cheesecloth (4.32 by 13.45 meshes/cm), and a 1.90 cm grid wire screen was chosen to represent the peanuts. Each resistance plate with the six layers was calibrated individually with a specific collar, for flowrates ranging from 1 to 2.8 m³/s and later extending to 4.1 m³/s.

Each collar was fitted with its own resistance plate. Each test consisted of eight flowrates, and three replications were done for each flowrate for each of the eight collars. For each flowrate, the motor rpm, the static pressure upstream of the nozzle, the pressure drop across the nozzle, and the pressure drop across the resistance plate were taken. The pressure drop across the nozzle was used to calculate total flow using the Equations [12] through [16] from AMCA (1985). The wet and dry bulb temperatures were measured for each test, and the barometric pressure was taken periodically throughout the day. These values were used to compute air density and viscosity.

Power Measurements

Power measurements were originally obtained using a hand-held meter. This approach proved to be inadequate in the field as the readings fluctuated severely, and differences in power consumption for various tests were difficult to detect.

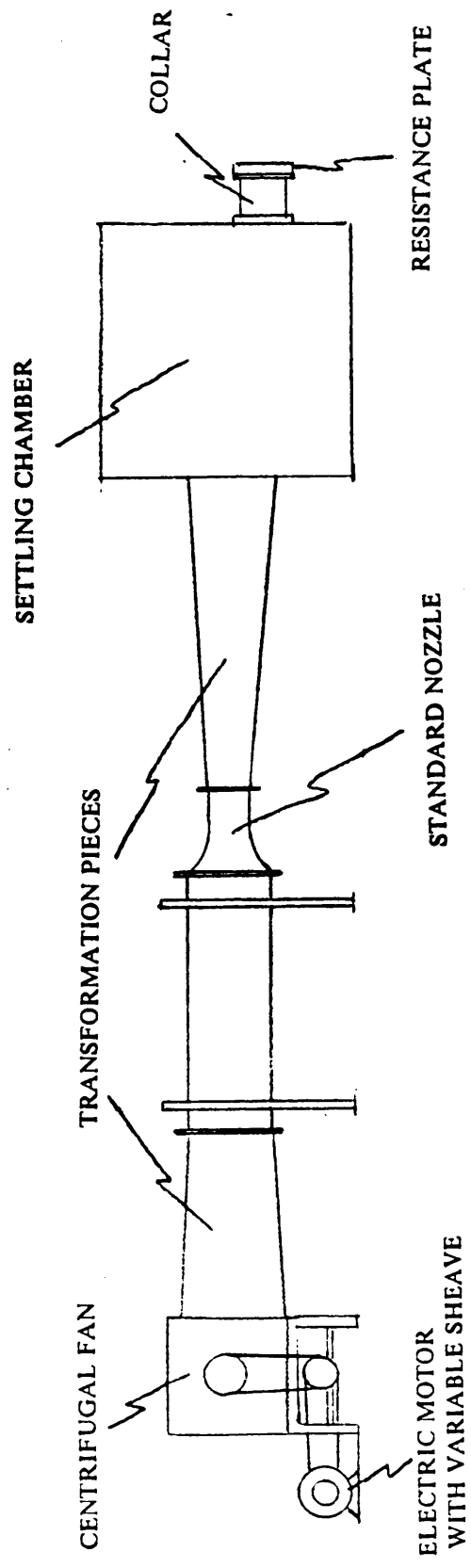


Figure 13. Experimental setup for calibration of resistance plates.

To ensure more reliable power measurements, a power transducer (Scientific Columbus Model XL34-2K5-A2-6070-1) was purchased, specifically designed for three-phase power. This transducer emitted one electrical pulse for each watt-hour of electricity that passed through it. Since the fan power draw was above the capacity of the transducer, current transformers were installed to reduce line current, which simply introduced a multiplicative factor in the power calculations. The emitted pulses were counted by a frequency meter. A programmable gate was built to act as a switch between the transducer and the frequency meter. Once a test was started, the operator would activate the programmable gate to count pulses for a given time period, such as five minutes. The total energy consumed by the fan was measured over this five minute period, and fan power determined.

Field Test Setup

Since peanut dryers normally have sheds built over them, the fan on dryers to be tested had to be close to the edge of the shed, or have sufficient clearance above it, to allow the end plate from the fan test unit to fit into place with the dryer fan inlet protruding through the circular opening in the end plate. If this condition was met, the fan test unit was backed into place in front of the dryer (Figure 14). The end plate, which must be disassembled for transport, was reassembled and the connecting canvas was bolted to it. The end plate was positioned over the dryer fan inlet, and the fan inlet canvas was attached around the dryer fan. Stakes and guy lines prevented the end plate from tipping over. Once in place, the fan test unit was pulled forward to tighten the connecting canvas. An inclined manometer, mounted on a tripod, was used to measure the pressure drop across the perforated plate.

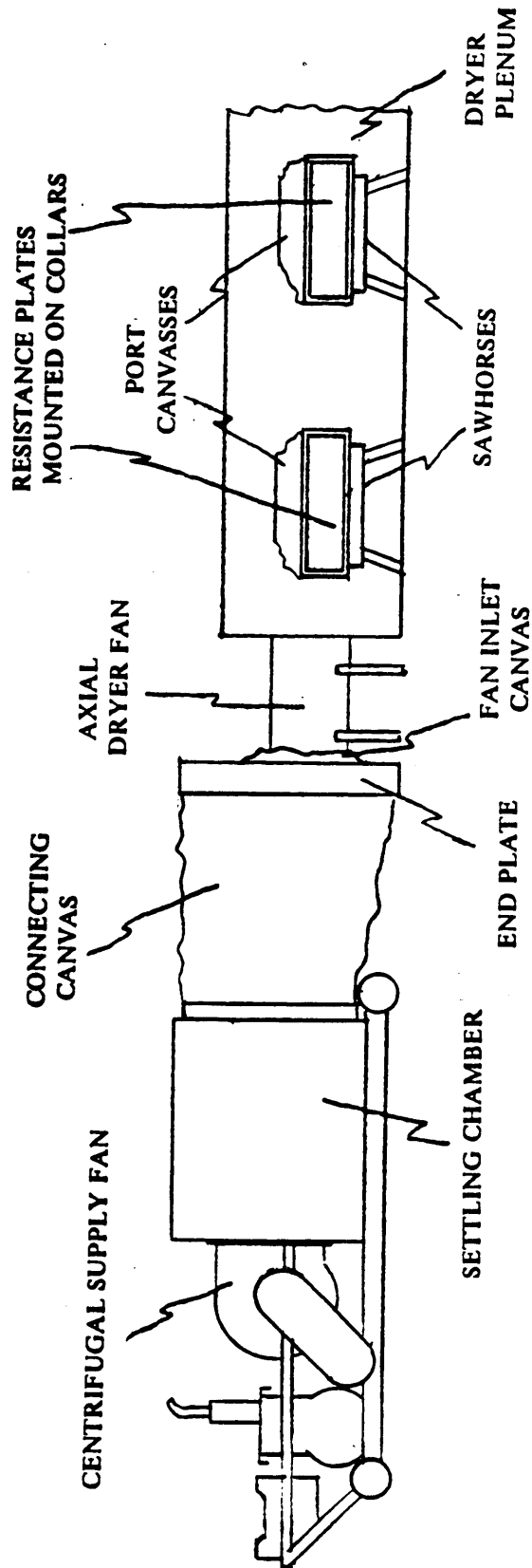


Figure 14. Experimental configuration for on-site testing of peanut dryer fans.

A collar with a piezometer ring was placed on a sawhorse in front of each of the plenum ports. The wooden frame at the end of the port canvas, which normally connects to the trailers, was inserted into the collar and held in place with clamps. Two inclined manometers, one on either side of the plenum, were used to measure the pressure across the resistance plates, which represent trailers filled with peanuts. Rubber tubing connected the piezometer ring on each collar to the manometers. Tubes were numbered at the manometer to correspond to the port, so several pressure drops could be measured by switching tubes, without moving the manometers. The dryer ports were numbered such that, if one were to look downstream from the fan, Port No. 1 would be the port on the immediate right. The ports were then numbered consecutively counterclockwise around the plenum. The collar/resistance plate combinations, which were also numbered, were always placed at the port having the same number. This allowed easier computer programming, as a certain port number would always identify a particular collar. A frequency meter counted the pulses from a 60-tooth sprocket mounted on the supply fan shaft, and this aided in maintaining a constant fan speed. After opening the required ports for a given test, and zeroing the manometers, testing was begun.

Field Test Procedures

Fan Balancing

To begin a test, the supply fan and dryer fan were started simultaneously, and the speed of the supply fan was adjusted until the pressure in the connecting canvas was zero. The required supply fan speed was unknown at the beginning of a test. An undersupply or oversupply of air to the dryer

fan caused the connecting canvas to be either sucked in or blown out. In addition, the dryer fan came up to speed much more quickly than the supply fan. To prevent excess pressure from building up in the connecting canvas, the dryer fan was turned off and on by a second operator as the supply fan speed was increased by the primary operator. Once the two fans were close enough in balance for the dryer fan to remain on, the supply fan speed was more finely adjusted. It was assumed that the fans were in balance, i.e., the supply fan was delivering the same amount of air into the connecting canvas as the dryer fan would require under normal operating conditions, when the connecting canvas was loose and fluttered slightly. At this point, the pressure at the dryer fan inlet was approximately equal to atmospheric pressure. Since there is a slight velocity pressure in the connecting canvas, a negative static pressure, causing the canvas to be sucked in, should exist. However, this kind of condition would be difficult to observe and hence to maintain. From an observation point of view, a fluttering canvas is much more practical than one that is slightly sucked in. Small adjustments had to be made to the supply fan speed during the test, and an operator stood by the controls to make these adjustments.

Data Collection

Data collection began once the two fans were balanced. First, the pressure drop across the perforated plate was taken, to define total flow into the dryer, followed by those across each of the resistance plates, to define flow out each port. After this, the pressure across the perforated plate was retaken, to check if variation occurred during the time it took to collect the resistance plate data. The supply fan speed and the dryer fan power consumption were also measured. The wet and dry bulb temperatures were also taken periodically, and the daily barometric pressure was obtained from the nearest meteorological station.

Description of Dryers Tested

A total of six different peanut dryers were tested (Table 2). Two of these, a six-trailer unit and an eight-trailer unit, were tested on site in Lewiston, North Carolina. Both dryers were equipped with 4-blade, 1.07-m diameter Aerovent fans, driven by 11.2-kW, three-phase motors. A six-trailer unit, with a 7.46-kW, three-phase motor, driving a 6-blade Aerovent fan, was tested near Holland, Virginia. These three dryers were tested in November, 1987. In addition, four dryers were tested in Blacksburg in the spring of 1988. These consisted of a six-trailer unit and a four-trailer unit tested with a 5.60-kW motor driving a 0.91 m diameter, 9-blade Long fan, and a six-trailer unit and an eight-trailer unit tested with a 7.46-kW motor driving a 1.12 m diameter, 9-blade Long fan. The fan curves were obtained from the manufacturers and are shown in Figure 15 to Figure 18. Aerovent supplied tabular data, whereas Long gave the entire curve.

At each location, the resistance plates were placed, and a "dry" run was first carried out without the fan test unit connected. This was done to study whether the fan test unit affected the flow measured at the various ports. Next, the fan test unit was connected, and the dryer was tested without any modifications. A third set of tests was conducted after "repairs" had been made. These repairs consisted largely of using duct tape to fix the holes in the port canvasses. At the Holland location, holes were essentially non-existent so that tests after "repairs" became a repetition of the first test.

For the second and third tests, different combinations of port gates were opened and closed. Not all possible choices of open and closed gates were employed, as this would be too time-consuming. The combinations were selected to give a general idea of the leakage and flow distribution within the plenum when a farmer does not have loaded trailers connected to all ports.

Table 2. Description of fan configurations tested.

Location	Fan Size and Type	Dryer Plenum Size
Lewiston, North Carolina	11.19-kW Aerovent	Eight-trailer unit
Lewiston, North Carolina	11.19-kW Aerovent	Six-trailer unit
Holland, Virginia	7.46-kW Aerovent	Six-trailer unit
Blacksburg, Virginia	5.60-kW Long	Four-trailer unit
Blacksburg, Virginia	5.60-kW Long	Six-trailer unit
Blacksburg, Virginia	7.46-kW Long	Six-trailer unit
Blacksburg, Virginia	7.46-kW Long	Eight-trailer unit

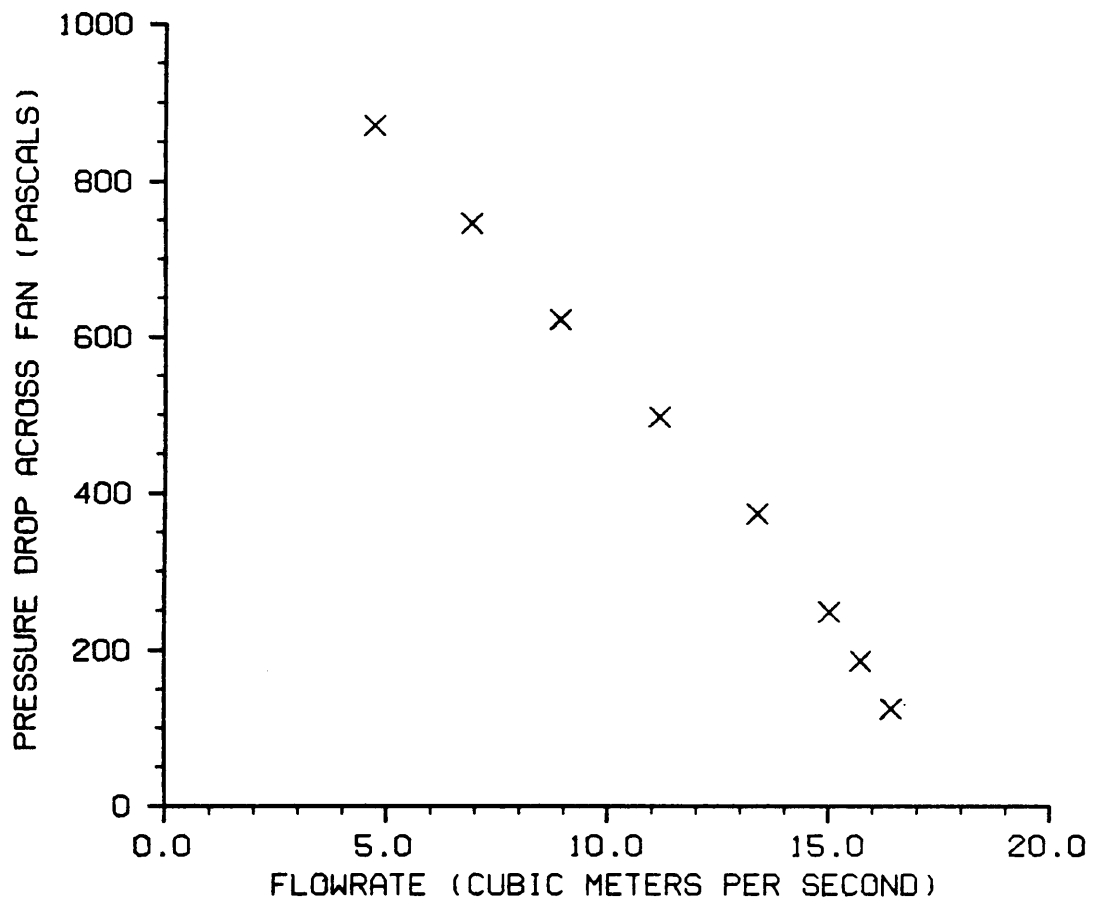


Figure 15. Manufacturer's fan rating curve for 11.2-kW Aerovent (Adapted from Aerovent performance data).

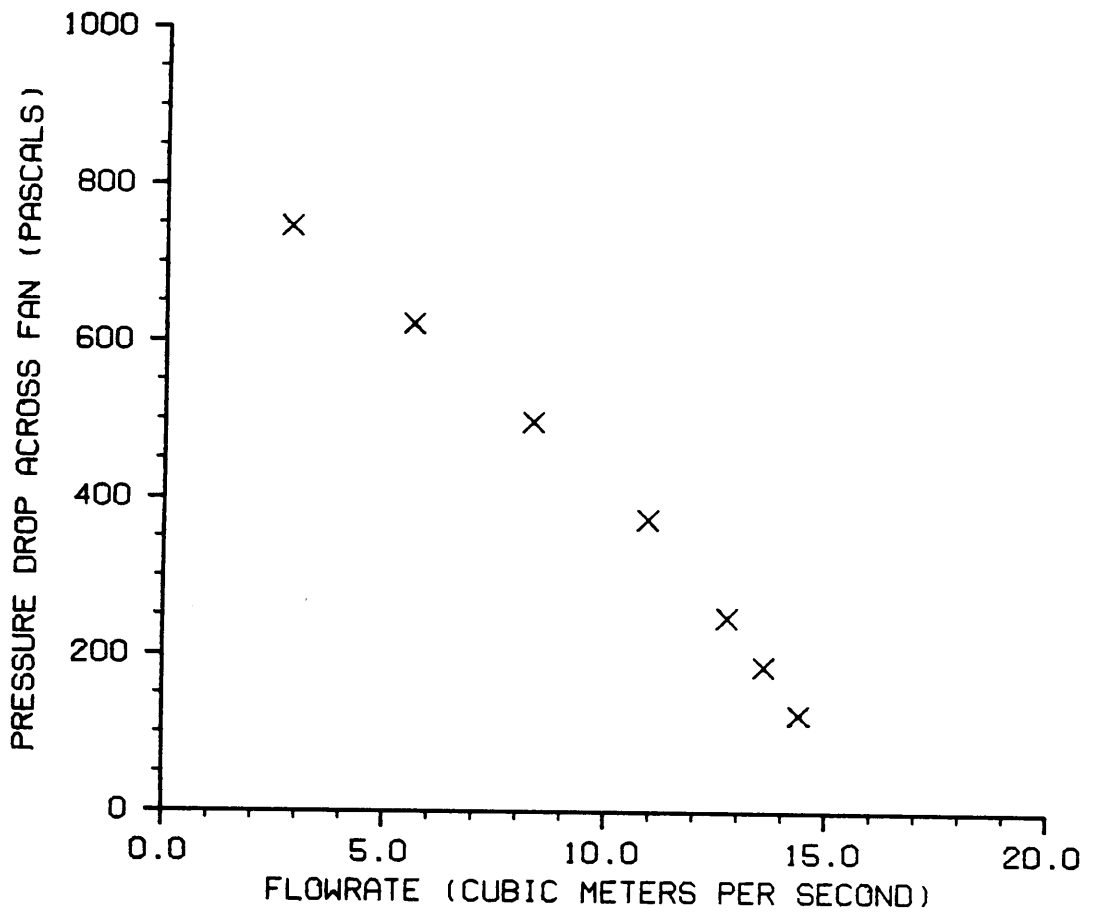


Figure 16. Manufacturer's fan rating curve for 7.46-kW Aerovent (Adapted from Aerovent performance data).

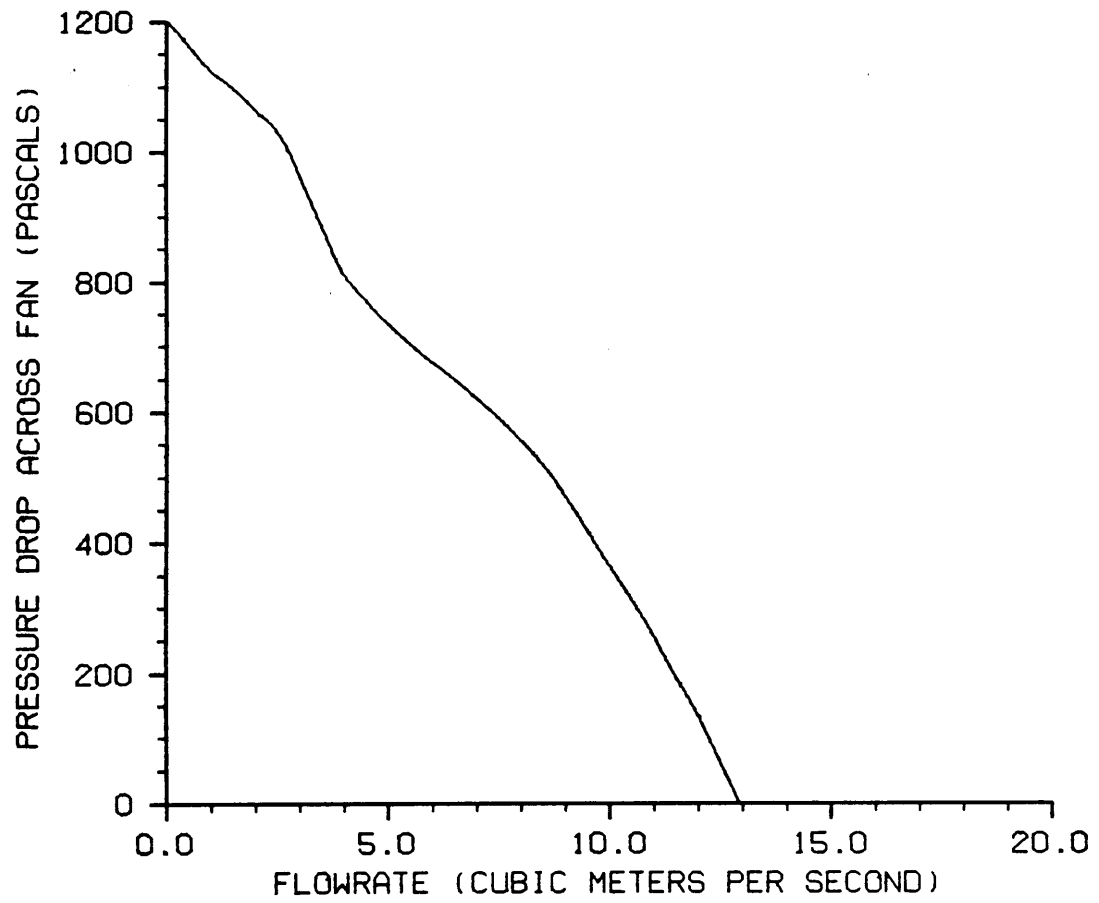


Figure 17. Manufacturer's fan rating curve for 5.60-kW Long (Adapted from Long performance data).

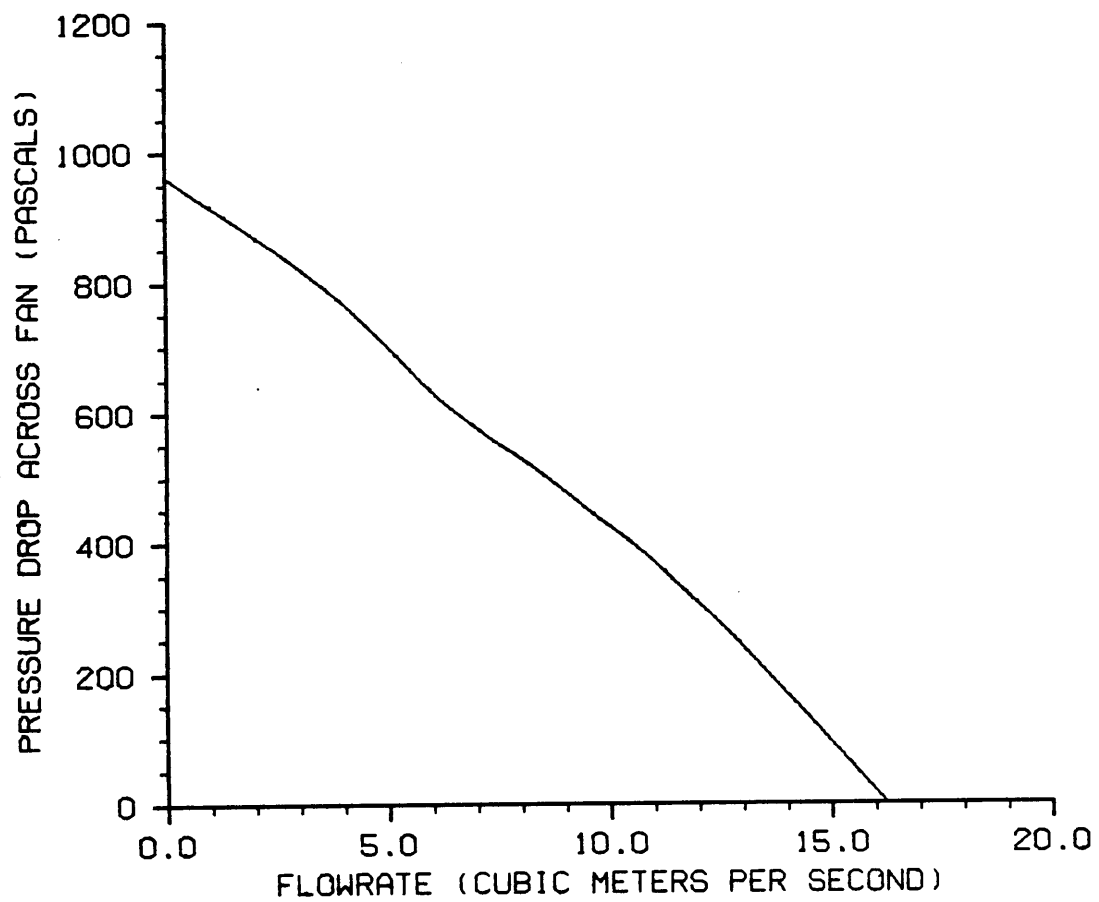


Figure 18. Manufacturer's fan rating curve for 7.46-kW Long (Adapted from Long performance data).

The dryers tested in Blacksburg were constructed from two four-trailer dryers were purchased in North Carolina. Both were manufactured by Long Mfg. Co., Tarboro, North Carolina, and equipped with 9-blade fans. One had a 5.60-kW motor with a 0.91 m diameter fan, and the second had a 7.46-kW motor with a 1.12 m diameter fan. The 5.60-kW fan was tested on a four-trailer plenum in its original condition and retested after repairing all holes in the fan housings and plenums with sheet metal and caulking. In addition, the frames on the port canvasses which connected to the trailer plenums were repaired. After testing, weatherstripping was added to the frames and the tests were done a third time. Unlike the dryers tested previously, this dryer plenum had a baffle to divert more air to the ports closest to the fan. The baffle consisted of a folded piece of sheet metal supported by two angle iron uprights (Figure 19).

After the testing of the four trailer unit was complete, the end of the dryer plenum was removed, and two sections from the end of the second four-trailer unit were cut off and bolted to the original four-trailer unit. This "new" six-trailer unit was then tested in a similar manner to the four-trailer unit. Both the 5.60- and 7.46-kW fans were bolted onto the six-trailer unit for individual tests. For each fan, the dryer was tested with and without the baffle installed to determine its effectiveness in distributing the flow.

On some commercial dryers, fans move more air than the $0.167 \text{ m}^3/\text{s}$ per m^3 of peanuts which is needed. In addition, dryers are sometimes only partially loaded towards the end of the drying season because there are not enough filled trailers for the available ports. This causes the trailers to receive more than the desired airflow. One method of reducing the flow is to partially close the port gates. This method is also used to reduce airflow to trailers which are only partially filled (which also occurs at the end of the drying season). The consequence of this management technique is that it tends to force more air through the ports that remain fully open, and energy is wasted.

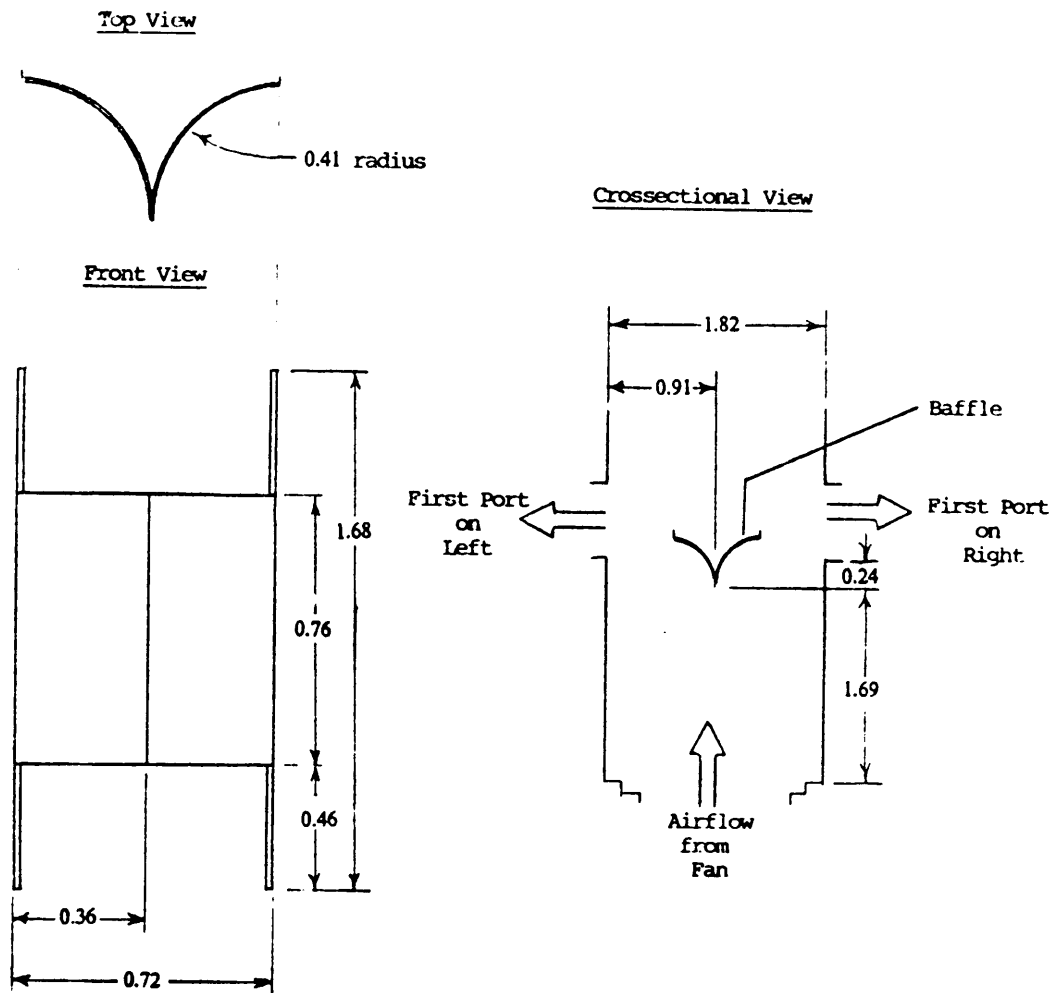


Figure 19. Baffle dimensions and position in dryer plenum (All dimensions in meters).

A better management technique would be to restrict the amount of air entering the dryer. One method would be to install exhaust dampers on the fan outlet. However, the propane burner is attached to the fan housing just downstream of the fan, leaving little available space for any additional accessories. Furthermore, restricting flow on the exhaust side of the fan would have only negligible effects on energy consumption since the flowrate is reduced simply by increasing the working pressure. Preliminary tests indicated that increasing the working pressure always led to a rise in power consumption. For these reasons, any attempts to control the fan flow by use of exhaust dampers was considered futile.

In order to test the inlet restriction option, plywood sheets, 0.006 m thick, were sawn into pieces the diameter of the fan inlet. In the center of each piece, a circular opening was cut, the size of which depended on the amount of restriction required. As more ports in the plenum were closed, the restriction had to increase, and the size of the opening had to decrease. With an even distribution in the dryer, the opening was considered to be the correct size when it allowed approximately $1.82 \text{ m}^3/\text{s}$ through each of the open ports. Restricted inlets were used in the six-trailer unit with two to four ports open for the 5.60-kW fan, and two to six ports open for the 7.46-kW fan. The needed restrictions required the construction of eight plywood rings.

Results and Discussion

Performance of Field Testing Equipment

Perforated Plate Calibration

Calibration of both perforated plates was accomplished without problems. The indicator needle on the micromanometer used to measure flow velocity at the outlet of the calibration nozzle showed some wavering, particularly on a windy day, when the errors introduced were on the order of ± 0.5 Pa for a pressure of 25 Pa, a variation of ± 2 percent. The inclined manometer used to measure the pressure drop across the perforated plate gave a steady reading for a given fan speed setting.

Static pressure readings were not taken for each velocity pressure measurement. Since these measurements were taken close to the nozzle outlet, the static pressure was small. The associated errors

with the static pressure had little influence on the velocity pressure. For this reason, corrections to readings, as given by Pope and Harper (1966), were not necessary to account for tip and stem effects.

Since the traverse was taken over a period of time, some of the measured non-uniformities encountered was found to be actually due to unsteady flow. During some tests, the centrifugal supply fan speed drifted upward, and the measured pressure readings would indicate this. In these tests, grid points that were spatially adjacent had similar velocity pressures only if readings were taken within a short period of time. This problem was, however, easily detected.

To account for drifting of the fan speed, a centerline velocity pressure could have been measured for each grid point. Instead, tests which showed obvious drift were redone until steady flow occurred. In these cases, the flow was found to be very uniform. At an average velocity of 9.43 m/s, the velocity non-uniformities ranged from -1.7 percent to 0.7 percent. At an average velocity of 37.74 m/s, the flow deviation was ± 0.46 percent. This last value falls within the ± 0.5 percent given by Mehta and Bradshaw (1979). The flow was considered sufficiently uniform to allow the calibration of the perforated plate to be done using only the centerline velocity.

Two sets of four runs were done, on two separate days. These data were used to make two curves of pressure drop versus flowrate. The measured velocity was converted to flowrate by multiplying by the flow area. The nozzle exit was measured to be 0.886 by 0.883 m, giving an area of 0.782 m². Air temperature and barometric pressure were sufficiently different to allow a comparison between tests of different fluid densities.

Ignoring density differences, a slight scatter of points existed within each set, with a noticeable difference between the two sets. To account for this discrepancy, the pressure drop across the plate was assumed proportional to the air density for a given flowrate,

$$\frac{\Delta P_m}{\Delta P_n} = \frac{\rho_m}{\rho_n} \quad [58]$$

where ΔP_m = measured pressure drop across perforated plate [Pa]

ΔP_n = nominal pressure drop across perforated plate [Pa]

ρ_m = measured air density [kg/m^3]

ρ_n = nominal air density [kg/m^3]

A nominal density was calculated, based on a dry bulb temperature of 20°C, a wet bulb temperature of 13°C, and a barometric pressure of 101.325 kPa. At these conditions, nominal air density was 1.200 kg/m^3 .

The field data was processed by FANPER1 FORTRAN, Appendix B, and the results are shown in Figure 20. When air densities were different, calibration curves were also different. These differences in air densities were accounted for by converting the measured pressure drop to a nominal pressure drop based on the ratio of the measured density to the nominal density. With these adjustments, the data points fell essentially on the same line. These results indicated that flowrate could be determined by measuring the pressure drop across the plate if the air density was known.

These data points were used to fit to several curves. Using a curve of the form of Equation [8] produced ($R^2 = 0.9995$),

$$\Delta P_n = 1.6622 Q_p^{2.054} \quad [59]$$

where Q_p = flowrate of air passing through perforated plate [m^3/s]

It was expected that no flow would occur when there was no pressure drop across the plate. This meant that the calibration curve should pass through the origin. Although this was the case in

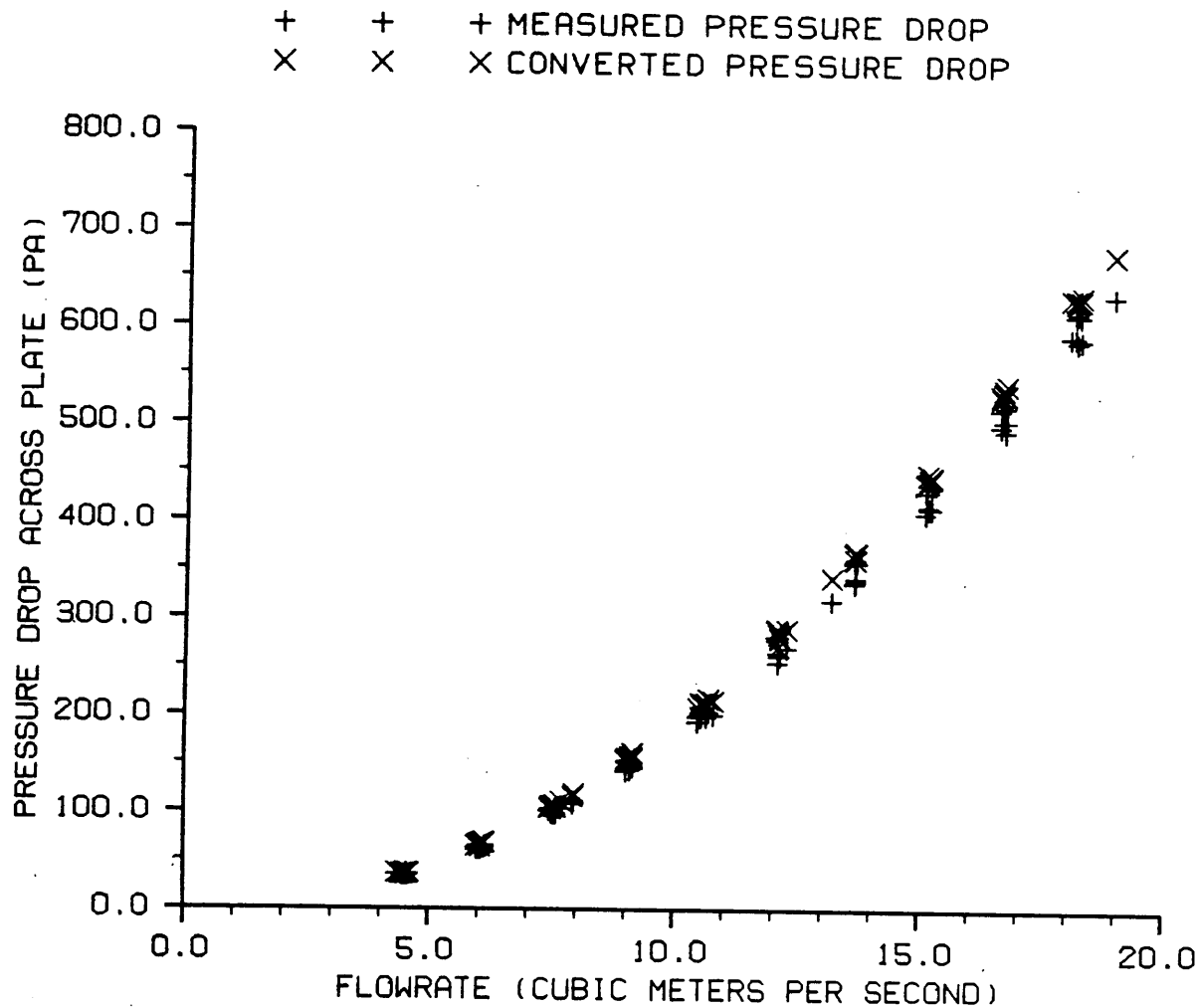


Figure 20. Measured flowrates, and measured and adjusted pressure drops on two separate days.

Equation [59], the exponent of the flowrate was not as expected. For turbulent flow through the plate, the flowrate exponent of 2 should result, corresponding to a line with zero slope in the Moody diagram. A value greater than two should not occur, corresponding to a line with a slight positive slope in the Moody diagram.

For this reason, Equation [59] was replaced with Equation [8], setting n equal to 2. The new calibration curve was ($R^2 = 0.9994$),

$$\Delta P_n = 1.9165 Q_p^2 \quad [60]$$

Although R^2 was reduced slightly, the general equation more closely followed the theory. This equation was valid for flowrates ranging from 4.4 to 18.9 m³/s.

Equation [60] allows evaluation of plate performance in terms of dimensionless parameters, in particular, the pressure coefficient. Without correction factors,

$$C_{pp} = \frac{\Delta P}{\frac{1}{2} \rho V_n^2} \quad [61]$$

where C_{pp} = pressure coefficient for perforated plate

ΔP = pressure across perforated plate, nominal or measured [Pa]

ρ = air density, nominal or measured [kg/m³]

V_n = air velocity exiting nozzle [m/s]

Rewriting Equation [60],

$$\Delta P_m \frac{\rho_n}{\rho_m} = 1.9165 Q_p^2 \quad [62]$$

Rearranging Equation [62], and noting that $Q = VA$,

$$\frac{2 (1.9165 A_n^2)}{\rho_n} = \frac{\Delta P_m}{\frac{1}{2} \rho_m V_n^2} \quad [63]$$

where $A_n =$ nozzle flow area [m^2]

A_n and ρ_n were replaced with their constant values of 1.200 kg/m^3 and 0.782 m^2 , respectively. This result showed that, for Equation [62], C_{pp} had a constant value of 1.9533.

To check this assumption, values of C_{pp} were calculated for each measurement taken during the calibration. A form of Equation [23] was used,

$$C_{pp} = \frac{\Delta P_m}{\frac{1}{2} \rho_m V_n^2} \quad [64]$$

If the pressure coefficient is not constant, it may be related to the Reynolds number or Mach number. The Reynolds number for the perforated plate is defined as,

$$Re_p = \frac{D_p V_n \rho_m}{\mu_m} \quad [65]$$

where $Re_p =$ Reynolds number for the perforated plate

$D_p =$ diameter of holes in perforated plate [m]

$\mu_m =$ measured value of air viscosity [$N \text{ s/m}^2$]

The Reynolds number is based on the measured velocity, which is not measured at the holes of the perforated plate. However, the average velocity through a hole in the perforated plate only differs by a multiplicative factor from the nozzle exit velocity, so that no error is introduced. The total area of the 1628 holes (0.825 m^2) differs only slightly from the total area of the nozzle exit (0.782 m^2).

The Mach number is determined from

$$M_p = \frac{V_n}{\sqrt{\gamma P_m / \rho_m}} \quad [66]$$

where P_m = total measured pressure [Pa]

The pressure coefficient was plotted against the Reynolds number and Mach number, and are shown in Figure 21 and Figure 22, respectively.

The pressure coefficient was not found to be a constant, as was previously assumed. Although Equation [56] had an R^2 of 0.9994, Figure 21 reveals that some effects were not taken into account. The pressure coefficient increased with the Reynolds number up to $Re \simeq 28,000$, and then decreased. The same trend occurred on both days, so it is unlikely that random error can account for the non-constant value of C_{pp} .

Several methods of correcting for the curvature in Figure 21 were considered, such as combining the Reynolds number and Mach number. Multiplying the two values together exaggerated the curvature, whereas dividing one into the other eliminated the velocity component, which is necessary for the determination of the flowrate. A cubic equation was fit to the data to give the pressure coefficient as a function of the Reynolds number. (Since the Mach number showed a similar trend, this one equation was considered sufficient to account for the variation in the pressure coefficient.) The equation was found to be ($R^2 = 0.7002$),

$$C_{pp} = 1.8308 - 5.5625 \times 10^{-6} Re + 8.5454 \times 10^{-10} Re^2 - 1.67 \times 10^{-14} Re^3 \quad [67]$$

It is worthwhile to compare the results obtained using Equations [59], [60] and [67] with the actual measured value. With an R^2 of only 0.7002, it appeared that nothing had been gained. To properly

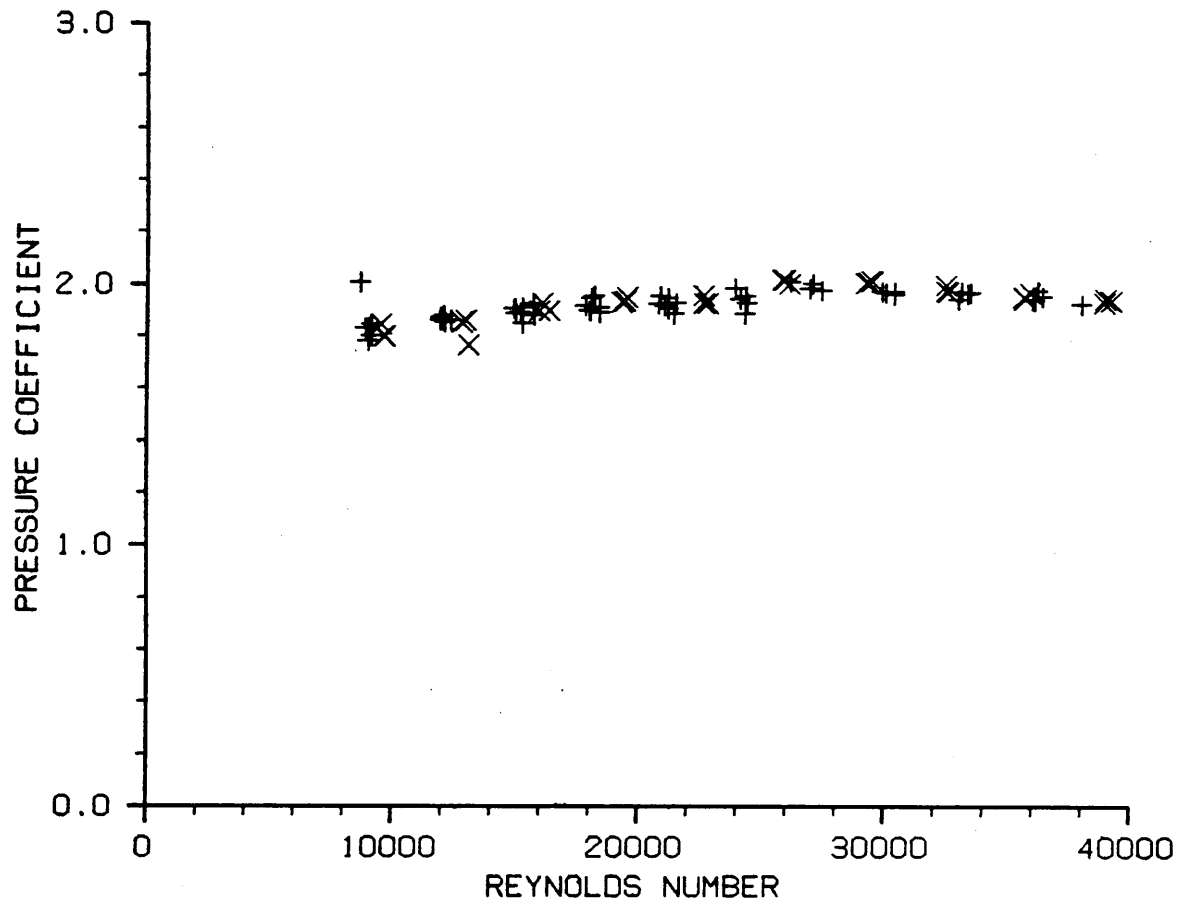


Figure 21. Pressure coefficient vs. Reynolds number for perforated plate.

compare the three equations, Equation [67] must be rewritten to a form similar to Equations [59] and [60],

$$\frac{\Delta P_m}{\rho_m} = c_0 \left(\frac{1}{2} V_n^2 \right) + c_1 \left(\frac{1}{2} V_n^2 \right) Re_p + c_2 \left(\frac{1}{2} V_n^2 \right) Re_p^2 + c_3 \left(\frac{1}{2} V_n^2 \right) Re_p^3 \quad [68]$$

where $c_0, c_1, c_2, c_3 = \text{constants}$

No ρ_n term is included in the equation. However, it is a constant and as such will not influence the goodness of fit. This equation resulted in a slight improvement over Equation [59] or [60], with an R^2 of 0.9997. Using additional terms with Equation [60] would have increased its R^2 value as well. There was no great difference seen among the three equations in predicting the pressure drop from the flowrate.

It was noted, however, that a greater scatter of the data points occurred when plotted as the pressure coefficient and Reynolds number than simply as the pressure drop and flowrate. Some points which appear to fall on a curve in Figure 20 no longer do so when plotted as in Figure 21. Hence, it would appear that any errors that are small and difficult to detect using either Equation [59] or [60], are greatly magnified when plotted using the pressure coefficient and the Reynolds number.

Equations [59] and [60] produced negative residuals near the endpoints and positive residuals near the mean value of ΔP . These results may explain the curvature produced when the pressure coefficient was plotted against the Reynolds number, as in Figure 21. Although Equation [67] was found to be the most accurate, one must consider whether the nozzle had any effects on the pressure drop - flowrate relationship of the perforated plate. In other words, does the calibration change when the nozzle is removed and the connecting canvas reinstalled? Unfortunately, it was not possible to verify if any changes occurred.

The pressure coefficient did not behave exactly as expected. The variation in the pressure coefficient may have been caused by some slight flow separation in the exit section of the nozzle, by a changing boundary layer thickness, or a combination of the two. Although these effects could not be substantiated, they may account for the non-constant value of the pressure coefficient, as well as a flowrate exponent greater than 2 in Equation [59].

It is also interesting to note the constant value of the pressure coefficient using Equation [63]. The value was 1.9533, which is not equal to the average of the individually calculated values of the pressure coefficient, 1.9223. The constant value was closer to the maximum of the calculated values. Referring to Figure 21, it can be deduced that, when the slope is positive, the exponent of the flowrate, or velocity, is greater than 2. When the pressure coefficient reaches a maximum, the slope is zero, and the exponent is equal to 2. When the slope is negative, it is less than 2. In theory, the slope should never be positive, as is demonstrated by the Moody diagram, where slopes are always less than or equal to zero.

At first glance, Equation [67] was not very suitable for field testing. Field tests involved measuring the pressure drop across the perforated plate, which was converted to a flowrate. Both the pressure coefficient and the Reynolds number are functions of the air velocity, which is unknown from field tests. This method would require an iterative solution. However, only a few iterations were required when the velocity was first estimated using Equation [60]. The Reynolds number was estimated using this velocity, and the pressure coefficient was calculated using Equation [67]. This value, along with the measured pressure drop, was used in Equation [64] to determine the velocity for the next iteration.

During field tests, the pressure drop across the plate varied slightly during a run. Once the supply fan and dryer fan were balanced, adjustments still had to be made to the supply fan to maintain balance. Although these changes were small, the pressure reading at the plate changed slightly.

For this reason, the reading was taken both at the beginning and at the end of the run, and averaged to give one value.

Resistance Plate Calibration

Initially, the port resistance plates were calibrated up to a maximum flow of 2.8 m³/s. This maximum was found to be insufficient for the testing that was done in Lewiston and Holland. After the installation of a larger fan motor on the test stand in the laboratory, the resistance plates were recalibrated for a maximum flow of 4.1 m³/s which was the maximum the test setup could provide. For the testing of dryers with 11.46-kW fans and only two ports open, the airflow was higher than 4.1 m³/s, so some minor extrapolation of data was necessary.

Figure 23 shows the calibration curve for Resistance Plate No. 7. Similar results were obtained for the other resistance plates. Some differences were noted between calibration runs, and were more pronounced than those encountered in the calibration of the perforated plate. For comparison, the pressure drop-flowrate curve for peanuts as given by Steele (1974), Equation [10], is also plotted in Figure 23 for a peanut trailer depth of 1.3 m and a floor area of 8.4 m².

As with the perforated plate, several methods of obtaining a calibration equation were possible. In order to check how closely the plates followed the resistance of a trailer filled with peanuts, it was useful to present the calibration data for the resistance plates in the form of Equation [10],

$$\Delta P_{nr} = a Q^n \quad [69]$$

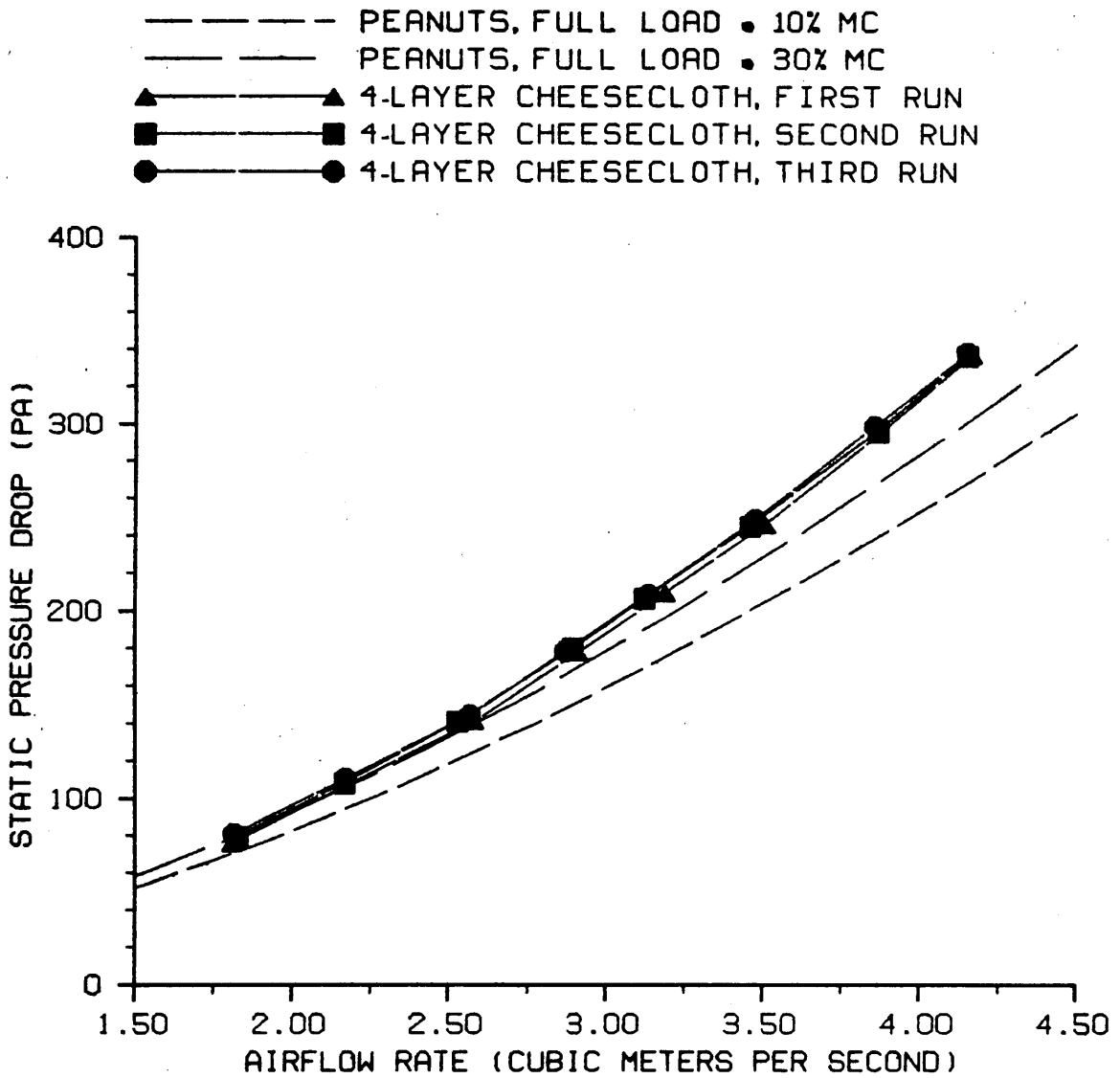


Figure 23. Pressure drop-flowrate for Resistance Plate No. 7, with resistance of a trailer filled with peanuts.

where $a, n = \text{constants}$

$\Delta P_{nr} = \text{nominal pressure drop across resistance plate [Pa]}$

$Q_r = \text{measured flowrate through resistance plate [m}^3/\text{s]}$

The results for the 8 resistance plates calibrated are shown in Table 3 and were obtained using PERF FORTRAN, Appendix C. Comparing these values with Equation [57] reveals some differences between the actual resistance of a trailer of peanuts, and that of the resistance plates used to simulate them. The difference was small at low flowrates, but, since the values of n for the resistance plates were higher than the 1.618 in Steele's equation for peanuts, the difference was greater at the higher flowrates.

Further analysis of the resistance plates was done using the pressure coefficient and Reynolds number. The greatest value of the Mach number encountered was 0.031, and, based on Figure 6, its effects on the pressure coefficient were considered negligible. Changes in the value of the pressure coefficient were taken into account using only the Reynolds number.

Since the values of n in Table 3 are less than 2, the pressure coefficient was expected to decrease as the Reynolds number increased. This result was confirmed by plotting the pressure coefficient against the Reynolds number for Resistance Plate No. 7 (Figure 24). Unlike the perforated plate, the pressure coefficient started at a maximum and decreased as the Reynolds number increased.

The three calibration runs did not fall on the same line. Successive runs produced higher values of the pressure coefficient. As with the perforated plate, minor differences were magnified when the same data points were plotted using the pressure coefficient. This upward drift was attributed to the collection of dust on the cheesecloth used for the resistance plates.

Table 3. Pressure drop-flowrate equations for the 8 resistance plates.

Resistance Plate	$\Delta P_n = a Q^n$		
	a	n	R^2
1	27.70	1.774	0.9983
2	27.76	1.725	0.9986
3	28.58	1.762	0.9977
4	29.29	1.745	0.9989
5	29.30	1.728	0.9992
6	29.39	1.710	0.9996
7	27.64	1.755	0.9990
8	33.19	1.711	0.9954

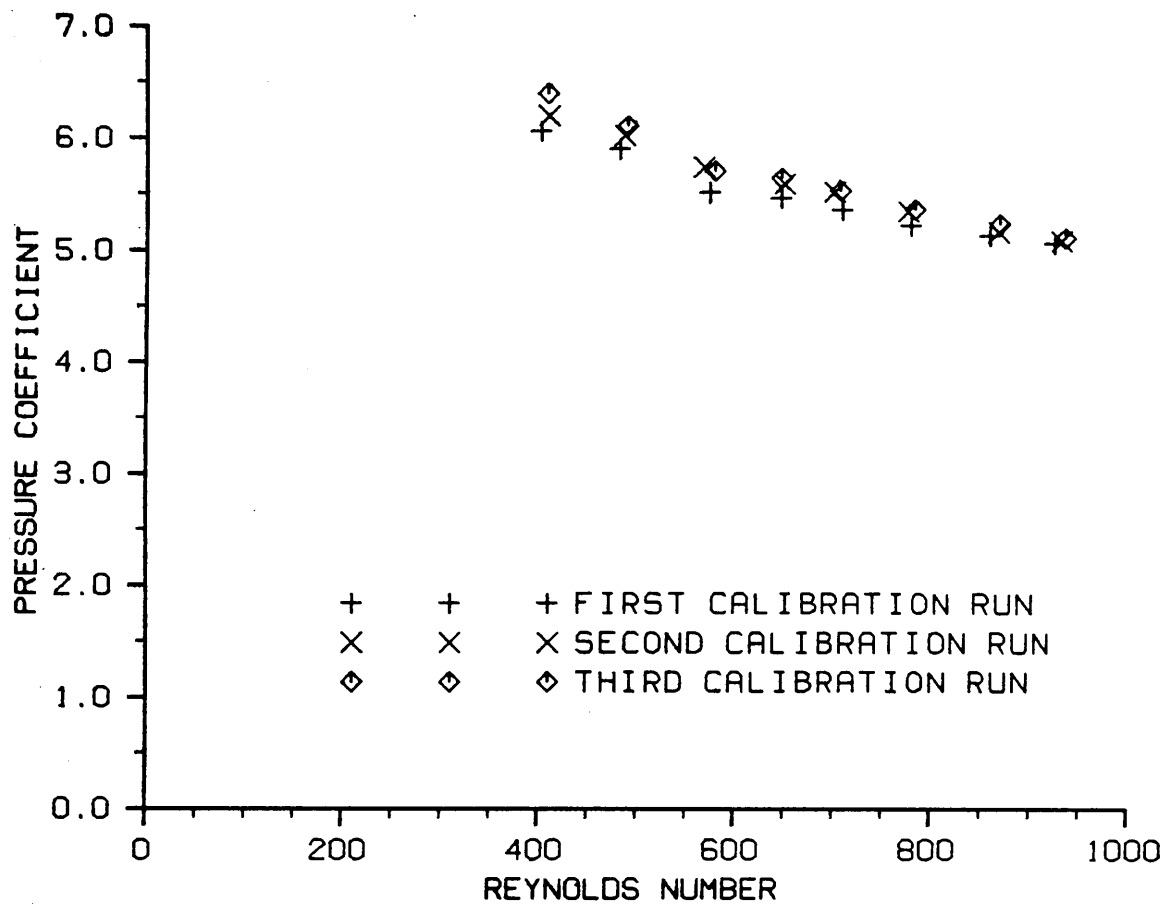


Figure 24. Pressure coefficient and Reynolds number for Resistance Plate No. 7.

This problem proved to be one of the major drawbacks to using cloth to simulate the resistance of peanuts. Unlike the perforated plate, the cloth allows a flowrate exponent to be less than 2, since the small flow areas forces the flow to be laminar or transitional. The dust collection results in a bias in the flowrate measurements. In reality, the resistance increases, decreasing the actual flowrate, but increasing the apparent flowrate, which is determined by referencing the measured pressure drop to the calibration curve. After extended use, the resistance plates had to be recalibrated.

The data from these new calibrations were used to determine the values of a and n as in Table 3, and are produced in Table 4. Resistance Plates 7 and 8 were used after the previous calibration, and were not recalibrated.

The data from these new calibrations were also used to determine the pressure coefficient as a function of the Reynolds number. The data were quite linear, and adding a squared term to the regression analysis did little to improve R^2 . The values obtained from the linear regression for all eight resistance plates are shown in Table 6. The R^2 values varied much more than they did in Table 4. This variance was assumed to be due to the error magnifying effect of the analysis. These linear equations were transformed to produce an equation similar to Equation [68],

$$\frac{\Delta P_{mr}}{\Delta \rho_m} = a_0 \left(\frac{1}{2} V_r^2 \right) + a_1 \left(\frac{1}{2} V_r^2 \right) Re_r \quad [70]$$

where $a_0, a_1 = \text{constants}$

$\Delta P_{mr} = \text{measured pressure drop across resistance plate [Pa]}$

$V_r = \text{measured velocity through resistance plate [m/s]}$

$Re_r = \text{Reynolds number for resistance plate}$

Table 4. Pressure drop-flowrate equations for the 8 resistance plates, recalibration.

Resistance Plate	$\Delta P_n = a Q^n$		
	a	n	R^2
1	33.11	1.702	0.9913
2	31.21	1.682	0.9978
3	32.42	1.719	0.9888
4	30.55	1.733	0.9988
5	30.99	1.729	0.9981
6	29.98	1.720	0.9985
7	27.64	1.755	0.9990
8	33.19	1.711	0.9954

The velocity was calculated by dividing the measured flowrate through the nozzle by the area of the resistance plate. Best-fit values for the constants, as well as the R^2 values are shown in Table 5. These R^2 values were similar to those in Table 4. It was concluded that the exponent of the flowrates, being less than 2, accounted for the negative, but relatively constant, slope in Figure 24. Hence, Equation [68] was considered sufficiently accurate for flow calculations from field collected data.

Error Analysis of Flow Measurement Devices

In order to properly determine original peanut dryer performance and then compare after modifications, an estimate of the error involved in the flowrate determined using the perforated plate and the resistance plates was essential.

Measurement errors result from two sources: precision error, and bias (Abernethy and Thompson, 1980). For most measurements, biases are unknown. In this case, measurement errors were assumed to be precision errors, so only Equation [47] was used. In other instances, only one error for a given measurement is used for analysis (Rabinowicz, 1970; AMCA, 1985). This type of analysis was used for most of the error estimation and was well suited when single error bounds were provided by the manufacturer. Due to dust collection in the resistance plates, error calculations must be adjusted to account for the drift in the calibration. Biases were introduced in a known direction and had to be estimated.

Table 5. Pressure drop as a function of Reynolds number for the 8 resistance plates, recalibration.

Resistance	$\Delta P_{m,r}/\rho_m = a_0(V_r^2) + a_1(V_r^2) Re_r$		
Plate	a_0	a_1	R^2
1	6.832	-1.682	0.9988
2	6.681	-1.955	0.9987
3	6.897	-1.616	0.9944
4	7.118	-1.876	0.9988
5	7.073	-2.045	0.9991
6	7.079	-2.187	0.9991
7	6.771	-1.826	0.9988
8	7.963	-2.333	0.9966

Table 6. Pressure coefficient and Reynolds number for the 8 resistance plates.

Resistance Plate	$C_{pe} = a_0 + a_1 Re_r$		
	a_0	a_1	R^2
1	8.326	-3.034	0.7389
2	7.792	-3.012	0.9083
3	8.185	-2.713	0.6841
4	7.714	-2.622	0.9172
5	7.822	-2.704	0.9049
6	7.524	-2.580	0.8913
7	7.003	-2.127	0.9180
8	8.389	-2.877	0.8131

Total Flow Measurement Error

Error was considered for the three flow prediction methods, Equations [59], [60], and [67]. Error was expected to be largest for Equation [60] and smallest for Equation [67]. In Equation [60], the pressure coefficient was assumed to be constant. Defining the nozzle area to be width times length, LW , the flowrate is determined from,

$$Q_p = L W \sqrt{\frac{2 \Delta P_m}{\rho_m C_{pp}}} \quad [71]$$

According to the manufacturer of the inclined manometer, the pressure drop across the plate was measurable to an accuracy of ± 2 percent. The width and length of the nozzle exit were measured to within 0.002 m. The air density is determined from the wet and dry bulb temperatures, barometric pressure, and saturated vapor pressure. If the temperatures are measured to within 1.1°C, and the barometric pressure within 170 Pa, the error in air density is approximately 0.005 (AMCA, 1985).

The pressure coefficient, C_{pp} , had a standard deviation, $S_{C_{pp}}$, of 0.05790, and mean, \bar{C}_{pp} , of 1.9223. The associated precision error is $t_{95} S_{C_{pp}}$. Hence, $e_{C_{pp}} \approx 0.116$. Error was also estimated using the error measurements associated with ΔP_m , ρ_m , and V_n . Errors in the velocity measurement resulted from velocity pressure measurements, as well as flow non-uniformities in the nozzle exit. This combined error was estimated to be 1 percent. Using Equations [36] and [64], $e_{C_{pp}}$ was estimated to be 0.056. The larger error estimate was used for the analysis.

From Equation [36], the error in estimating Q_p is

$$e_{Q_p} = \frac{Q}{2} \sqrt{(2e_L/L)^2 + (2e_W/W)^2 + (e_{\Delta P_m}/\Delta P_m)^2 + (-e_{\rho_m}/\rho_m)^2 + (-e_{C_{pp}}/C_{pp})^2} \quad [72]$$

With $L = 0.886$, $W = 0.883$, $\rho_m \approx 1.15$, $e_{C_{pp}} = 0.116$, $C_{pp} = 1.9533$, and $e_{\Delta P_m} = 0.02(\Delta P_m)$,

$$\frac{e_{Q_p}}{Q_p} = 0.032$$

The error bound increases if one considers that the standard deviation used for estimating the error in C_{pp} is 1.922, not the 1.9533 actually used. Recalculating the standard deviation to account for this results in errors of 3.5 percent.

Error associated with Equation [59] must be evaluated in a different manner since there is no measurable constant like C_{pp} to define a bound on precision error. Error was estimated for the equation

$$Q_p = k \Delta P_n^m \quad [73]$$

In this equation, $k = 0.782$ and $m = 0.487$. The value of m is determined from,

$$m = \frac{\ln V_n A_n - \ln k}{\ln \Delta P_n} \quad [74]$$

Similarly, k is determined from,

$$k = \frac{V_n A_n}{\Delta P_n^m} \quad [75]$$

Errors were estimated for m and k based on the measurement errors associated with ΔP_n , V_n , and A_n . The estimated measurement error in m , e_m , was 0.0063 and 0.0086 for pressure drops across the perforated plate of 60 and 650 Pa, respectively. These pressure drops correspond to flowrates of 5.73 and 18.27 m³/s. The error in estimating k , e_k , was 0.011.

Error was also estimated by using the standard deviation of both m and k , from Equations [75] and [76]. With m held constant in Equation [75], a k value was determined for each set of A_n , V_n , and ΔP_n . The standard deviation was estimated from,

$$S_k = \left[\frac{\sum (k - V_n A_n / \Delta P_n^m)^2}{n - 1} \right]^{1/2} \quad [76]$$

S_k was determined to be 0.0076, and the error, e_k , was estimated to be 0.015. Similarly, $e_m \approx 0.0042$.

The error in determining Q_p is

$$e_{Q_p} = \sqrt{\left(\frac{\partial Q_p}{\partial k} e_k\right)^2 + \left(\frac{\partial Q_p}{\partial \Delta P_n} e_{\Delta P_n}\right)^2 + \left(\frac{\partial Q_p}{\partial n} e_n\right)^2} \quad [77]$$

Using an error of 2 percent for the pressure drop, and maximum errors of 0.0086 and 0.015 for m and k , respectively,

$$\frac{e_{Q_p}}{Q_p} = 0.022$$

The error in Q_p was also estimated by determining the standard deviation of Q_p when using Equation [73],

$$S_{Q_p} = \left[\frac{\sum (Q_p - k \Delta P_n^m)^2}{n - 1} \right]^{1/2} \quad [78]$$

This method gave an error in Q_p of 0.21, corresponding to errors of 3.6 and 1.1 percent at flowrates of 5.73 and 18.27 m³/s, respectively.

Error was expected to be further reduced using Equation [67]. Assuming a viscosity error of 0.5 percent, measurement error in the Reynolds number was estimated to be 1.2 percent. Pressure drops of 60 and 650 Pa correspond to Reynolds numbers of 12,000 and 40,000. Corresponding measurement errors in C_{pp} , using Equation [67] resulted in $e_{C_{pp}} \simeq 0.0000053$.

Total error in the pressure coefficient was also estimated using the standard deviation, similar to Equation [78]. Error was estimated to be twice the standard deviation, or 0.063, which was much larger than the measurement error. Total error in estimating Q_p from ΔP_m was estimated from Equations [71] and [72]. This analysis resulted in,

$$\frac{e_{Q_p}}{Q_p} = 0.019$$

Thus, errors in total flow measurement using Equation [67] were determined to be less than 2 percent.

Resistance Plate Flow Measurement Error

The resistance plate errors were expected to be much higher than those of the perforated plate, based on the R^2 values. Following the method used for Equation [73], error analysis was done for the worst case, which was assumed to be recalibrated Resistance Plate 1, $R^2 = 0.9913$. Pressure drops across the resistance plate ranged from 80 to 360 Pa, corresponding to flowrates, Q_r , of 1.69 to 4.05 m³/s. Using Equation [73], k and m were found to be 0.132 and 0.582, respectively.

Flowrate was assumed accurate to within 1.2 percent for the calibration, and the pressure drop, measured with a micromanometer, produced negligible error. Associated measurement error in k was 0.0070, and a maximum of 0.019 in m .

Using the standard deviations of m and k resulted in errors of $e_k \simeq 0.0068$ and $e_m \simeq 0.010$. With the larger error values, $e_k \simeq 0.070$ and $e_m \simeq 0.019$,

$$\frac{e_{Q_r}}{Q_r} = 0.020$$

Error was also estimated from the standard deviation of the flowrate, S_{Q_r} , using a form of Equation [78]. The error bounds were as follows,

$$\frac{e_{Q_R}}{Q_r} = 0.082, Q_r = 1.69 \text{ m}^3/\text{s}$$

$$\frac{e_{Q_R}}{Q_r} = 0.034, Q_r = 4.05 \text{ m}^3/\text{s}$$

In the worst case, the flowrate exiting a resistance plate was measured within 8.2 percent. These values do not include bias resulting from dust collection after extensive use. Bias added additional error to the flow determination. Furthermore, this error accounted for only one of the resistance plates. For a six-trailer unit, with all ports in use, and assuming consistent 5 percent error, the total error would be 12.2 percent. This result led to the conclusion that the total flow defined by the perforated plate is much more accurate. Additional problems arose due to pressure drop fluctuations, both for the resistance plates and the perforated plate. Although these may reflect flow fluctuations, and are therefore not true errors, errors were introduced in leakage calculations since it was not possible to make all pressure measurements simultaneously. The range of fluctuation was recorded to indicate possible sources of error, but averages were used to process the data.

Resistance Plate and Perforated Plate Correlation

Since some leaks from the dryer plenum are expected, the total flow computed from the pressure drop across the perforated plate should be higher than the sum of flows through the resistance plates, which was usually the case, but negative leakage did occur, usually when leaks were difficult to detect. (Leakage is defined as the the total flow minus the sum of flows out the ports.) The calculated negative leakage ran as high as 6.5 percent of the total airflow. This value may have resulted from fluctuating pressure drops during a test run which gave some error in calculating the flows from the individual ports as well as the perforated plate.

There are three possible explanations for any discrepancy between the total flow measured with the perforated plate and the total flow calculated by summing the measured flows at all the ports.

1. Error in the total measured with the perforated plate.
2. Errors in the flows measured with the resistance plates.
3. Leakage.

The measurement of total flow with the perforated plate was determined to be the most accurate of all the flow measurements. Since this error is small, discrepancies between total flow measurements were mainly due to leakage and errors associated with the resistance plates.

For tests on the best-maintained plenums, meaning that all practical means were used to seal leaks, the discrepancy between perforated plate total flow and resistance plates total flow ranged from -0.6 to 3.45 percent. These values are based on results obtained at Blacksburg for the four-trailer unit since the resistance plates were calibrated just prior to testing, and hence would be the most reliable

means of estimating discrepancy between the perforated plate and the resistance plates. However, since these percentages fell within the error associated with the resistance plates, an accurate assessment of dryer leakage was impossible. Even in the worst-maintained dryer, measured leakage was 7 percent, which is still within the error bound.

Considerable effort would have to be expended to reduce the resistance plate error to the point where it can be neglected. A very accurate manometer which will record and average the pressure drop across a resistance plate for some time interval, say five minutes, would be needed for both the calibration curve and collection of the best data. The resistance plate itself would need to be constructed from a more durable material than cheesecloth, and then would have to be carefully maintained and frequently recalibrated. It is questionable if the return gained, in an improvement in the leakage measurement, which is only 7 percent of the total flow for even the worst-maintained plenum, is worth the additional effort. If all resistance plates in a six-trailer unit were accurate to within 1 percent, the combined error would be 2.4 percent, which is a large percentage of any calculated leakage.

Supply Fan Effects on Dryer Fan

Another possible source of error can exist if the supply fan provides a positive total pressure to the dryer fan. Since the connecting canvas was not always kept at a slight negative pressure as it should be, the dryer fan may have a more favorable inlet condition than normal. To check the consequence of this error, the dryer was tested both with and without the fan test unit connected. With all ports open, the total flow was determined by summing all the flows from the individual ports. This summation was done for each of the six dryer configurations tested. After connecting the fan test unit, the total flow increased 1.1 to 3.8 percent, with an average increase of 2.8 percent, which

is within the error bound for the resistance plate measurements. Consequently, no definite statement can be made concerning the effect of the supply fan. It appears that its effect is negligible, which is the hoped for result.

Errors were increased on windy days. Gusts would cause the connecting canvas to flutter considerably, resulting in fluctuating pressure drops across the perforated plate. This problem was partially solved by increasing the pressure in the canvas, to reduce the fluttering. Although readings were steadier, dryer fan overfeeding was increased.

Dryer Performance

Data collected in the field had to be processed in order to evaluate performance. Conversions of pressure drops to flowrates, accounting for barometric pressure and temperature was done by FIELD FORTRAN, Appendix D.

Effects of Repairs

The effects of repairing the two dryers tested in Lewiston were determined by taping over all holes found in the plenum or the plenum canvasses. For the eight-trailer unit, these repairs caused an increase in total flowrate of only 2.2 percent. (Total flow was obtained by summing the resistance plate flows.) Total flow into the dryer fan, as measured at the perforated plate, remained constant. As the effect of taping could only be compared on one test, this value is not conclusive. The six-trailer unit was tested more extensively, and for the five combinations compared, the total flow in-

creased from 2.9 up to 5.1 percent. A general inspection of the dryer before testing indicated a unit in relatively poor repair. The losses appeared to be totally independent of the number of ports open. The greatest loss, 5.1 percent, represents a flow of $0.76 \text{ m}^3/\text{s}$, or approximately enough for a trailer 40% full, so the resultant energy losses were significant. Total flow into the fan decreased by 0.3 to 3.6 percent. Repairing increased the resistance of the system, causing the flowrate to decrease.

By contrast, the six-trailer unit tested in Holland appeared in remarkably good condition. Taping the few holes that were detected increased the total flow from -0.7 to 1.2 percent. These percentages were obtained from summing the flows from the individual ports before and after taping, and comparing tests with the same ports open and closed. Differences in measurements before and after repair were comparable to differences measured for repetitions of the same test, which led to the conclusion that the repairs did not improve performance. Total flow increased from -0.9 to 0.8 percent, which is within the error bound of the perforated plate.

The planned method for determining the improvement from repairs was to compare the leakage before and after, leakage being defined as the perforated plate flow minus the sum of the resistance plate flows. Because this method for defining leakage includes the perforated plate error, resistance plate error, and the true leakage, the values obtained often varied by up to $0.2 \text{ m}^3/\text{s}$. This handicapped assessment of the improvement derived from repairs, since the leakage values were very small compared to the total flow.

The four-trailer unit tested in Blacksburg was repaired thoroughly. A general inspection of the dryer would indicate that repairs should make a noticeable increase in air delivered. The fan housing on the 0.905 m Long fan had numerous holes. The plenum had several places where the joints, particularly at the ports, had come apart. Some of the port canvasses were torn and cracked and these were replaced. With no weatherstripping added to the frames, the total flow increased

5.35 percent. With the weatherstripping, flowrate increased 6.80 to 7.04 percent compared to the dryer before repairs, an increase of about 0.6 m³/s. These leakages were determined by summing resistance plate flow before and after repair. By plugging some of the leaks, the resistance was increased, the fan built a higher pressure, and the resulting flow through the resistance plates was increased.

Since the six trailer unit tested in Blacksburg was made by adding extra sections to the four trailer unit, the increase in airflow after repairs applied only to the added sections and varied from 2.6 to 4.4 percent.

Measured Ratings versus Manufacturers' Ratings

One of the means of evaluating dryer performance is to determine if the fans deliver air according to the manufacturers' ratings. Losses in the peanut dryer resulted from flow disturbances caused by the motor, propane burner, abrupt expansion into the plenum, as well as entrance losses into the supply ports. These losses could not be directly measured. As the pressure drop across the fan was not known, several methods of estimating it were explored. Livesey and Hugh (1966) described several methods of determining mean pressure values. They computed an average pressure using 5 methods: mass weighted, area weighted, availability, mixed, and mass derived. The availability method, using mass flowrates and the logarithms of the pressures, was preferred. The other methods were compared to it. At low Mach numbers, the mass weighted method agreed very well with the availability method. The mass weighted pressure is given by,

$$\bar{P}_{mw} = \frac{1}{\dot{m}} \left[\sum P \, d\dot{m} + P_0 \, d\dot{m} \right] \quad [79]$$

where \bar{P}_{mw} = mass weighted pressure

P = measured pressure

P_0 = reference pressure

\dot{m} = mass flowrate

In the case of peanut dryers, the pressures measured were generally low, less than 250 Pa. Since air density differences within this range were negligible, the volumetric flowrate is comparable to the mass flowrate. Hence, a weighted pressure drop based on the volumetric flowrate should give good results. The weighted pressure is given by,

$$P_w = \sum_{i=1}^n \Delta P_i \frac{Q_i}{Q_t} \quad [80]$$

where P_w = weighted pressure drop [Pa]

ΔP_i = pressure drop measured at the i th port [Pa]

Q_i = flow at the i th port [m^3/s]

Q_t = total flow delivered by fan [m^3/s]

$$Q_t = \sum_{i=1}^n Q_i$$

n = number of open ports

Since the resistance plate pressure drops were taken considerably downstream of the fan outlet, these pressure drops were expected to be lower than the actual pressure drop across the fan. The total pressure "seen" by the fan is a sum of the pressure drop in the fan housing and plenum, plus the pressure drop at the resistance plates. A lower pressure referenced to the manufacturer's curve

will give a higher rated flow. For this reason, measured flow should be less than rated flow. The measured airflow and its corresponding weighted pressure drop were plotted alongside the rating curve as supplied by the manufacturer to give an indication of the losses encountered in the dryer. Three additional curves are included showing 90, 80 and 70 percent of rated delivery at the rated pressure, respectively. These results are depicted in Figure 25 through Figure 33. Both the eight and six trailer units tested in Lewiston were equipped with the same fan model, as shown in Figure 25 and Figure 26, respectively. Both of these dryers delivered more than 90 percent of their rated flows. The eight-trailer unit was found to perform better than the six-trailer unit. Several of the operating points actually exceeded the rating, which was thought to be caused either by the fan test unit oversupplying the dryer fan or experimental error. In addition, the speed of a three-phase motor increases as its load decreases. If the fan is underloaded, its speed may be above the rated speed, hence the airflow would be above its rating. However, fan speed was not measured. Since the perforated plate method for measurement of total flow is accurate to within 2 percent, errors in the rating curve as supplied by the manufacturer were suspected as the major cause of the operating points exceeding the rating. Because all measured values are included, both before and after repairs, measured flowrates varied at the same measured pressure drops.

Since both dryers tested at Lewiston, the six-trailer and the eight-trailer unit, had the same fan, it is worthwhile to compare Figure 25 to Figure 26. For one test (Figure 26), the fan developed 175 Pa and delivered 16.5 m³/s to six trailers (resistance plates), averaging 2.75 m³/s per trailer. The same fan developed 125 Pa and delivered 17.5 m³/s to eight trailers, averaging 2.19 m³/s per trailer. Measured average airflow was equivalent to 0.255 m³/s per m³ of peanuts in the six-trailer unit and 0.205 m³/s in the eight-trailer unit. Desired minimum airflow is 0.167 m³/s per m³ of peanuts, so adequate average airflow is available, even in the eight-trailer unit. Dryer capacity was increased 33 percent by adding two additional ports to the six-trailer unit, and total airflow was increased by only 7 percent.

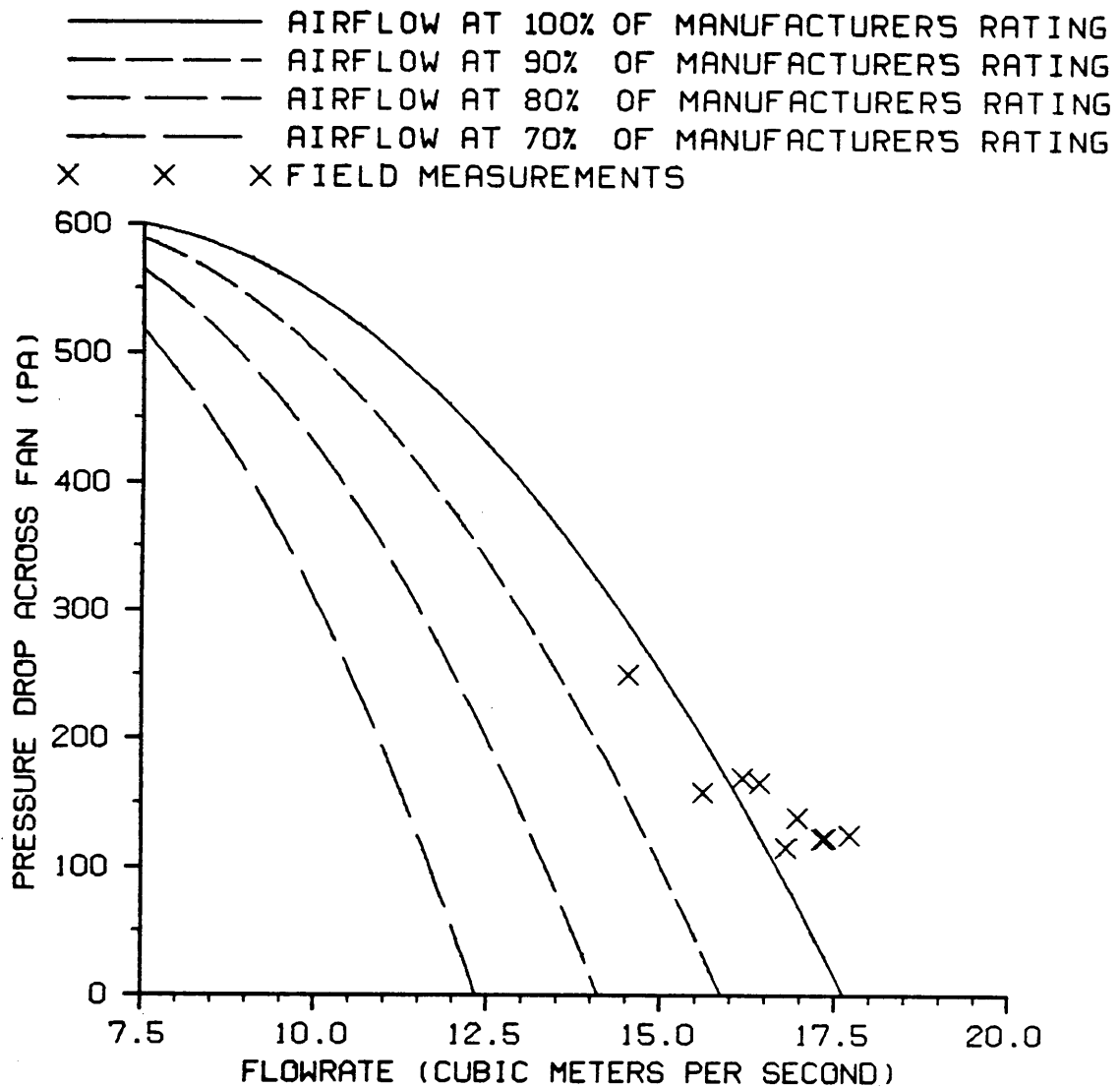


Figure 25. Pressure drop vs. flowrate for an eight-trailer unit equipped with an 11.2-kW Aerovent fan (Lewiston, NC).

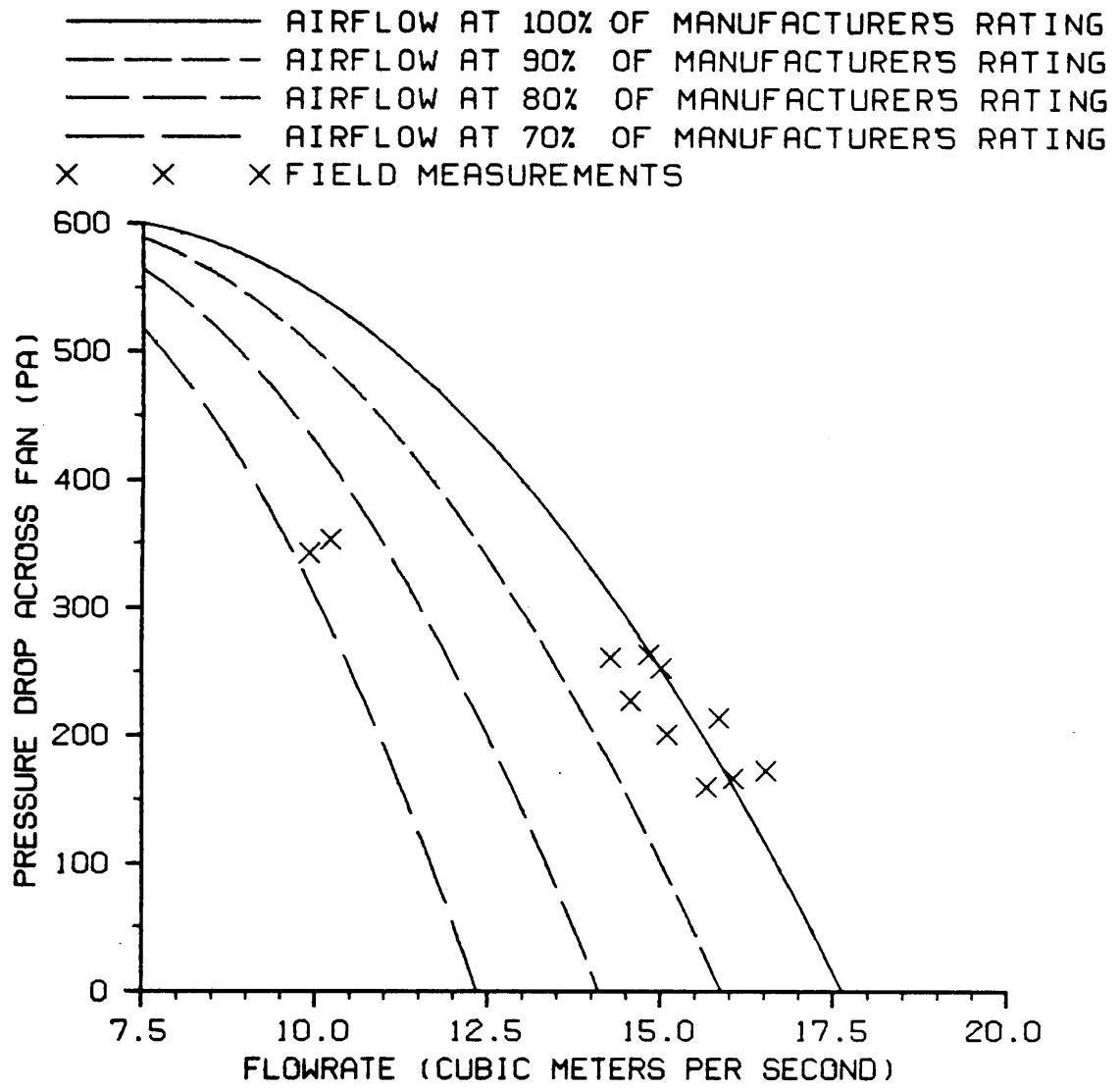


Figure 26. Pressure drop vs. flowrate for a six-trailer unit equipped with an 11.2-kW Aerovent fan (Lewiston, NC).

The six-trailer unit tested in Holland did not perform as well as those in Lewiston, as shown in Figure 27. A restricted inlet was at least partially responsible for the loss of performance. The shed housing the dryer was open on the sides for the trailers, but had a wall on the end, close to the dryer fan inlet. The air was drawn by the fan through a rectangular opening in the wall. This opening was not large enough to allow free entry of the air into the inlet. The problem was aggravated since the wall prevented the end plate of the fan test unit from being properly positioned over the inlet, causing the canvas connecting the end plate to the inlet to be sucked onto a portion of the fan screen.

With all six ports open, the flow averaged $0.187 \text{ m}^3/\text{s}$ per m^3 of peanut trailer volume, or 12 percent above the recommended flow. When one port was closed, the average flow to the five open ports was $0.208 \text{ m}^3/\text{s}$ per m^3 , and with two closed it increased to $0.256 \text{ m}^3/\text{s}$ per m^3 .

As the number of closed ports increased, the pressure drop the fan was working against went up, and the fan delivered a still smaller percentage of its rating. Closing ports did not proportionally change the total flowrate, as more air was forced through those ports left open. The resulting higher velocities added to turbulence losses in the plenum.

When installed on a six-trailer unit, the 7.46-kW Long fan delivered up to 85 percent of its rating (Figure 28). The 5.60-kW model did not perform as well, and delivered a maximum of 80 percent of its rating (Figure 29). As the plenum was identical for both fans, additional losses were attributed to differences in the fan housings. The smaller fan had a large disk in the center of the gas burner, which was not included in the larger fan.

The 7.46-kW Long fan delivered an average of $0.200 \text{ m}^3/\text{s}$ per m^3 of peanut trailer volume in a six-trailer unit compared to $0.151 \text{ m}^3/\text{s}$ per m^3 for the 5.60-kW Long fan. (The six-trailer unit at Lewiston averaged $0.255 \text{ m}^3/\text{s}$ per m^3 , and the six-trailer unit at Holland averaged $0.187 \text{ m}^3/\text{s}$ per

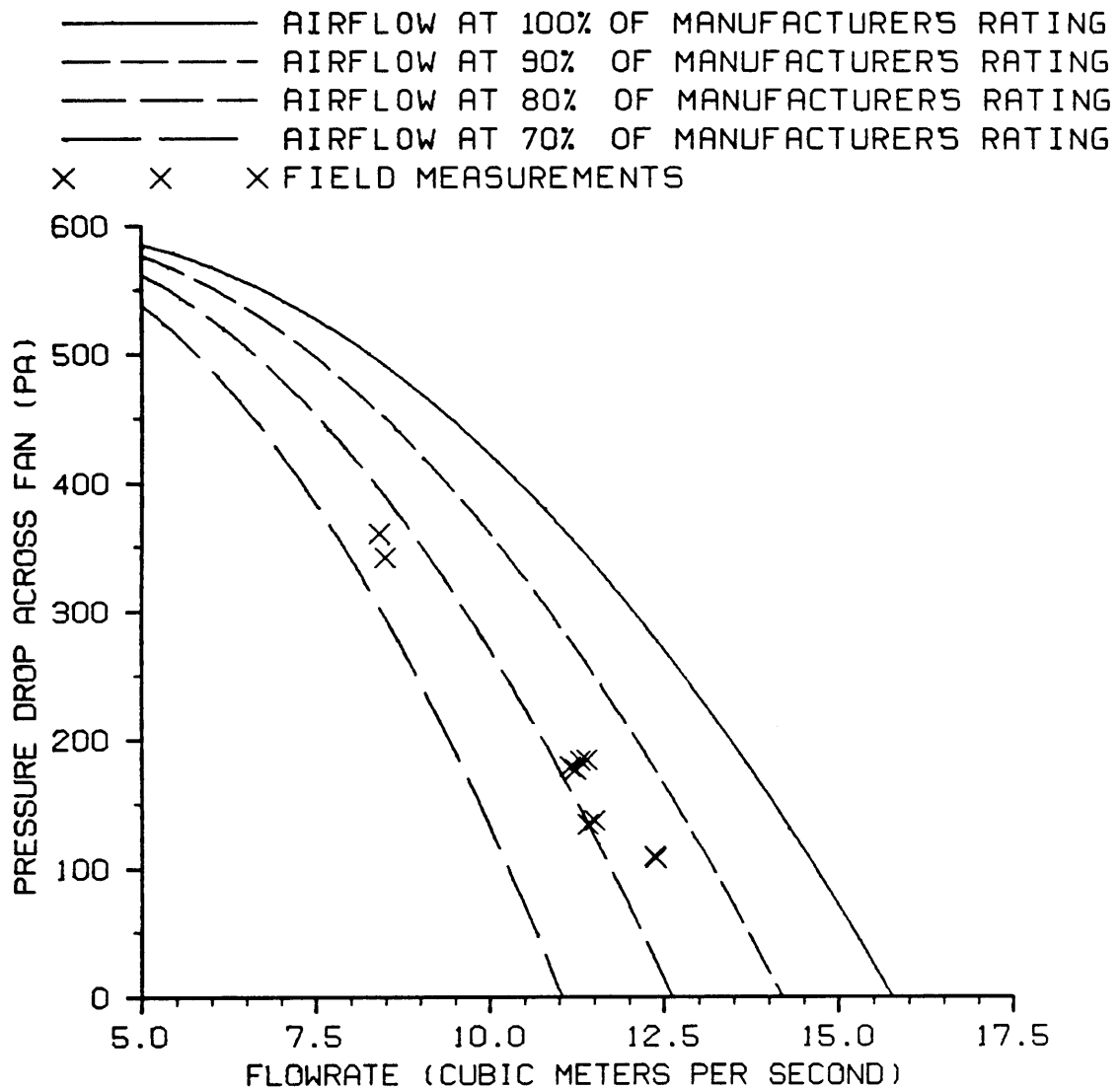


Figure 27. Pressure drop vs. flowrate for a six-trailer unit equipped with a 7.46-kW Aerovent fan (Holland, VA).

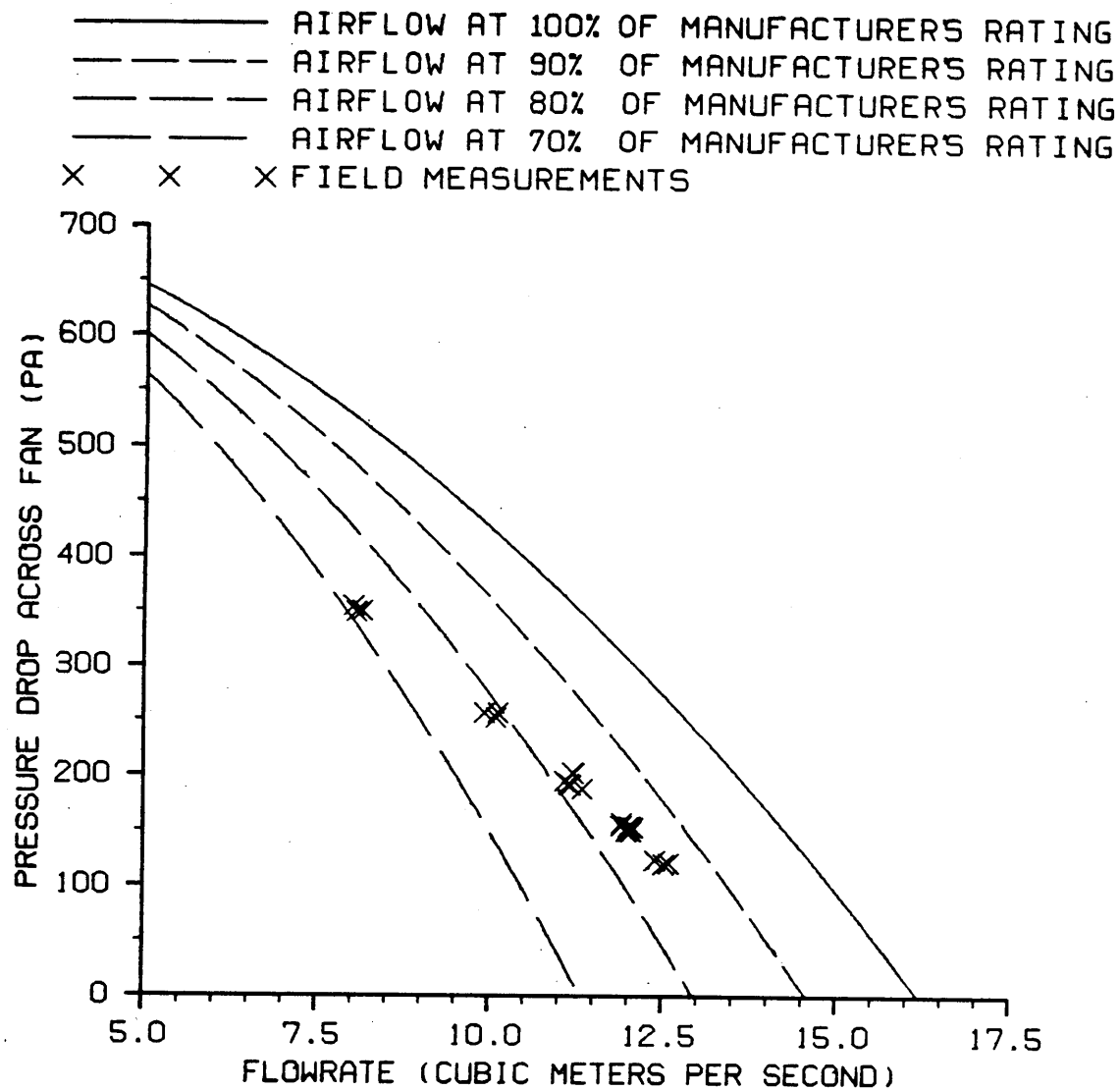


Figure 28. Pressure drop vs. flowrate for a six-trailer unit equipped with a 7.46-kW Long fan (Blacksburg, VA).

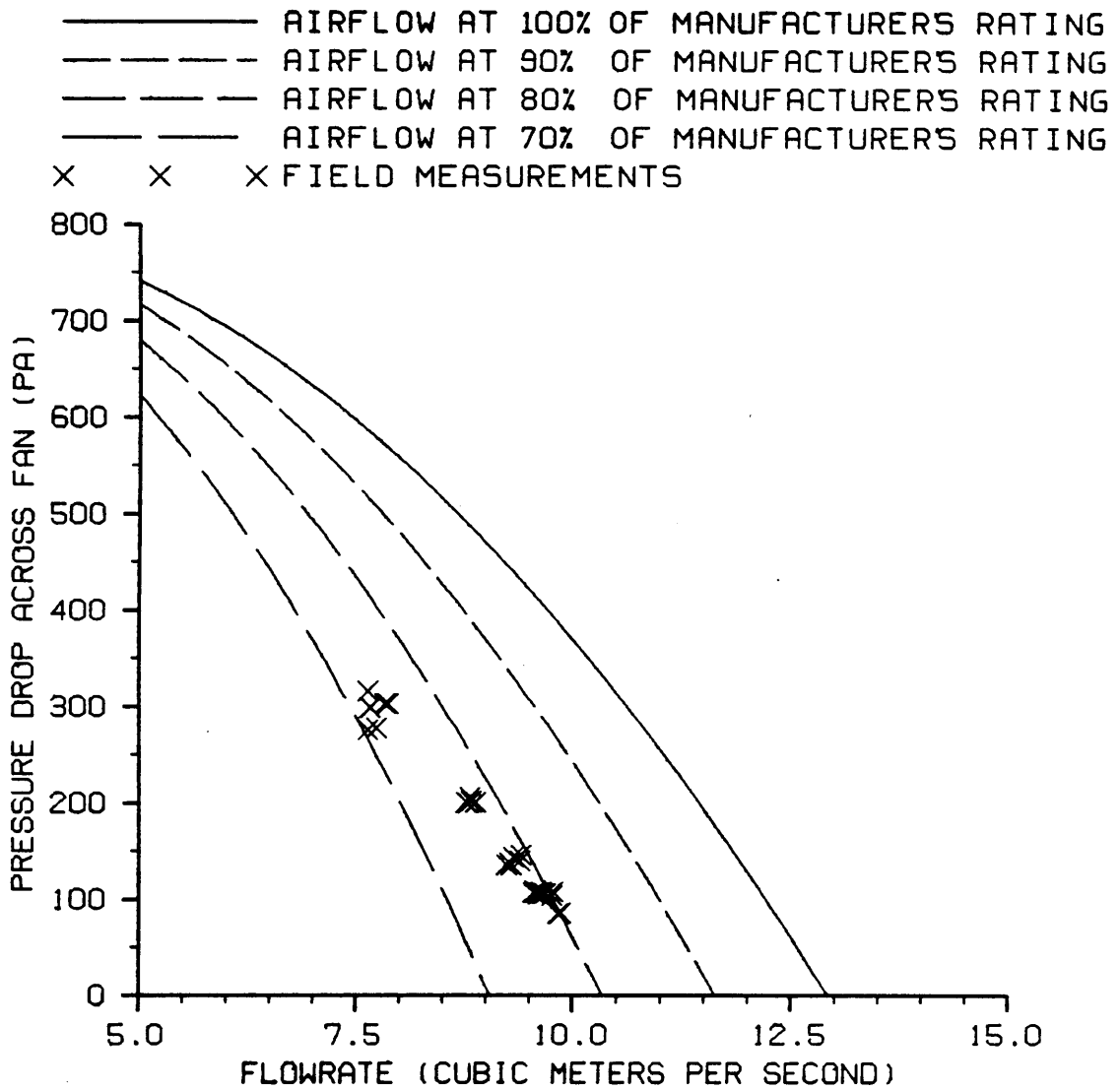


Figure 29. Pressure drop vs. flowrate for a six-trailer unit equipped with a 5.60-kW Long fan (Blacksburg, VA).

m³. With one and two ports closed, the 7.46-kW Long fan averaged 0.228 and 0.277 m³/s per m³, respectively. The 5.60-kW Long fan averaged 0.177 and 0.213 m³/s per m³ with one and two ports closed. When installed on a four-trailer unit equipped with a baffle, the 5.60-kW fan delivered 0.208 m³/s per m³ with all ports open. When the 7.46-kW Long fan was installed on an eight-trailer unit equipped with a baffle, it averaged 0.156 m³/s per m³. These results are summarized in Table 7.

The effect of the baffle in the Long dryer is revealed by comparing Figure 28 to Figure 30 for the 7.46-kW fan, and Figure 29 to Figure 31 for the 5.60-kW fan. The addition of the baffle in the dryer with the smaller fan resulted in a total flow decrease from 0 to 5 percent for the range of combinations tested. Adding the baffle to the dryer with the larger fan had only negligible effects on total output. These results are of prime importance as they show that air can be evenly distributed to the supply ports with a total flow loss of less than 5 percent. Furthermore, this can be achieved readily, since the baffle requires a minimum amount of investment, both in time and money. These losses and costs are well worth the benefit gained by having uniform air distribution to each of the supply ports.

In all cases, the difference between the measured and rated performance was greater at higher pressure drops. Thus, closing port gates reduced dryer efficiency. For example, the data in Figure 28 shows that for a weighted pressure of 350 Pa, the total airflow was 70 percent of rated. When the pressure was reduced to 125 Pa, the total flow was 85 percent of rated.

Fans delivered a smaller proportion of their rated flow when installed on smaller dryers. This is demonstrated by comparing a six-trailer unit with an eight-trailer unit, each equipped with the same 11.2-kW fan (Figure 25 and Figure 26). The 7.46-kW Long fan delivered a greater percentage of its rated flow to the eight-trailer unit than to the six-trailer unit (Figure 30 and Figure 32). Similarly, the 5.60-kW Long fan delivered a greater percentage of its rated flow to the six-trailer unit than to the four-trailer unit (Figure 31 and Figure 33).

Table 7. Average airflow for configurations tested.

Fan Size and Type	Dryer Plenum	Average Airflow (m ³ /s per m ³)	Percentage Increase Over Recommended ¹
11.2-kW Aerovent	Eight-Trailer	0.205	23
11.2-kW Aerovent	Six-Trailer	0.255	53
7.46-kW Aerovent	Six-Trailer	0.187	12
5.60-kW Long	Six-Trailer	0.151	-10
5.60-kW Long	Four-Trailer	0.208	25
7.46-kW Long	Eight-Trailer	0.156	6.4
7.46-kW Long	Six-Trailer	0.200	20

¹ Recommended airflow 0.167 m³/s per m³ of peanuts at a 1.3 m depth.

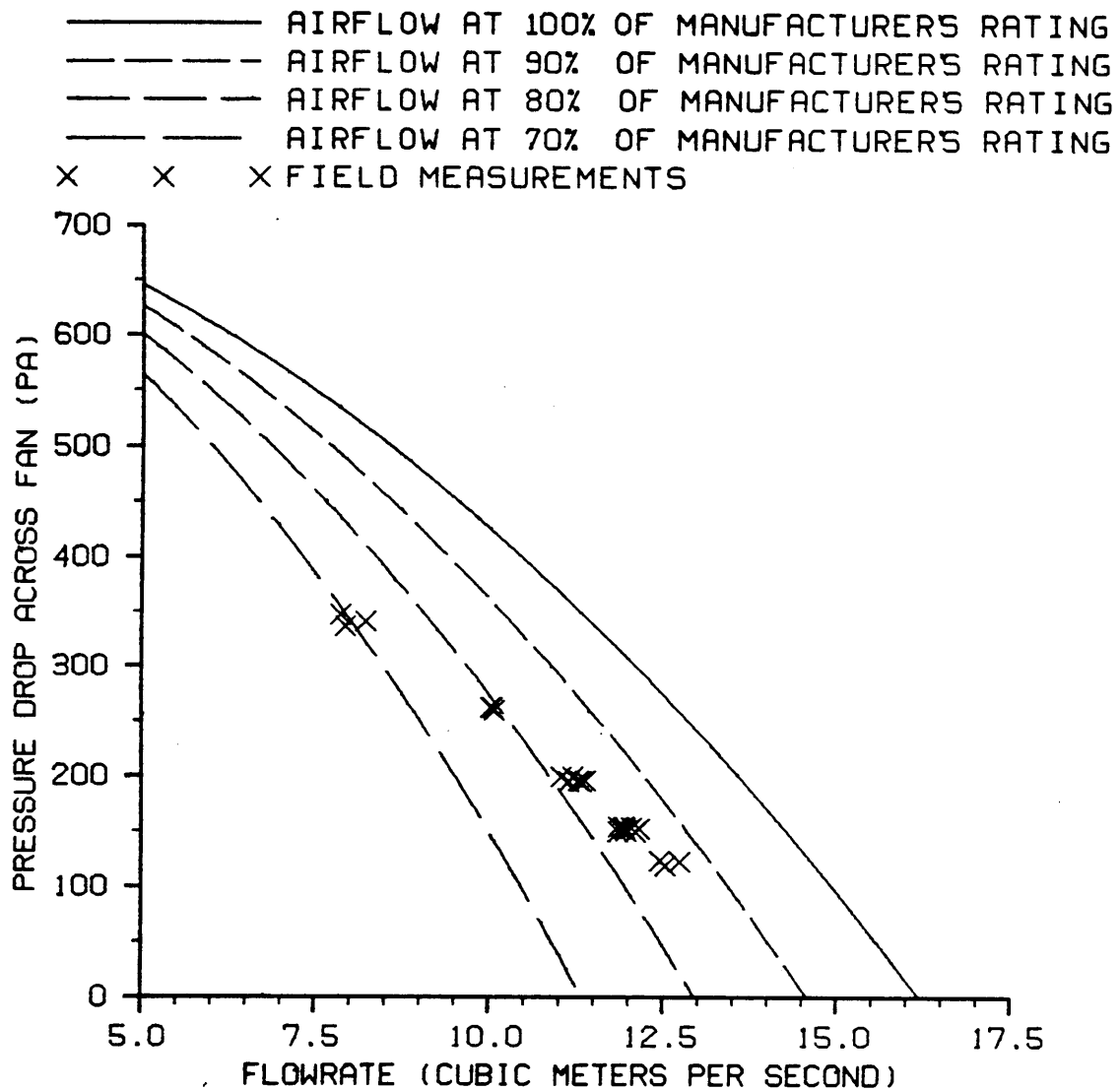


Figure 30. Pressure drop vs. flowrate for a six-trailer unit equipped with a 7.46-kW Long fan, with baffle (Blacksburg, VA).

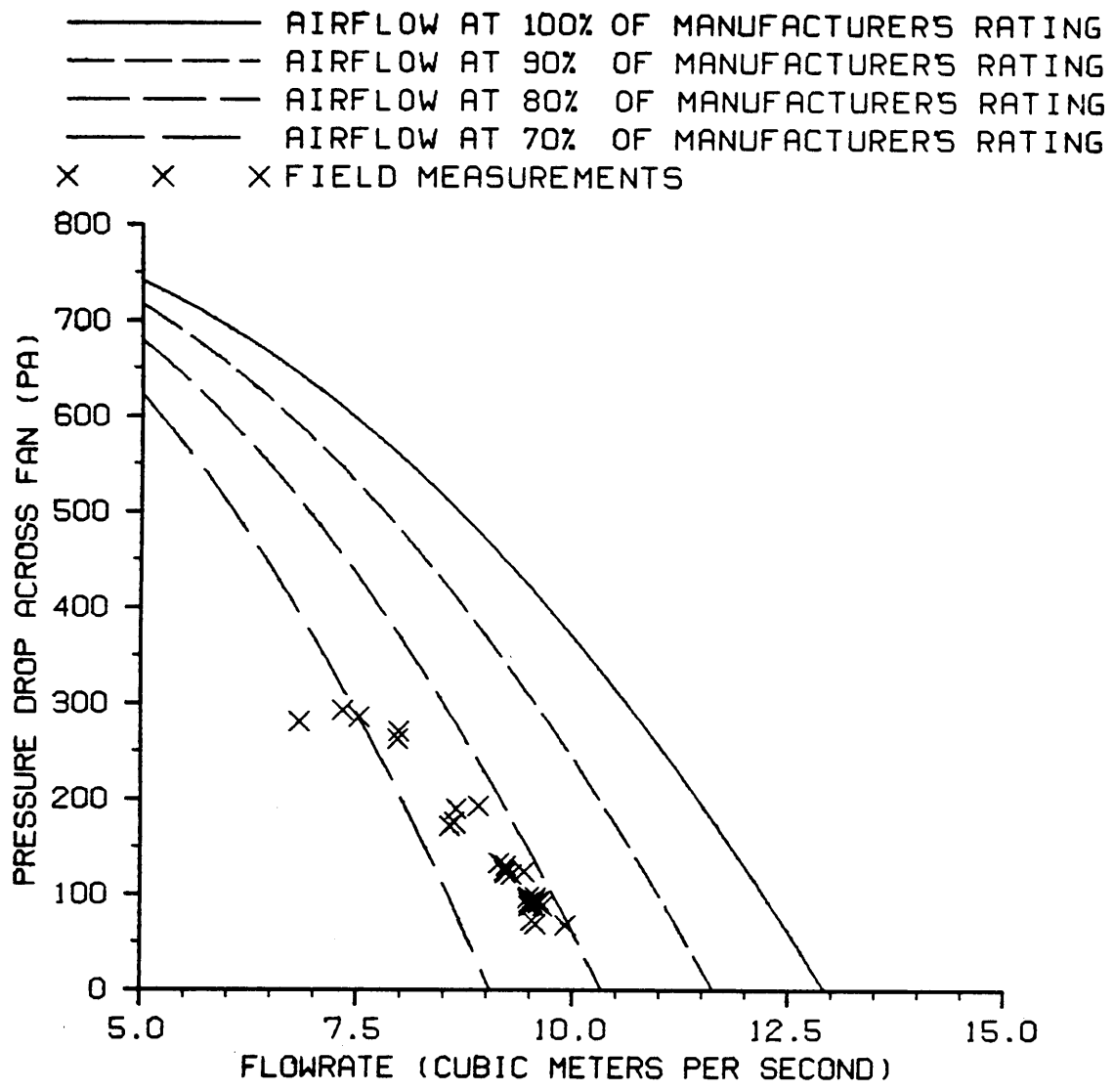


Figure 31. Pressure drop vs. flowrate for a six-trailer unit equipped with a 5.60-kW Long fan, with baffle (Blacksburg, VA).

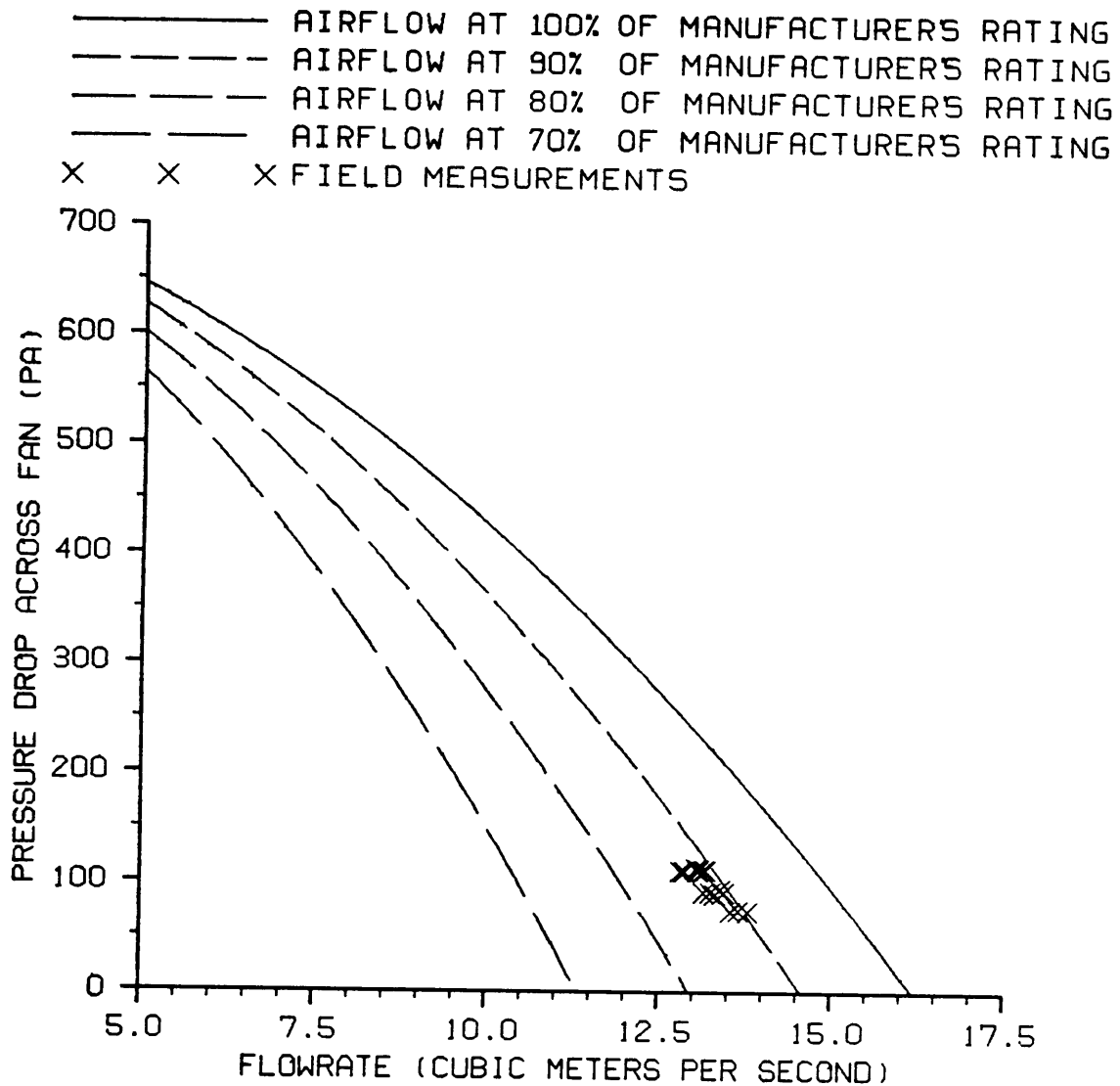


Figure 32. Pressure drop vs. flowrate for an eight-trailer unit equipped with a 7.46-kW Long fan, with baffle (Blacksburg, VA).

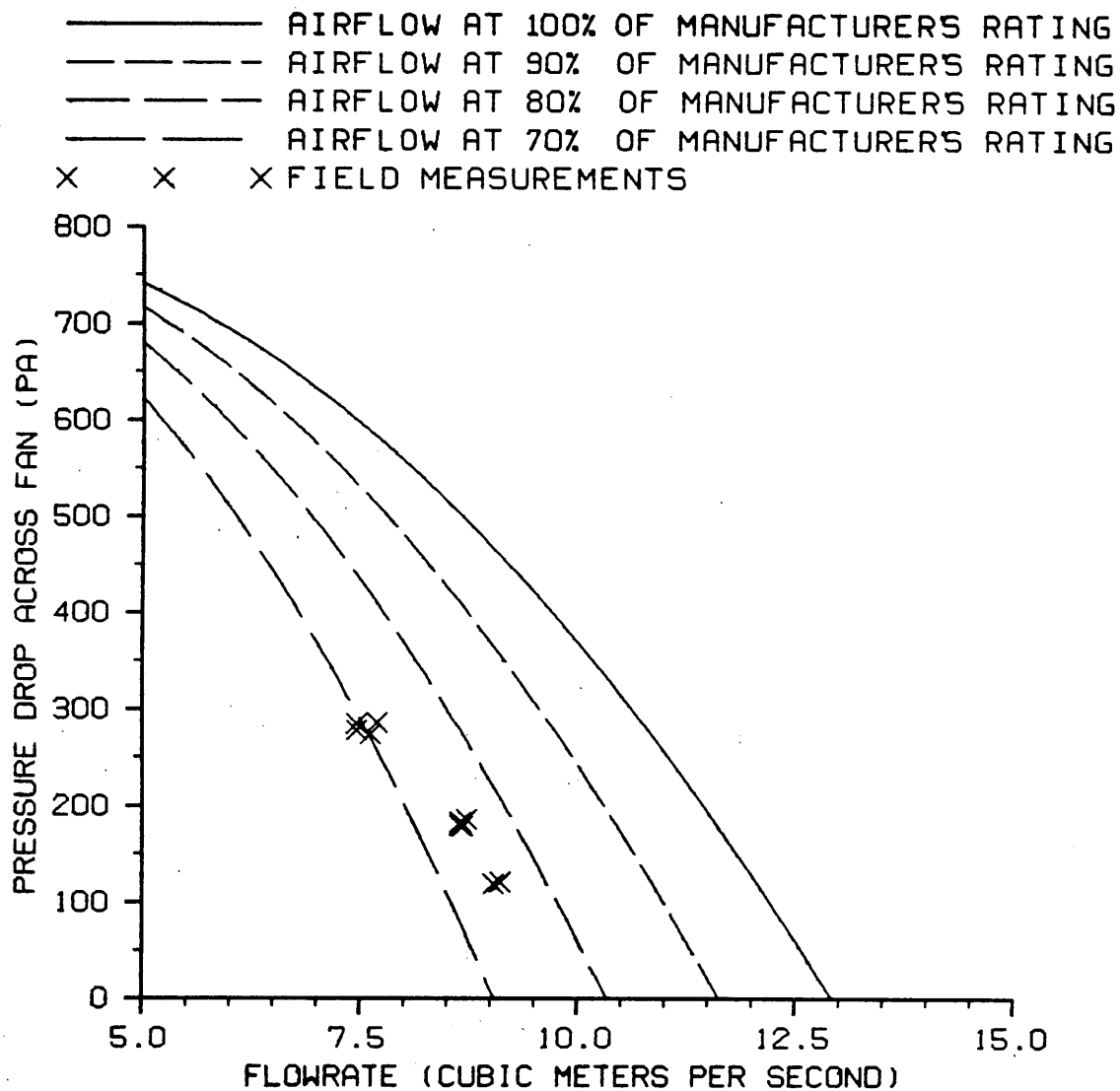


Figure 33. Pressure drop vs. flowrate for a four-trailer unit equipped with a 5.60-kW Long fan, with baffle (Blacksburg, VA).

Air Distribution within the Plenum

The air distributions within the plenums of the six units when all ports were open are shown in Figure 34 to Figure 41. The large rectangular outline between the dashed lines represents the dryer plenum, with the air entering from the left. The dashed lines indicate balanced flowrate through the port. Balanced flowrate is defined to be the flowrate out a port when the measured total flow is equally divided to all the ports. Measured flowrate is that obtained during testing, and is shown as a percentage (either increase or decrease) of the balanced flowrate. For example, in a six-trailer dryer with all the supply ports open, the balanced flowrate through each port would be $1/6$, or 16.67 percent of the total flow entering the dryer. If the measured flowrate at a port were 25 percent of the total flowrate, it would be delivering 50 percent above its balanced flowrate. When the measured flowrate is above the balanced flowrate, the value is plotted as a thick bar on the positive scale. When the measured flowrate is below the balanced flowrate, this bar appears on the negative side of the scale. Solid lines indicate the recommended flowrate, based on $0.167 \text{ m}^3/\text{s}$ per m^3 of peanuts, or $1.82 \text{ m}^3/\text{s}$ per trailer port. When the solid line is on the negative side of the dashed line, the total flow supplied by the fan is above the total requirements for drying. A bar on the positive side of the solid line indicates that the port receives more than the recommended flowrate.

Air distribution could not be determined using the perforated plate, but only by the resistance plates, implying the possibility of large errors. Comparison of many tests showed that error was relatively small. Bias was not expected to affect the distribution measurements since all resistance plate calibrations would shift in a similar fashion.

The eight-trailer unit tested in Lewiston (Figure 34) showed a severe distribution problem, with the two ports closest to the fan receiving much less air than the others. These two ports received less than the recommended flow, while the remaining six were oversupplied. Distribution improved

slightly when the same fan was installed on a six-trailer unit, though all ports received more than the recommended flowrate (Figure 35).

Some differences in distribution occurred between tests with the fan test unit connected, and disconnected for the dryer tested in Holland. These differences were possibly due to the fan inlet canvas being sucked onto a portion of the fan screen, as discussed earlier. For this reason, the measured distribution with the fan test unit disconnected was used to prepare Figure 36. Once again, total flow exceeded recommended flow. Figure 37 shows a 5.60-kW fan on a six-trailer unit. Distribution was poor, similar to the eight-trailer unit (Figure 34). Installing a larger, 7.46-kW fan on the same plenum revealed that distribution could be improved (Figure 38). Installing a larger fan on the same plenum, or using the same fan on a smaller plenum resulted in slightly improved airflow distribution. In other words, fans operating against higher pressure drops deliver air more evenly to the supply ports than those operating against smaller pressure drops. The larger fans, however, supply more air than needed, thus increasing operating costs.

A marked improvement resulted from the installation of a baffle (Figure 39 to Figure 41). The measured flowrate as a percentage of balanced flowrate was consistently higher at Port No. 1 in the six-trailer unit with the 5.60-kW Long fan (Figure 39), than with the 7.46-kW fan (Figure 40). It was suspected that noticeable differences in clearance between the fan blade and housing caused this behavior. The same fan caused similar problems in the four-trailer unit (Figure 41). The baffle was not as effective in distributing the air in an eight-trailer unit (Figure 42).

Closing ports in the dryer plenums changed the flow distribution (Figure 43 to Figure 45). Measured flowrate as a percentage of balanced flowrate is based on the number of open ports. (For example, if four port gates are closed in an eight-trailer unit, the balanced flowrate through each of the four open ports would be 25 percent of the total. If the measured value were 30 percent of the total, the port would be delivering 20 percent above its balanced flowrate.) Recommended

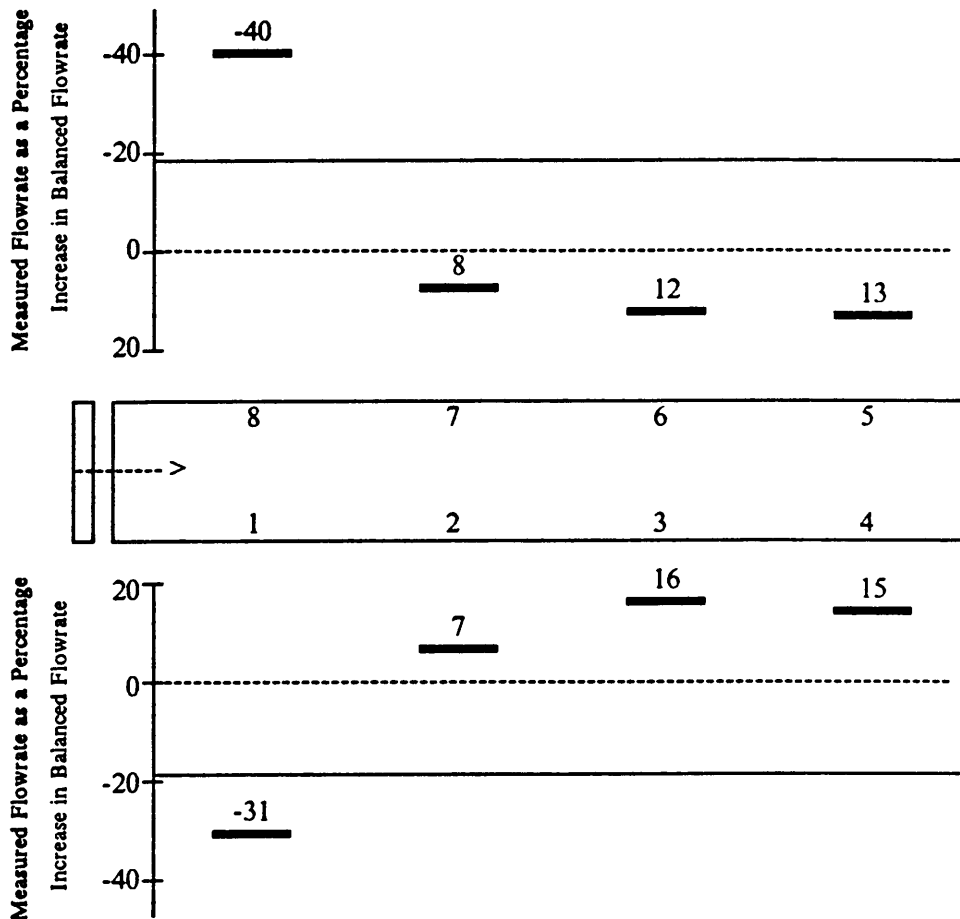


Figure 34. Deviation of measured from balanced flowrate with all ports open in an eight-trailer unit, 11.2-kW Aerovent fan (Lewiston, NC). Dashed lines indicate balanced flow. Solid lines indicate recommended flow which is 19% below balanced flow.

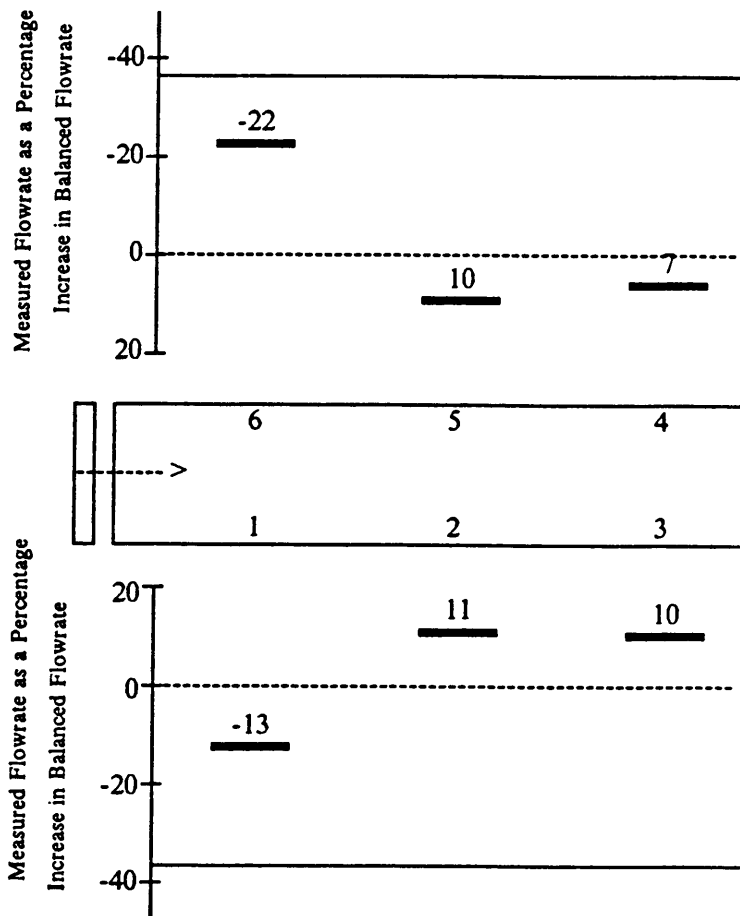


Figure 35. Deviation of measured from balanced flowrate with all ports open in a six-trailer unit, 11.2-kW Aerovent fan (Lewiston, NC). Dashed lines indicate balanced flow. Solid lines indicate recommended flow which is 37% below balanced flow.

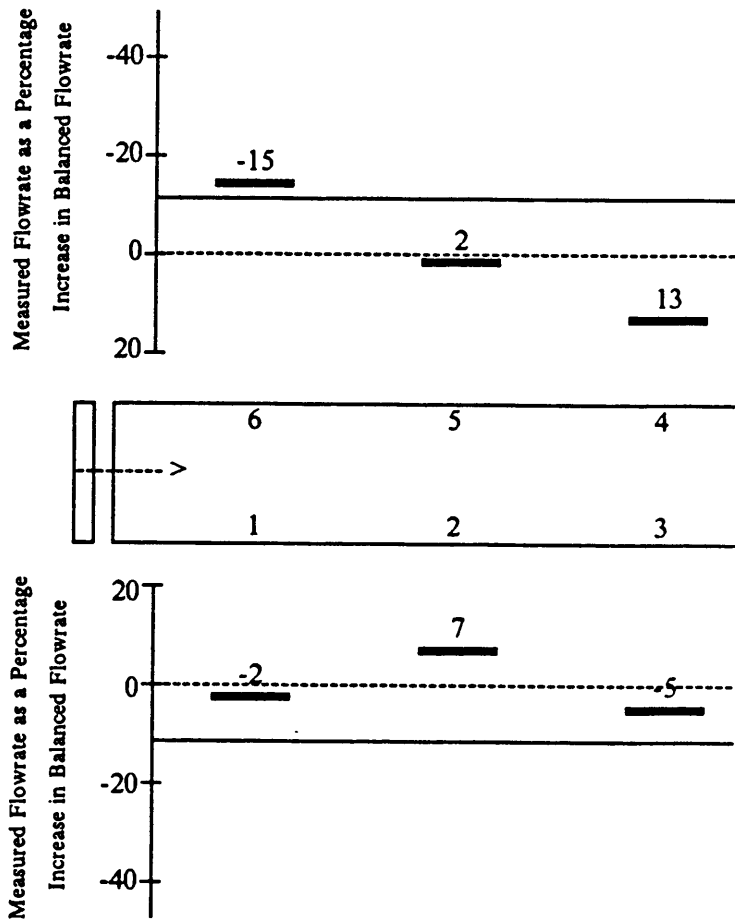


Figure 36. Deviation of measured from balanced flowrate with all ports open in a six-trailer unit, 7.46-kW Aerovent fan (Holland, VA). Dashed lines indicate balanced flow. Solid lines indicate recommended flow which is 11% below balanced flow.

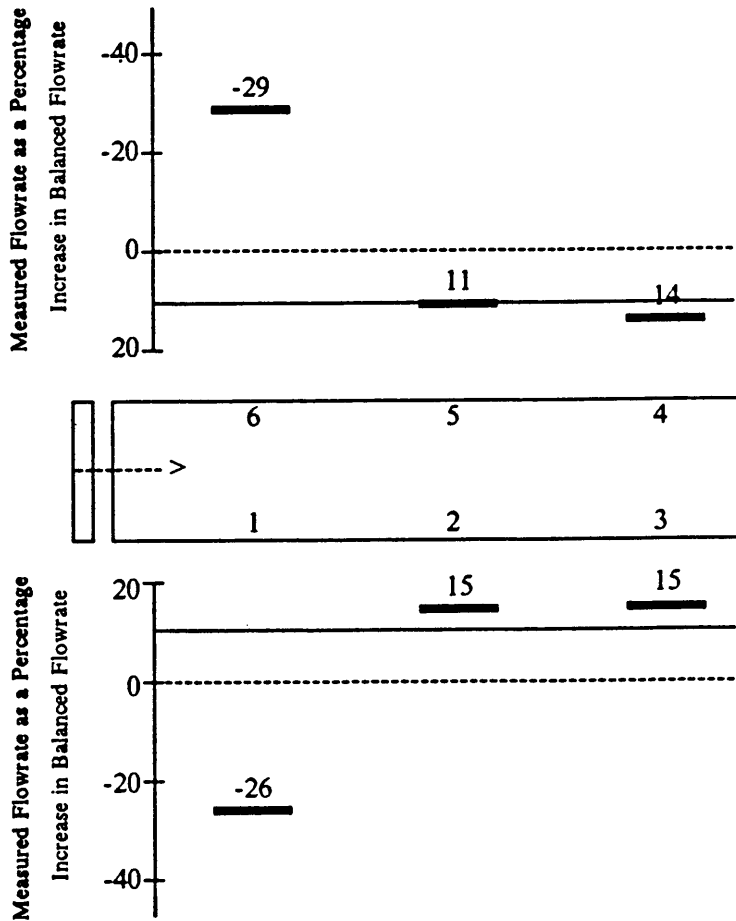


Figure 37. Deviation of measured from balanced flowrate with all ports open in a six-trailer unit, 5.60-kW Long fan (Blacksburg, VA). Dashed lines indicate balanced flow. Solid lines indicate recommended flow which is 11% above balanced flow.

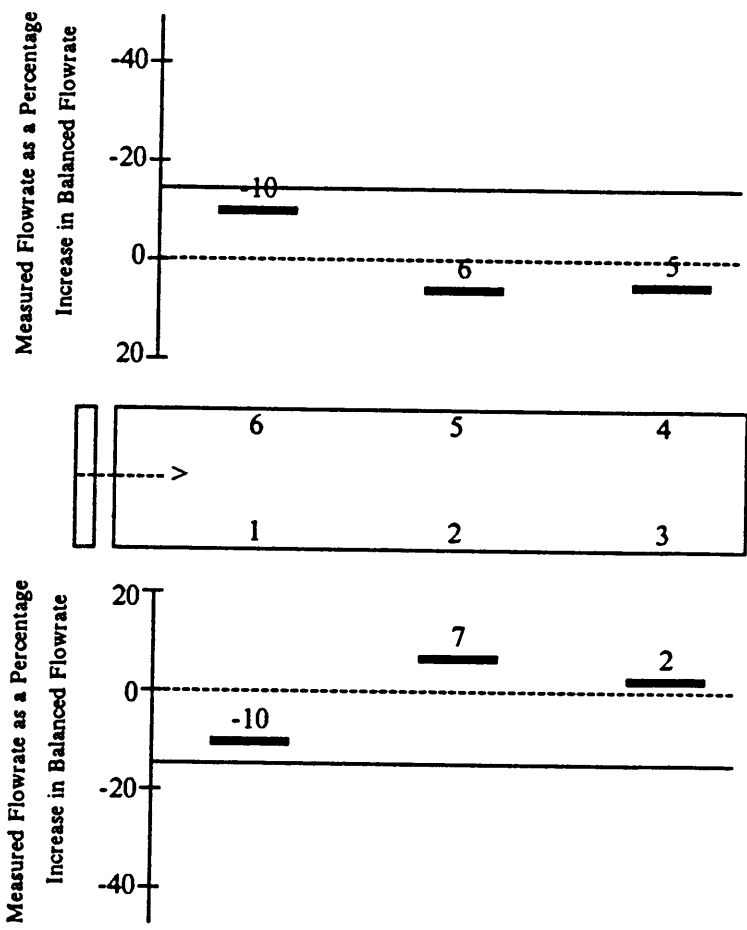


Figure 38. Deviation of measured from balanced flowrate with all ports open in a six-trailer unit, 7.46-kW Long fan (Blacksburg, VA). Dashed lines indicate balanced flow. Solid lines indicate recommended flow which is 16% below balanced flow.

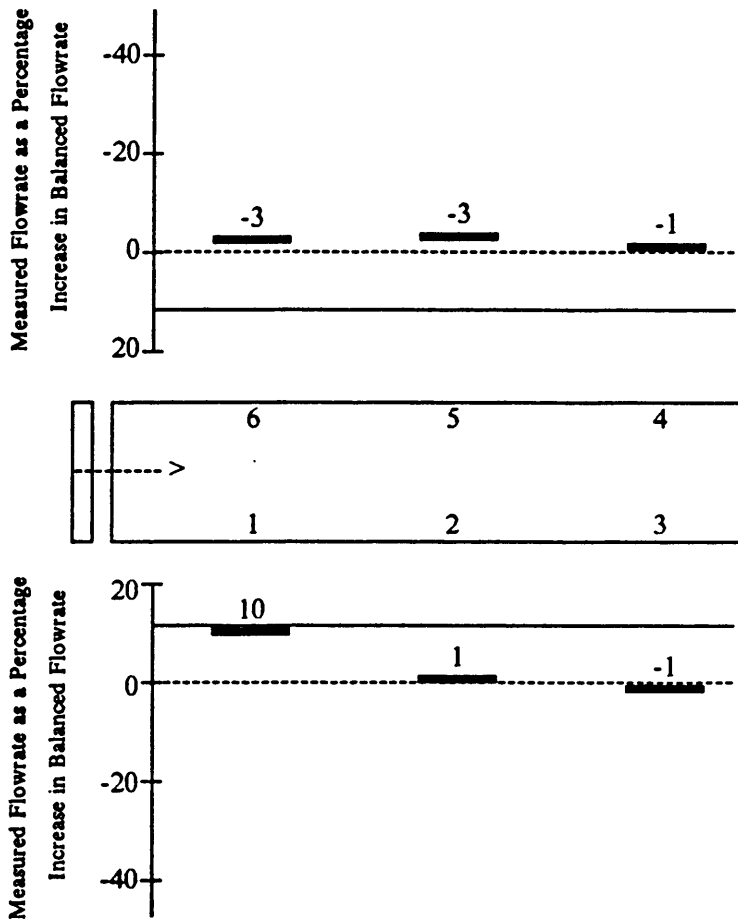


Figure 39. Deviation of measured from balanced flowrate with all ports open in a six-trailer unit, 5.60-kW Long fan, with baffle (Blacksbrug, VA). Dashed lines indicate balanced flow. Solid lines indicate recommended flow which is 12% above balanced flow.

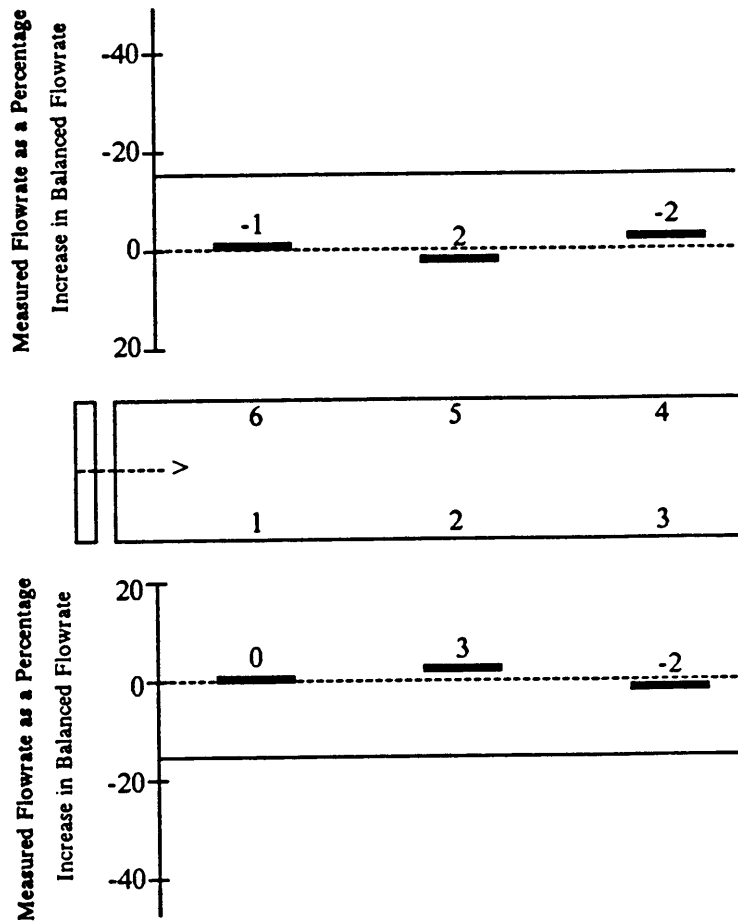


Figure 40. Deviation of measured from balanced flowrate with all ports open in a six-trailer unit, 7.46-kW Long fan, with baffle (Blacksburg, VA). Dashed lines indicate balanced flow. Solid lines indicate recommended flow which is 15% below balanced flow.

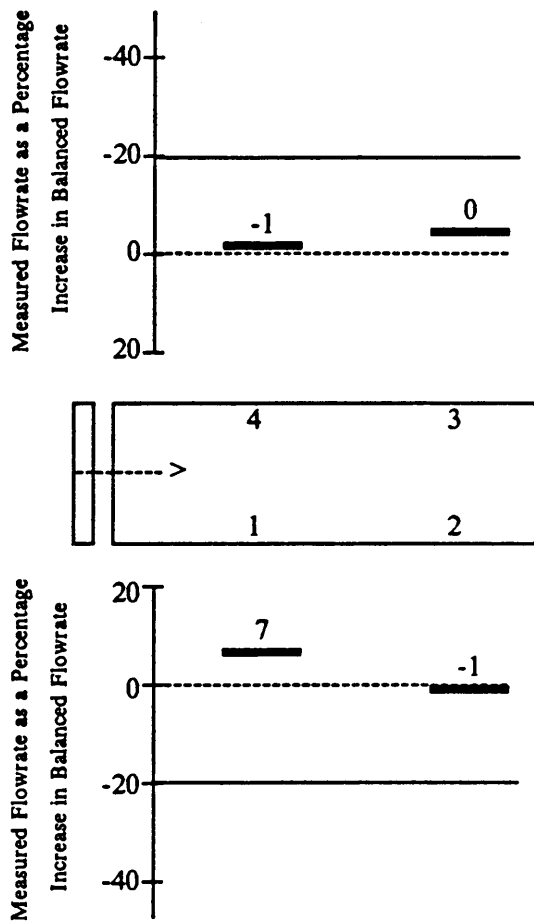


Figure 41. Deviation of measured from balanced flowrate with all ports open in a four-trailer unit, 5.60-kW Long fan, with baffle (Blacksburg, VA). Dashed lines indicate balanced flow. Solid lines indicate recommended flow which is 20% below balanced flow.

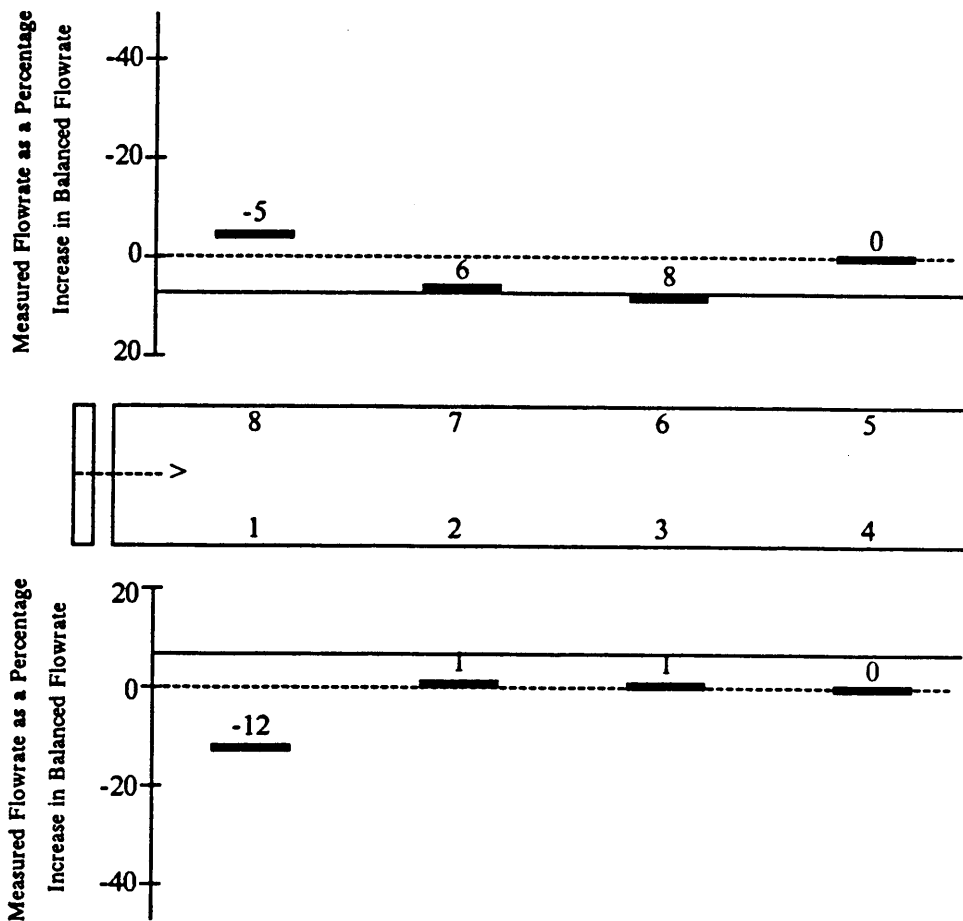


Figure 42. Deviation of measured from balanced flowrate with all ports open in an eight-trailer unit, 7.46-kW Long fan, with baffle (Blacksburg, VA). Dashed lines indicate balanced flow. Solid lines indicate recommended flow which is 7% above balanced flow.

flowrate as a percentage increase in balanced flowrate is calculated in a similar manner. In some cases, closing ports resulted in well-distributed flow, as seen in the data for the eight-trailer unit with four ports closed (Figure 43). However, when either or both of the two ports nearest the fan were left open, they did not receive the correct proportion of the total flow (Figure 44 and Figure 45).

Flow distribution is summarized in Figure 46 to Figure 53. For example, combining Figure 46 and Figure 43 to Figure 45, as well as results from additional combinations, produced the distribution represented by the graph in Figure 46. The deviation of measured flowrate from balanced flowrate for the different combination of ports closed is represented by the bar graph, and shows the extremes that can be expected. A plenum with good air distribution would have bar graphs that are short and are centered over the dashed line.

The installation of a baffle (Figure 51 to Figure 54) greatly reduced the range of deviation. This means that the air is well-distributed regardless of the number of ports being used. Use of a baffle would allow farmers to remove trailers and close ports, and still expect uniform drying rates in the remaining trailers.

One problem that occurs in all cases, is that port No. 1 always receives more than the one opposite. One possible explanation is that many dryers have thermostats that are in a metal box screwed to the plenum on the left side when facing downstream. The gas line and associated fittings are also located on the left. Testing showed that these obstructions caused a greater flow to port No. 1 as compared to the one opposite.

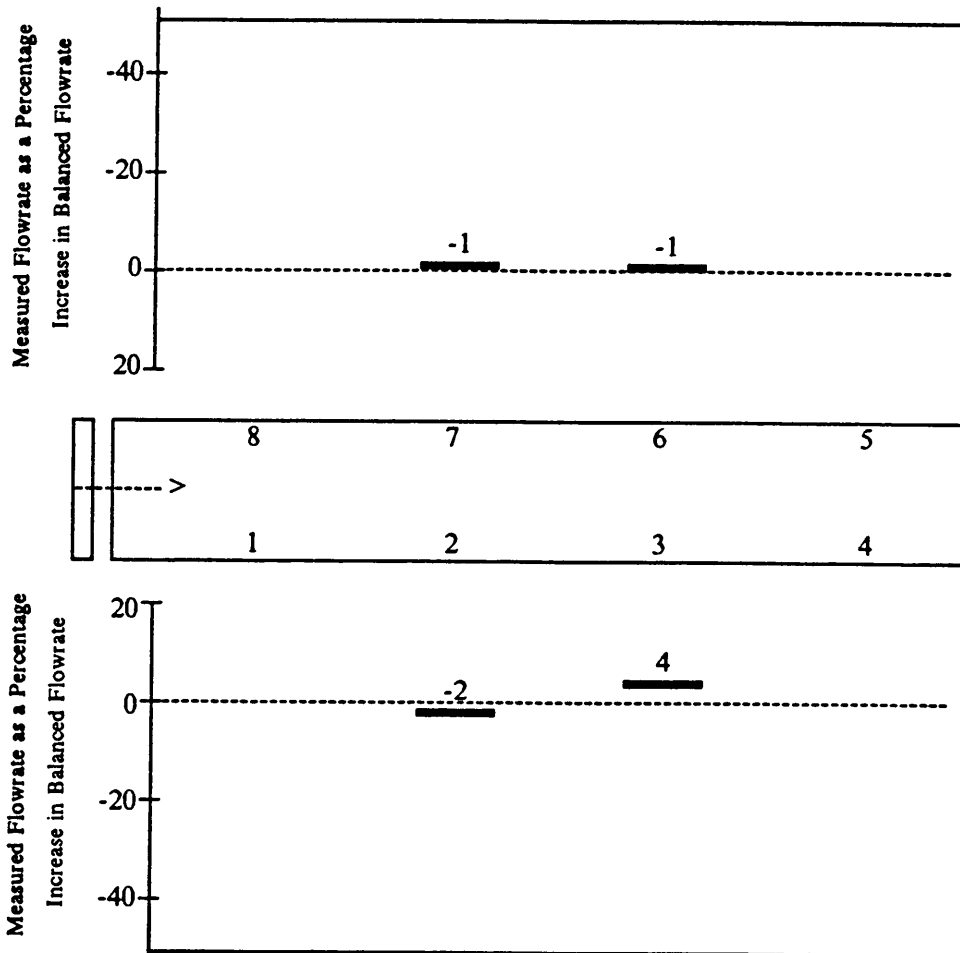


Figure 43. Deviation of measured from balanced flowrate with four ports open in an eight-trailer unit, 11.2-kW Aerovent fan (Lewiston, NC). Dashed lines indicate balanced flow. Solid lines indicate recommended flow which is 51% below balanced flow.

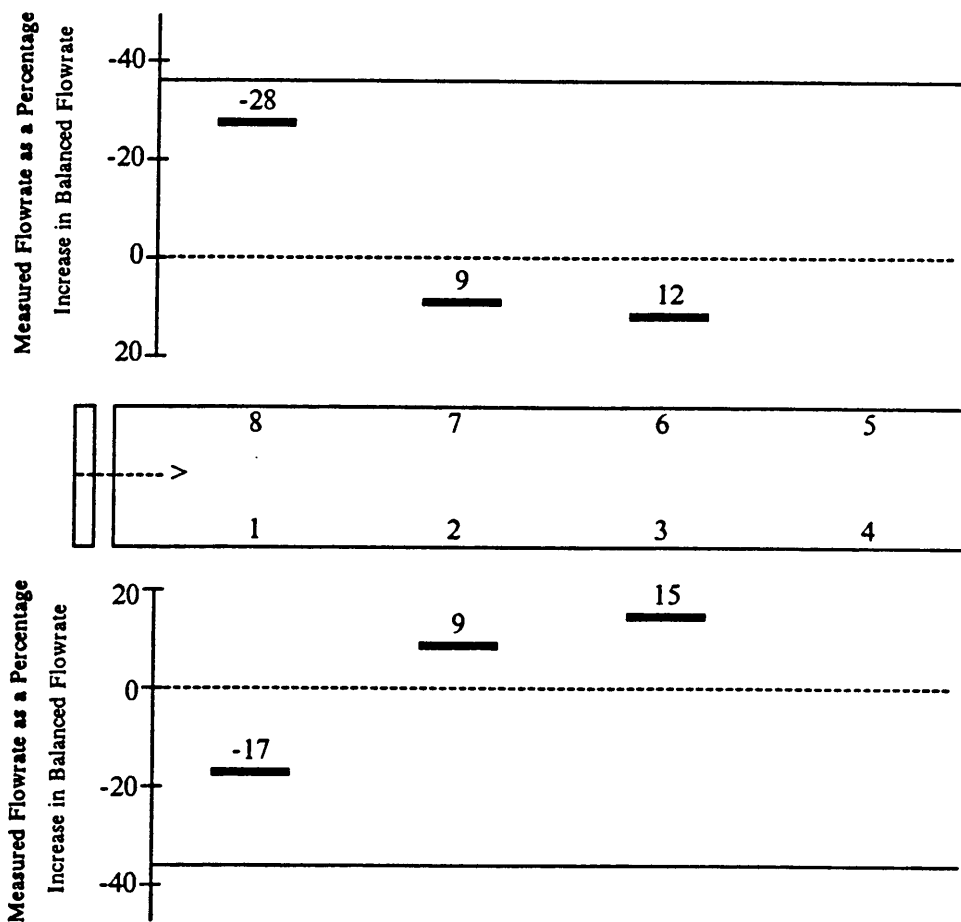


Figure 44. Deviation of measured from balanced flowrate with six ports open in an eight-trailer unit, 11.2-kW Aerovent fan (Lewiston, NC). Dashed lines indicate balanced flow. Solid lines indicate recommended flow which is 36% below balanced flow.

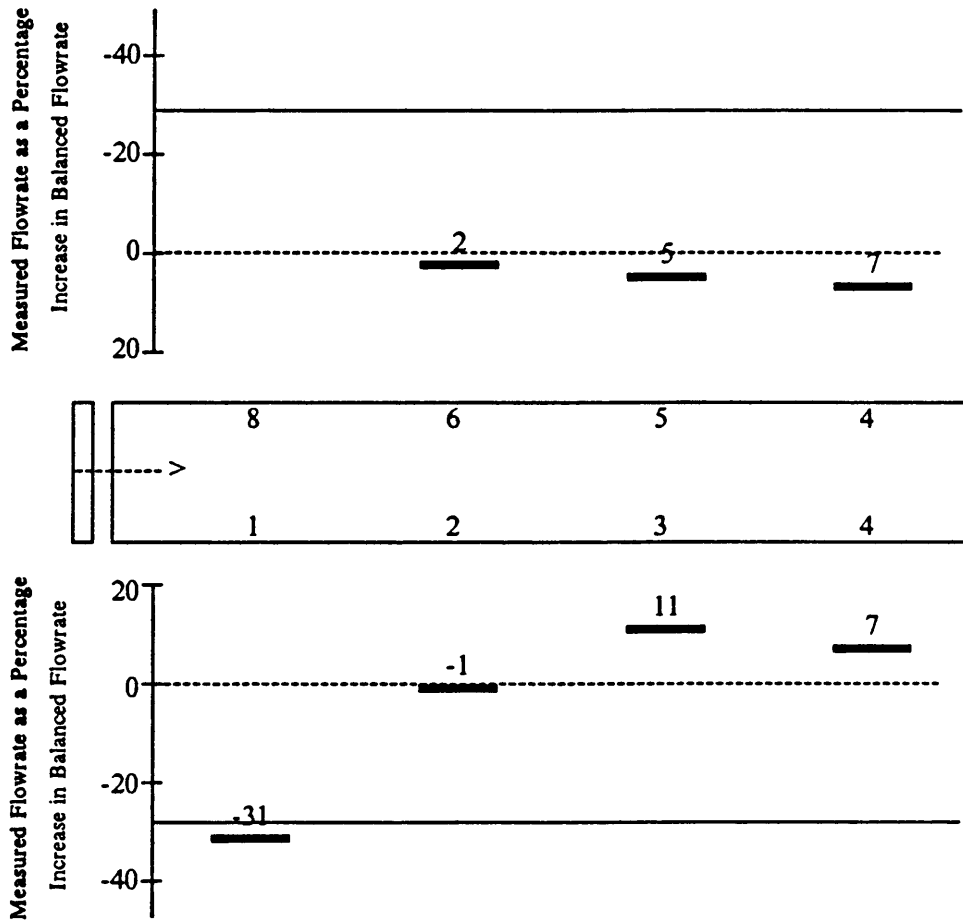


Figure 45. Deviation of measured from balanced flowrate with seven ports open in an eight-trailer unit, 11.2-kW Aerovent fan (Lewiston, NC). Dashed lines indicate balanced flow. Solid lines indicate recommended flow which is 28% below balanced flow.

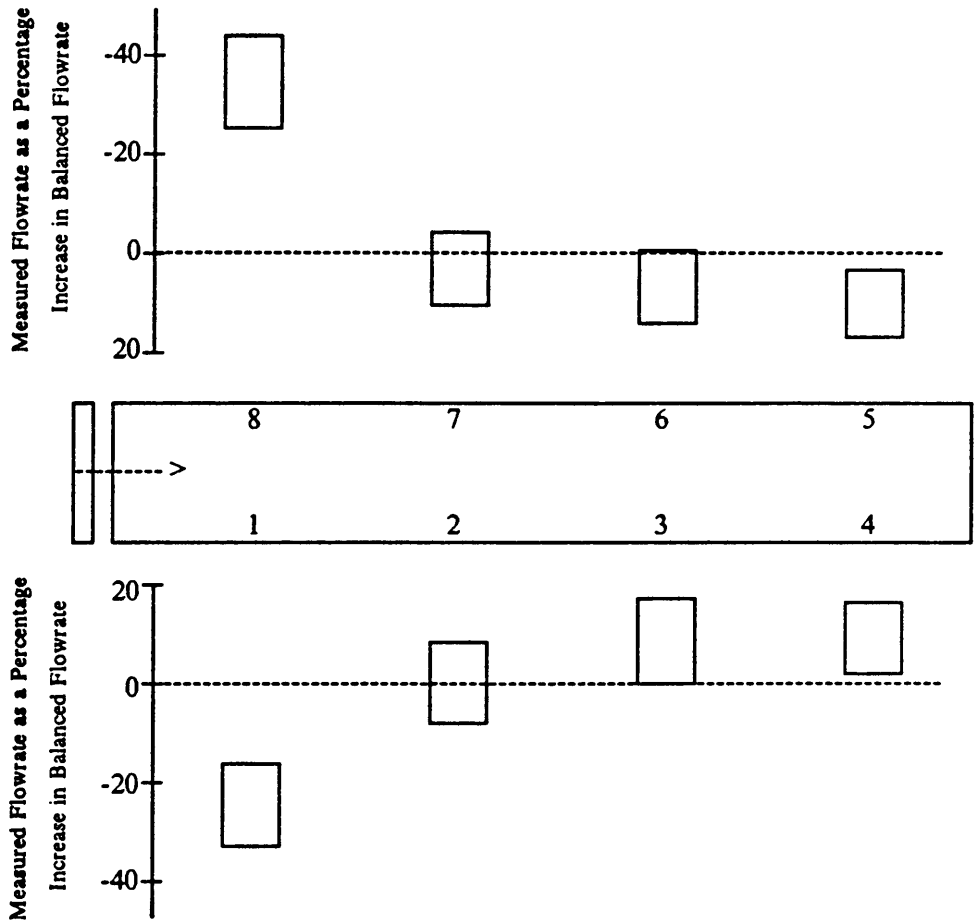


Figure 46. Deviation of measured from balanced flowrate, all combinations in an eight-trailer unit, 11.2-kW Aerovent fan (Lewiston, NC).

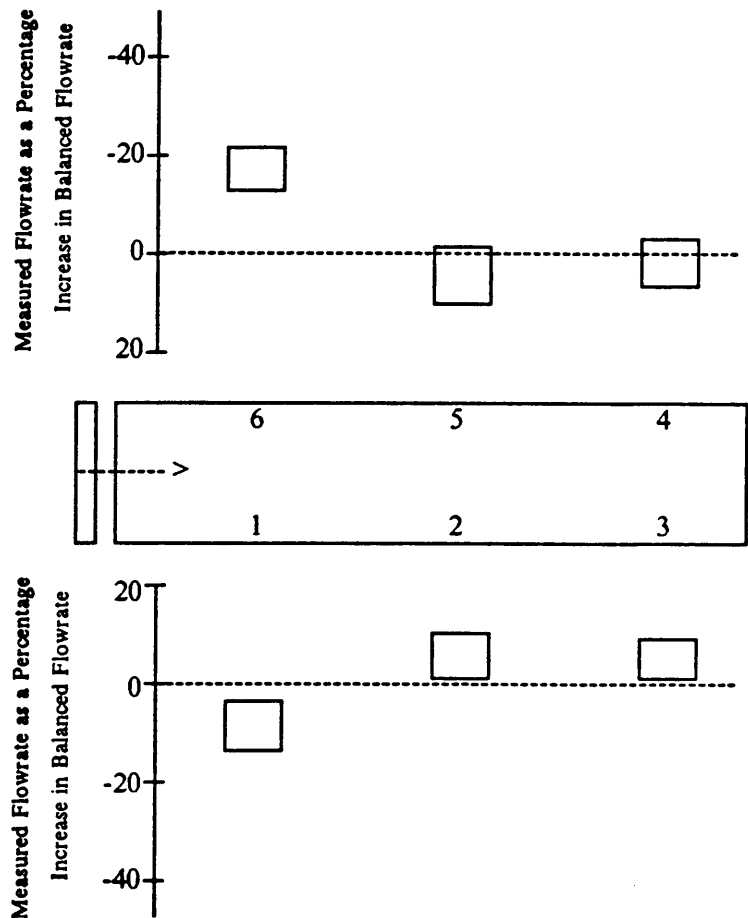


Figure 47. Deviation of measured from balanced flowrate, all combinations in a six-trailer unit, 11.2-kW Aerovent fan (Lewiston, NC).

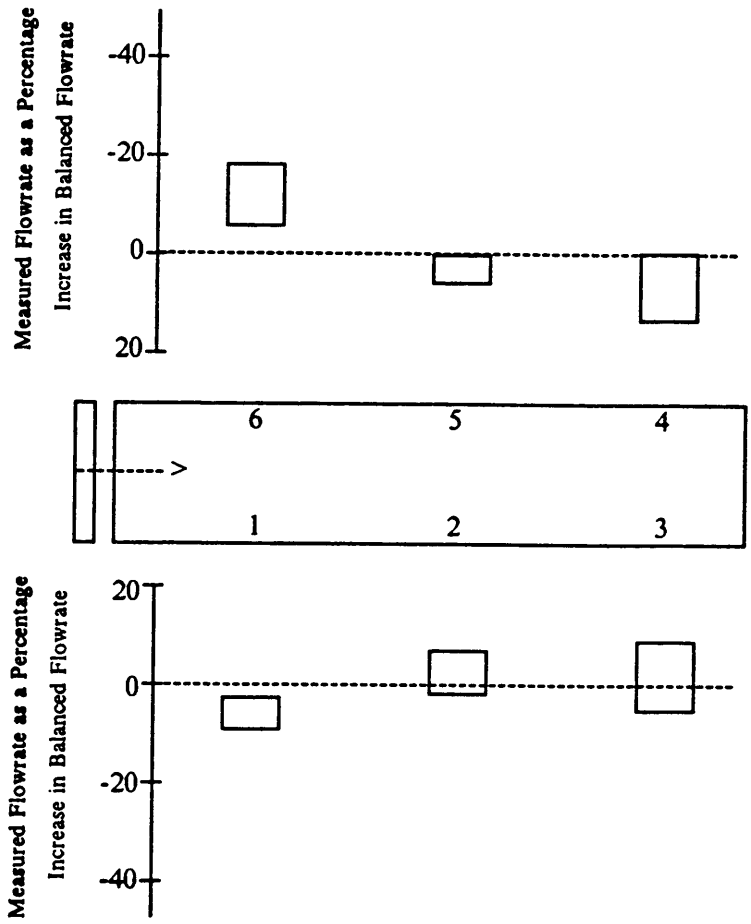


Figure 48. Deviation of measured from balanced flowrate, all combinations in a six-trailer unit, 7.46-kW Aerovent fan (Holland, VA).

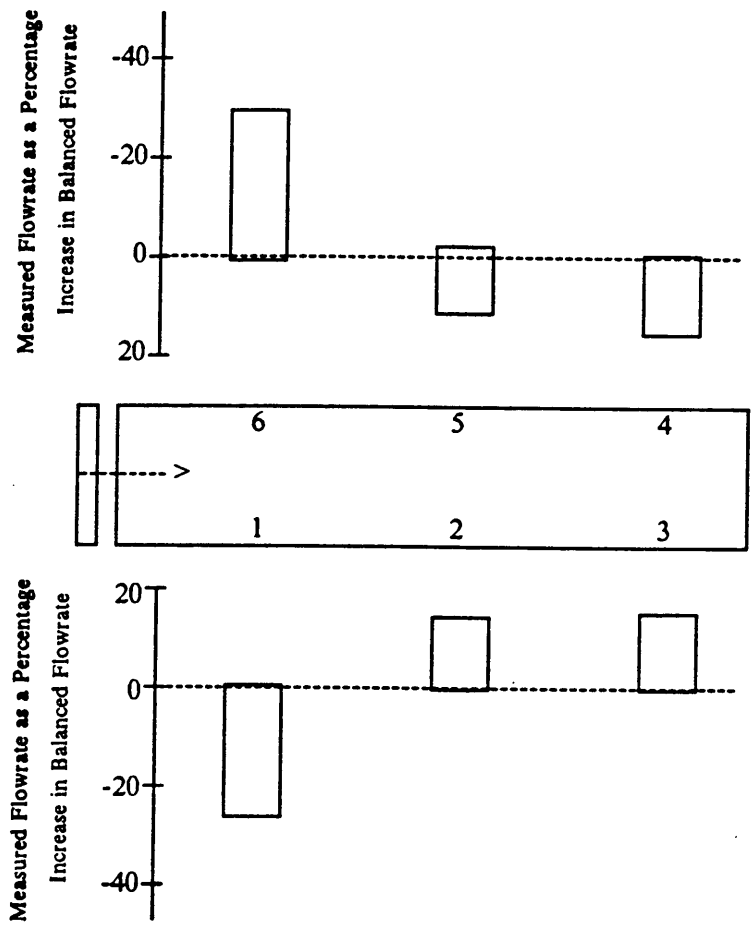


Figure 49. Deviation of measured from balanced flowrate, all combinations in a six-trailer unit, 5.60-kW Long fan (Blacksburg, VA).

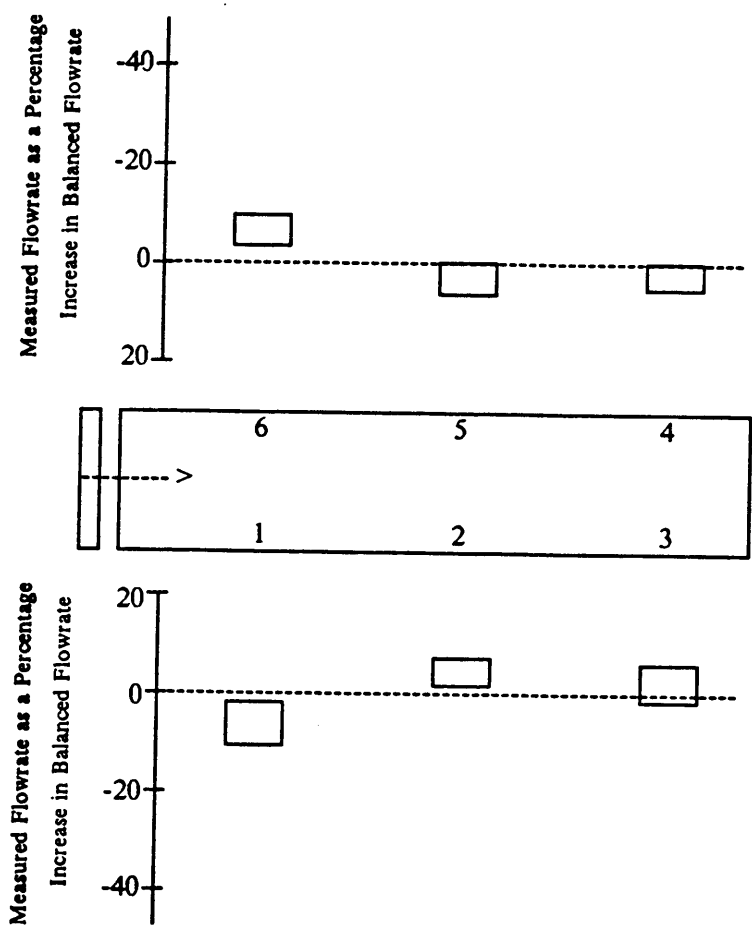


Figure 50. Deviation of measured from balanced flowrate, all combinations in a six-trailer unit, 7.46-kW Long fan (Blacksburg, VA).

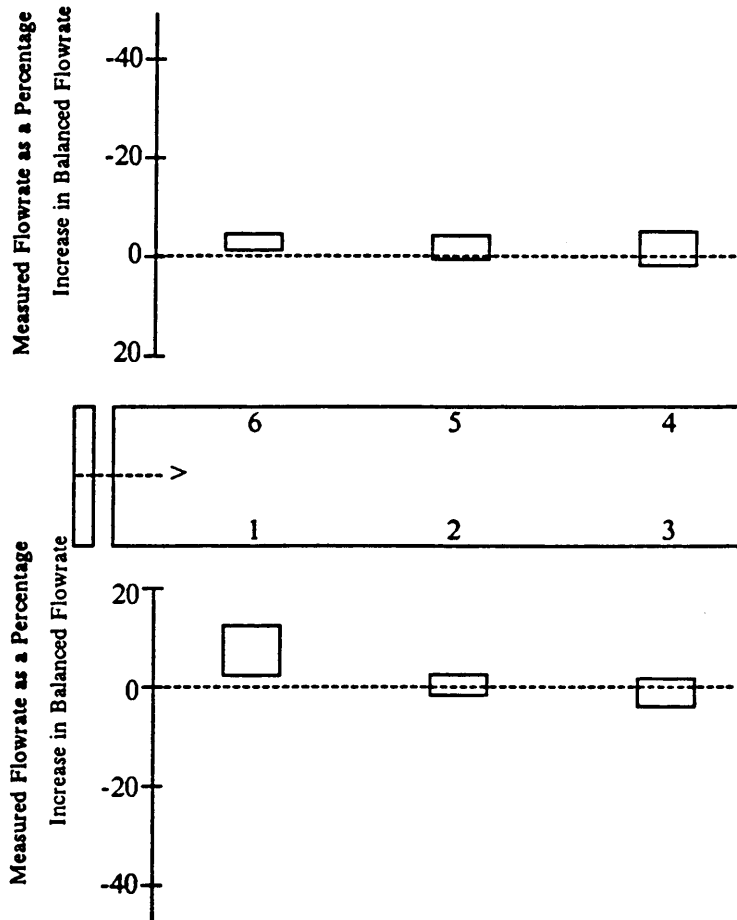


Figure 51. Deviation of measured from balanced flowrate, all combinations in a six-trailer unit, 5.60-kW Long fan, with baffle (Blacksburg, VA).

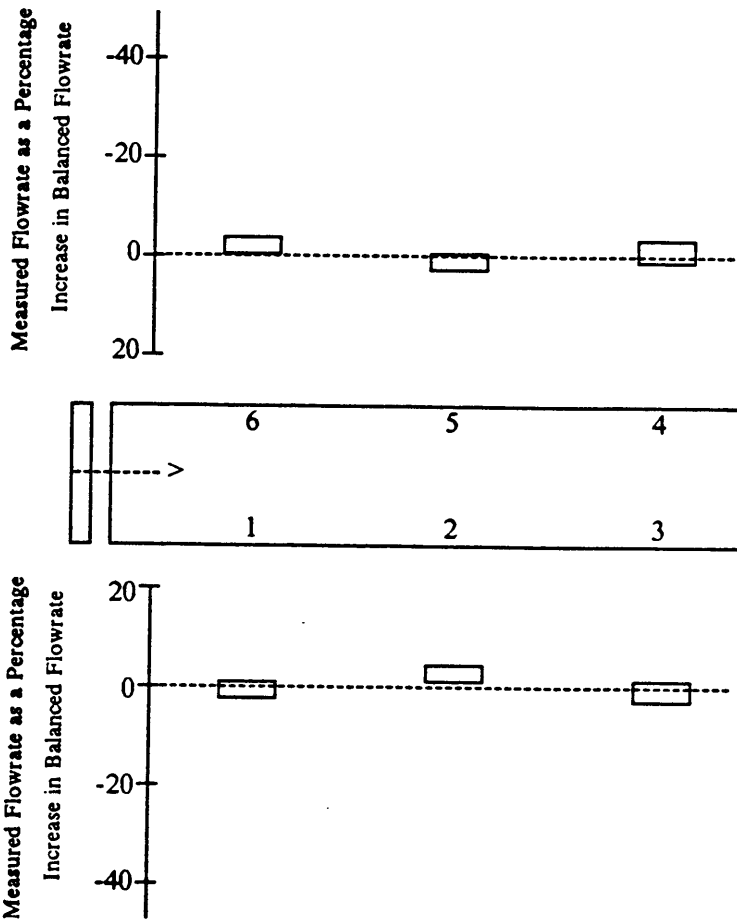


Figure 52. Deviation of measured from balanced flowrate, all combinations in a six-trailer unit, 7.46-kW Long fan, with baffle (Blacksburg, VA).

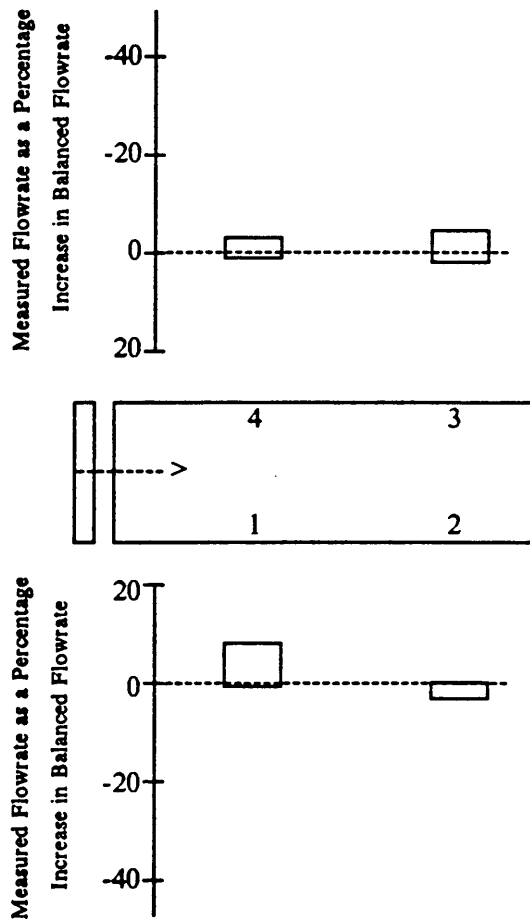


Figure 53. Deviation of measured from balanced flowrate, all combinations in a four-trailer unit, 5.60-kW Long fan, with baffle (Blacksburg, VA).

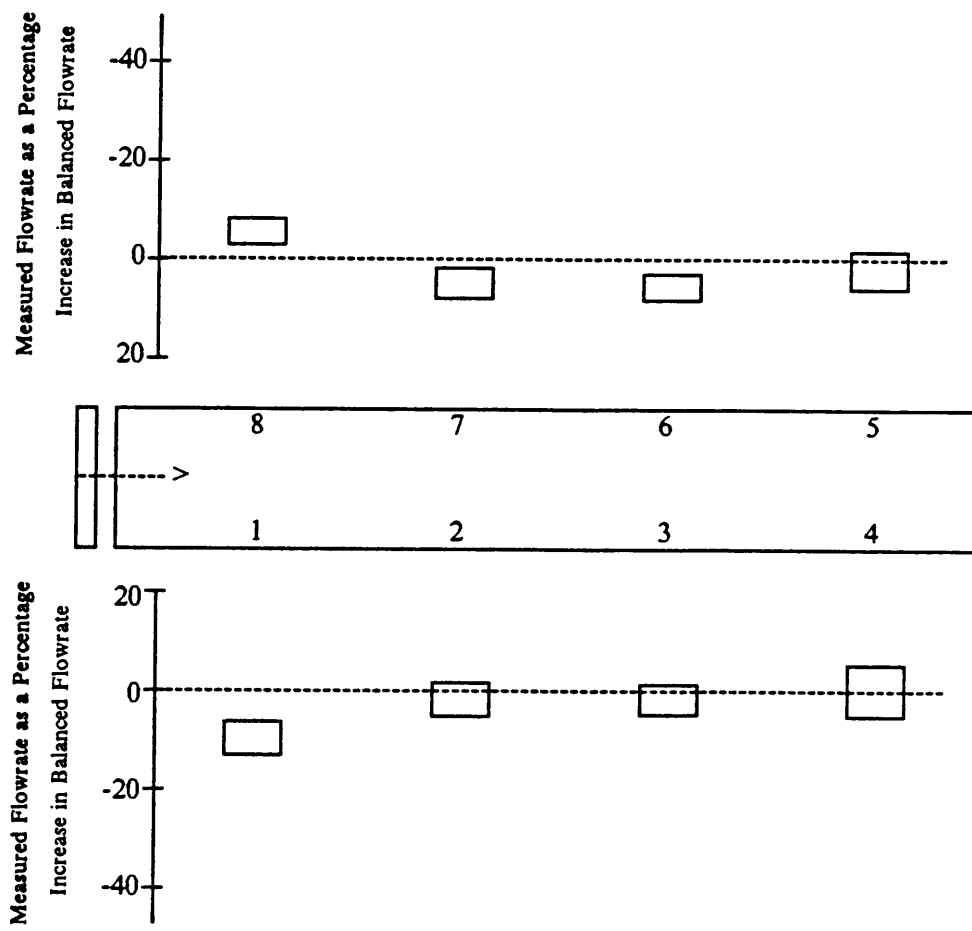


Figure 54. Deviation of measured from balanced flowrate, all combinations in an eight-trailer unit, 7.46-kW Long fan, with baffle (Blacksburg, VA).

Power Consumption

Power measurements revealed that dryer fans were operating close to motor capacities. A fully loaded 5.60-kW motor, at 70 percent efficiency, would use approximately 8000 W. Tests showed power consumption ranged from 8040 to 8280 W. At 80 percent efficiency, the 7.46-kW motor was expected to use 9300 W, whereas measurements ranged from 8960 to 9600 W.

Knowing the fan power consumption, as well as the flowrate, gives an indication of fan efficiency, based on the amount of air delivered per watt of power consumed. Both the 5.60- and 7.46-kW Long fans delivered more air per watt of energy consumed as the pressure drops across them decreased. The 5.60-kW fan delivered 0.00093 to 0.00123 m³/s/W at pressure drops ranging from 270 down to 70 Pa, respectively. The 7.46-kW fan delivered 0.00108 to 0.00142 m³/s/W, with corresponding pressure drops of 266 to 120 Pa. With two ports open in the six-trailer plenum, the pressure drop across the smaller fan was 271 Pa, and it delivered 0.00093 m³/s/W. With three ports open in the same plenum, the pressure drop across the larger fan was 266 Pa, and it delivered 0.00108 m³/s/W. Thus, at the same pressure drop, the larger fan delivered 16 percent more air per unit of electrical energy consumed than the smaller fan.

Inlet restrictions were used to decrease the flowrate. The size of the opening in the restriction was increased until the flowrate through each open port was approximately 1.82 m³/s. The size of the opening and the total flow exiting the open ports is shown in Table 8. Although the restrictions were initially sized to deliver 1.82 m³/s per port, the measured average flowrate was approximately 1.74 m³/s per port. Total flow without restriction is included for comparison.

Table 8. Total flowrate with and without inlet restrictions.

Number of Open Ports	Total Flow		Restriction Opening (m)
	Without Restrictions	With Restrictions	
6	12.58	10.50	0.965
5	12.13	8.63	0.865
4	11.36	6.95	0.797
3	10.22	5.19	0.711
2	8.17	3.52	0.641

The inlet restrictions proved to be very effective. Depending on the amount of inlet area reduction, energy consumption was reduced from 18 to 36 percent, while total airflow was reduced from 17 to 57 percent. For a four-trailer plenum, energy consumption for both the 5.60- and 7.46-kW fans was similar when the same airflow was delivered across the same pressure drop. (This pressure drop is measured at the resistance plates, and therefore includes the pressure drop across the inlet restriction.)

The test results for the 7.46-kW fan on a six-trailer unit equipped with a baffle is shown in Figure 55. As the gates were closed on the supply ports, energy consumption increased slightly from 8960 to 9600W, when no inlet restrictions were used. Airflow through each port increased much faster than energy consumption as the port gates were closed. (Total airflow to the plenum can be determined by multiplying the airflow through each port by the number of ports open.) Results were similar for the 5.60-kW fan.

As already mentioned, average flowrate per port increased much faster than the total electric energy consumption as ports were closed. When restrictions were used to maintain a constant average flowrate per port, the total electric energy consumption decreased as ports were closed. It was reduced from 7320 watts with all ports open to 6120 watts with four ports closed, while maintaining a constant average flowrate of $1.74 \text{ m}^3/\text{s}$ to all open ports. Though total electrical energy was reduced, the units of air delivered per watt of power consumed was decreased from $0.00143 \text{ m}^3/\text{s}/\text{W}$ with all ports open to $0.00130 \text{ m}^3/\text{s}/\text{W}$ with one port closed, $0.00113 \text{ m}^3/\text{s}/\text{W}$ with two ports closed, $0.000859 \text{ m}^3/\text{s}/\text{W}$ with three ports closed, and $0.000575 \text{ m}^3/\text{s}/\text{W}$ with four ports closed. By using the restriction the total electric energy consumption, when compared to energy consumption with no restrictions, was reduced 26 percent when one port was closed. However, the $\text{m}^3/\text{s}/\text{W}$ ratio was reduced 3 percent. With four ports closed the total electric energy was reduced 36 percent with the restriction, and the $\text{m}^3/\text{s}/\text{W}$ ratio was reduced 32 percent. Though the fan performance, defined

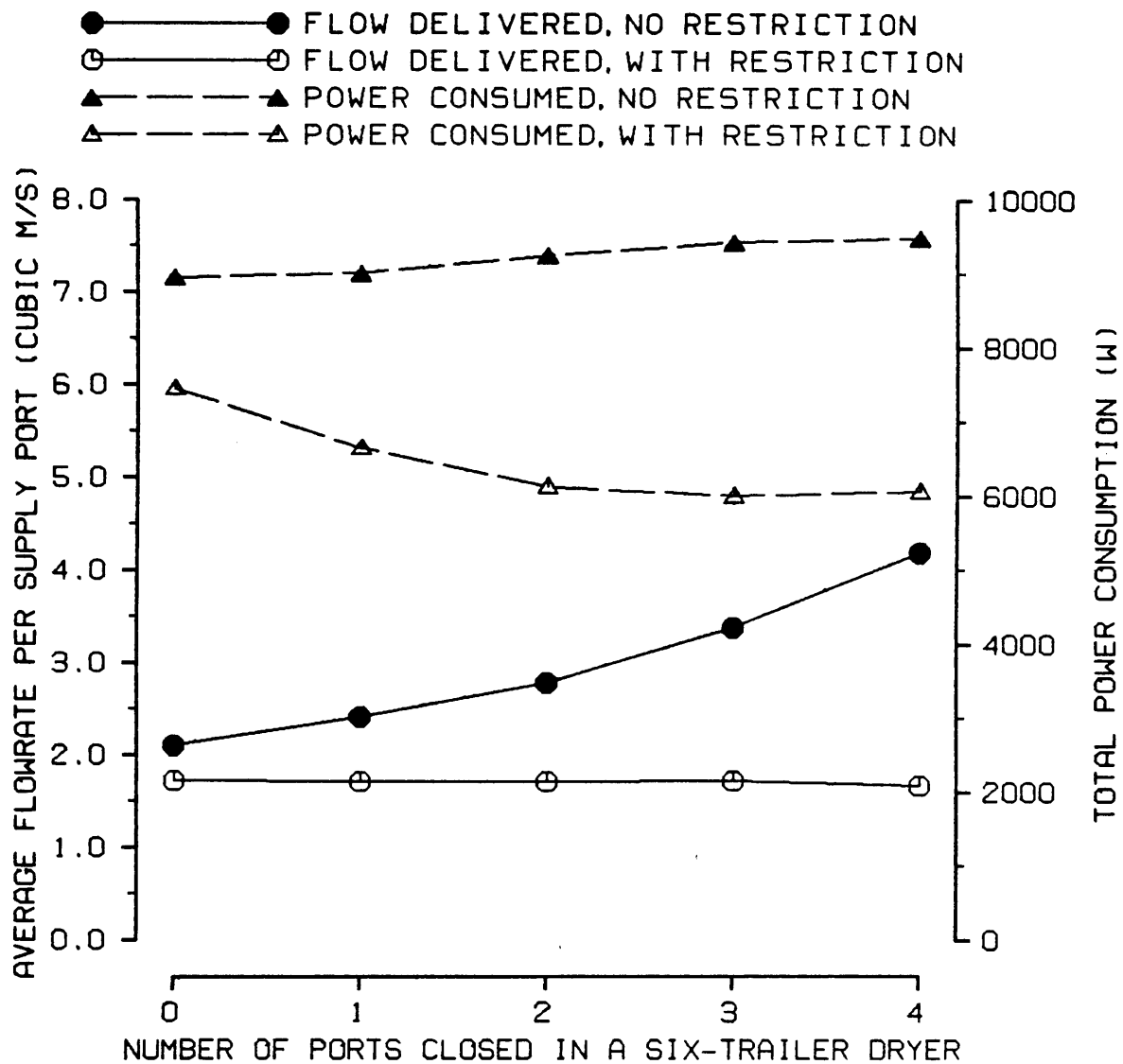


Figure 55. Flow reduction with inlet restrictions.

by the $\text{m}^3/\text{s}/\text{W}$ ratio, is reduced by the restriction, it is still a useful management tool because it reduces the total electric cost the farmer pays for drying his crop.

Summary and Conclusions

1. The perforated plate was found to be a good method of total flow measurement for on-site field testing of dryer fans. Error was determined to be less than 2 percent theoretically, and was substantiated by field measurements. Some slight calibration problems were detected by noting a rise and fall of the pressure coefficient, based on pressure drop across the plate, when plotted against its corresponding Reynolds number. Investigation and correction of the problem would probably not greatly improve flow measurement accuracy. The connecting canvas introduced error when it fluttered in the wind, causing fluctuations in the pressure drop. This problem was partially solved by increasing the pressure within the canvas, but this resulted in overfeeding of the dryer fan.
2. The resistance plate error was too large for accurate field measurements, particularly when using many of them, resulting in compounded error. Cheesecloth worked well in simulating peanuts since it prevented airflow through it from being totally turbulent. Being made of cotton, however, it lacked durability and was highly susceptible to dust collection, introducing bias to the calibration. Unlike the perforated plate, the resistance plates produced a steady decrease in the pressure coefficient as the Reynolds number increased. A resistance plate made

of strong material that is easily cleaned, while preventing totally turbulent flow, is needed to more accurately measure the airflow exiting the supply ports.

3. Despite errors in the flow determination using the resistance plates, they, along with the perforated plate, provided a successful method of on-site performance testing of commercial peanut dryers. However, accurate leakage measurements were not possible. Difficulties in using the method arose mainly in dryer sheds where the dryer fan inlet was not readily accessible, or where there was insufficient area to position the fan test unit.
4. Plotting the pressure coefficient against the Reynolds number, for both the resistance plates and the perforated plate, quickly revealed if any errors occurred during the calibration. A scatter of points that was slight when using the pressure drop and flowrate was greatly magnified when the pressure coefficient and Reynolds number were employed. A slope of zero indicated turbulent flow, where the pressure drop is proportional to the power of 2 of the velocity. A negative slope indicated a value of less than 2. A positive slope meant a power greater than 2, implying that problems existed with the calibration procedure.
5. Six peanut dryers were field tested and results compared with manufacturers' ratings. A weighted pressure drop at the resistance plates, and the total measured flow into the fan were used for the comparison. Peanut dryer fans delivered from 75 to 100 percent of their rated flow, based on the rating curves supplied by the manufacturers. Further decreases were encountered if port gates were closed, thus increasing the pressure drop across the fan. Slightly lower values occurred for dryers equipped with baffles, decreasing total flowrates up to 5 percent. Assuming efficiencies of 70 to 80 percent, electric energy consumed by the fan was close to its nameplate rating. Fans performed more closely to manufacturers' ratings with lower pressure drops across them. In some instances, fan delivered more than their rated flow. This discrepancy was attributed to errors in the manufacturers' ratings.

6. Dryer plenums normally deliver much too little air to the pair of supply ports closest to the fan. Increasing the fan size, or decreasing the dryer size resulted in slightly improved air distribution. However, additional modifications were required to bring the distribution to an acceptable level. To distribute air evenly, numerous flow vanes within the plenum were not found to be necessary. One baffle proved to adequately solve distribution problems. Beyond this, the port immediately to the right of the fan when looking downstream generally received more air than the port opposite it, which was attributed to the presence of the burner and accessories.

7. Inlet restrictions were found to be a promising means of flow control. Simple restrictions resulted in energy savings as high as 36 percent, while reducing total airflow up to 57 percent.

References

- Abernethy, R. B. and J. W. Thompson. 1980. Measurement uncertainty handbook. National Technical Information Service, Springfield, VA.
- AMCA. 1985. Laboratory methods of testing fans for rating. AMCA and ASHRAE.
- ASHRAE. 1981. Fundamentals. Measurements and instruments. ASHRAE, Atlanta, GA.
- Beasley, E. O. and J. W. Dickens. 1963. Engineering research in peanut curing. Tech. Bull. No. 155, North Carolina Agricultural Experiment Station, Raleigh, NC.
- Brooker, D. B. 1969. Computing air pressure and velocity distribution when air flows through a porous medium and nonlinear velocity-pressure relationship exist. Transactions of the ASAE 12(1):118-120.
- Clarke, M. S., J. T. Barnhart, F. T. Bubsey and E. Neitzel. 1978. The effects of system connections on fan performance. ASHRAE Transactions 84(II):227-263.
- Eck, B. 1973. Fans. Pergamon Press, Oxford.
- Engineering Sciences Data Unit. 1972. Pressure drops in ducts across round-wire gauzes normal to the flow. Paper No. 72009. Engineering Sciences Data Unit Ltd., London.
- Jorgensen, R. (editor). 1970. Fan engineering. Wm. J. Keller, Inc., Buffalo, NY, 729p.
- Lambert, A. J. 1969. Effects of peanut depth and air flow on dryer operation. Curing Virginia peanuts. Publication 269. Extension Division, Virginia Polytechnic Institute, Blacksburg, VA.
- Livesey, J. L. and T. Hugh. 1966. 'Suitable mean value' in one-dimensional gas dynamics. Journal Mechanical Engineering Science 8(4):374-383.

- Mehta, R. D. and P. Bradshaw. 1979. Design rules for low speed wind tunnels. *Aeronautical Journal* 83:443-449.
- Mikhail, M. N. 1979. Optimum design of wind tunnel contractions. *AIAA Journal* 17(5):471-477.
- Mirocha, C. J. and C. M. Christensen. 1982. Mycotoxins. Storage of cereal grains and their products. American Association of Cereal Chemists, Inc., St. Paul, MN.
- Osbourne, W. C. 1966. Fans. Pergamon Press, Oxford, 224p.
- Ower, E. and R. C. Pankhurst. 1977. Measurement of airflow. Pergamon Press, Oxford, 363p.
- Pope, A. and John J. Harper. 1966. Low speed wind tunnel testing. John Wiley and Sons, Inc., New York, 457p.
- Rabinowicz, E. 1970. An introduction to experimentation. Addison-Wesley Publishing Co., Reading, MA, 124p.
- Shedd, C. K. 1953. Resistance of grains and seeds to air flow. *Agricultural Engineering* 34(9):616-619.
- Shedd, C. K. 1954. Measuring air flow with perforated metal sheet. *Agricultural Engineering* 35(6):420.
- Steele, J. L. 1974. Resistance of peanuts to airflow. *Transactions of the ASAE* 17(3):573-577.
- Streeter, V. L. and E. B. Wylie. 1979. Fluid mechanics. McGraw-Hill Book Company, New York, 562p.
- Troeger, J. M. and J. L. Butler. 1980. Drying peanuts with intermittent airflow. *Transactions of the ASAE* 23(1):197-199.
- Wallis, R. A. 1983. Axial flow fans and ducts. John Wiley and Sons, Inc., New York, 444p.

Appendix A. CUBIC FORTRAN

```
C *****
C THIS PROGRAM IS TO DRAW A PROFILE OF A NOZZLE WITH A SHAPE
C DESCRIBED BY THE EQUATION:
C           Y = A * X ** 3
C THE AXES ARE ROTATED TO GIVE ZERO SLOPE AT THE EXIT AND
C INLET TO THE NOZZLE. INPUT DATA INCLUDES THE EXIT LENGTH
C AND DEPTH, AND THE LENGTH OF THE ENTRANCE.
C VARIABLES:
C XEP   THE LENGTH OF THE EXIT OF THE NOZZLE (M)
C YEPP  THE DEPTH OF THE EXIT OF THE NOZZLE (M)
C THETA THE AMOUNT OF ROTATION OF THE AXES (DEG)
C XIP   THE LENGTH OF THE INLET OF THE NOZZLE (M)
C YIPP  THE DEPTH OF THE INLET OF THE NOZZLE (M)
C SCALE SCALING FACTOR FOR INLET/EXIT DEPTH
C XNZHIT HEIGHT OF THE NOZZLE INLET (M)
C XNZWID WIDTH OF THE NOZZLE INLET (M)
C AI    COEFFICIENT A IN THE ABOVE EQUATION FOR THE INLET
C AE    COEFFICIENT A IN THE ABOVE EQUATION FOR THE EXIT
C YEP   VALUE OF Y IN THE ROTATED EQUATION AT X=XEP FOR EXIT, (M)
C       (YEPP IS USED AS A SCALING FACTOR FOR GRAPHING)
C XXE   X VALUE FOR EXIT IN THE ABOVE EQUATION (DIMENSIONED) (M)
C YYE   Y VALUE FOR EXIT IN THE ABOVE EQUATION (DIMENSIONED) (M)
C XXEP  X VALUE FOR EXIT IN THE ROTATED EQUATION (DIMENSIONED) (M)
C YYEP  Y VALUE FOR EXIT IN THE ROTATED EQUATION (DIMENSIONED) (M)
C *****
C       REAL XXE(51),YYE(51),YYEP(51),XXEP(51),XXI(51),XXIP(51),YYI(51)
C           @,YYIP(51),XE(51),XI(51),YE(51),YI(51),XH(51),ARCE(51),ARCI(51)
C           REAL XNAG(101), YNAG1(101), YNAG2(101)
C *****
C READ INPUT DATA
C *****
C       READ(10,111) XEP, YEPP, XIP, YIPP, XLENG, YLENG, THETA, XNZWID, XNZHIT
C       111 FORMAT(25X, F10.5)
C *****
C WRITE INPUT DATA
C *****
C       300 WRITE(20,112) THETA, XEP, YEPP, XIP, YIPP, XLENG, YLENG, XNZWID, XNZHIT
C       112 FORMAT(' THE VALUE OF THETA IS:', F10.5, /, ' THE EXIT LENGTH IS:',
C           @F10.5, /, ' THE EXIT HEIGHT IS:', F10.5, /, ' THE INLET LENGTH IS:',
C           @F10.5, /, ' THE INLET HEIGHT IS:', F10.5, /, ' THE VALUE OF XLENG:',
C           @F10.5, /, ' THE VALUE OF YLENG IS:', F10.5, /, ' THE NOZZLE WIDTH IS
C           @:', F10.5, /, ' THE NOZZLE HEIGHT IS:', F10.5)
C *****
C CONVERTING THETA TO RADIANS
C *****
```

```

      THETA=THETA*3.141592654/180.0
C *****
C DETERMINING NOZZLE EXIT DEPTH AND LENGTH
C *****
      YEP=(-2.0*XEP*SIN(THETA))/(3.0*COS(THETA)+SIN(THETA)*TAN(THETA))
      XEL=XEP*COS(THETA)-YEP*SIN(THETA)
C *****
C DETERMINING NOZZLE INLET HEIGHT AND LENGTH
C *****
      YIP=(-XIP/3.0*COS(THETA)*TAN(THETA)+XIP*SIN(THETA))/(COS(THETA)+
      @SIN(THETA)*TAN(THETA)/3.0)
      XIL=-XIP*COS(THETA)-YIP*SIN(THETA)
C *****
C DETERMINING CONSTANT VALUE "A" IN CUBIC EQUATION FOR EXIT AND INLET
C *****
      AE=TAN(THETA)/3.0/XEL**2
      AI=TAN(THETA)/3.0/XIL**2
C *****
C WRITING CALCULATED VALUES
C *****
      WRITE(20,114) AE,XEL,YEP,AI,XIL,YIP
      114 FORMAT(' THE VALUE OF AE IS:',F10.5,/, ' THE VALUE OF XEL IS',F10.5
      @,/, ' THE VALUE OF YEP IS:',F10.5,/, ' THE VALUE OF AI IS:',F10.5
      @,/, ' THE VALUE OF XIL IS:',F10.5,/, ' THE VALUE OF YIP IS:',F10.5)
C *****
C CALCULATING X AND Y VALUES FOR NOZZLE EXIT, UNROTATED
C *****
      DO 20 I=1,51
      XXE(I)=(FLOAT(I-1))*XEL/50.0
      YYE(I)=AE*XXE(I)*XXE(I)*XXE(I)
C *****
C CALCULATING X AND Y VALUES FOR NOZZLE EXIT, ROTATED
C *****
      SCALE=YEP/YEP
      XXE(I)=XXE(I)*COS(THETA)+YYE(I)*SIN(THETA)
      20 YYE(I)=(-XXE(I)*SIN(THETA)+YYE(I)*COS(THETA))*SCALE
C *****
C CALCULATING X AND Y VALUES FOR NOZZLE INLET, UNROTATED AND ROTATED
C *****
      SCALE=YIP/YIP
      DO 21 I=1,51
      XXI(I)=(FLOAT(I-1))*XIL/50.0
      YYI(I)=AI*XXI(I)*XXI(I)*XXI(I)
      XXIP(I)=XXI(I)*COS(THETA)+YYI(I)*SIN(THETA)
      YYIP(I)=(-XXI(I)*SIN(THETA)+YYI(I)*COS(THETA))*SCALE
      XI(I)=XXIP(I)*COS(THETA)-YYIP(I)*SIN(THETA)
      21 YI(I)=XXIP(I)*SIN(THETA)+YYIP(I)*COS(THETA)
C *****
C REASSIGNING VARIABLES
C *****
      XXEPL=XXEPL(51)
      XXEPO=XXEPL(1)
      YYEPL=YYEPL(51)
      YYEPO=YYEPL(1)
      WRITE(20,113) XXEPL,XXEPO,YYEPL,YYEPO
      113 FORMAT(' THE LENGTH OF XP IS:',F10.5,/, ' THE START OF XP IS:',F10.
      @5,/, ' THE LENGTH OF YP IS:',F10.5,/, ' THE START OF YP IS:',F10.5)
      115 FORMAT(' THE LAST XP VALUE IS:',F10.5,/, ' THE FIRST XP VALUE IS:',
      @F10.5,/, ' THE LAST YP VALUE IS:',F10.5,/, ' THE FIRST YP VALUE IS:'
      @,F10.5)
C *****
C THIS PART IS USED TO EVALUATE A DIFFERENTIAL EQUATION USING THE
C RUNGE-KUTTA METHOD.

```

```

C VARIABLES:
C XK1 FIRST EVALUATION
C XK2 SECOND EVALUATION
C XK3 THIRD EVALUATION
C XK4 FOURTH EVALUATION
C *****
  XH(1)=0.0
  ARCE(1)=0.0
  DO 180 I=2,51
  XH(I)=XKE(I)-XKE(I-1)
  CALL FUNCT(XKE(I-1),AE,DXDY)
  XK1=XH(I)*DXDY
  CALL FUNCT(XKE(I-1)+0.5*XH(I),AE,DXDY)
  XK2=XH(I)*DXDY
  CALL FUNCT(XKE(I-1)+0.5*XH(I),AE,DXDY)
  XK3=XH(I)*DXDY
  CALL FUNCT(XKE(I-1)+XH(I),AE,DXDY)
  XK4=XH(I)*DXDY
180 ARCE(I)=ARCE(I-1)+(XK1+2.0*XK2+2.0*XK3+XK4)/6.0
  ARCI(1)=0.0
  DO 170 I=2,51
  XH(I)=XXI(I)-XXI(I-1)
  CALL FUNCT(XXI(I-1),AI,DXDY)
  XK1=XH(I)*DXDY
  CALL FUNCT(XKE(I-1)+0.5*XH(I),AI,DXDY)
  XK2=XH(I)*DXDY
  CALL FUNCT(XXI(I-1)+0.5*XH(I),AI,DXDY)
  XK3=XH(I)*DXDY
  CALL FUNCT(XXI(I-1)+XH(I),AI,DXDY)
  XK4=XH(I)*DXDY
170 ARCI(I)=ARCI(I-1)+(XK1+2.0*XK2+2.0*XK3+XK4)/6.0
  WRITE(21,124) XNZWID,XNZHIT
124 FORMAT(' THESE VALUES ARE THE PHYSICAL DIMENSIONS OF THE PIECE OF'
  @,/, ' SHEET METAL TO BE CUT OUT. THE ARC LENGTH REPRESENTS',/, ' THE
  @ LENGTH OF THE METAL, AND "WIDTH" IS ITS',/, ' WIDTH. ALL DIMENSION
  @S ARE IN METRES.',/, ' THE INLET NOZZLE WIDTH IS:',F10.5,/, ' THE IN
  @LET NOZZLE HEIGHT IS:',F10.5,/, 'AXIAL ARC METAL',/,7
  @X, 'LENGTH LENGTH WIDTH',/)
  DO 200 I=1,51
200 WRITE(21,122) I,XKEP(I),ARCE(I),YYEP(I)
122 FORMAT(I5,3F10.3)
C *****
C CONVERTING AND PUTTING THE NOZZLE VALUES IN ANOTHER FILE FOR NAGPLOT
C *****
  DO 251 I=1,51
  XNAG(I)=XXIP(52-I)+1.80
251 YNAG1(I)=YYIP(52-I)+(2.421-0.385)
  DO 252 I=52,101
  XNAG(I)=XKEP(I-50)+1.800
252 YNAG1(I)=YYEP(I-50)+(2.421-0.385)
  DO 253 I=1,101
253 YNAG2(I)=2.421-YNAG1(I)
C 235 WRITE(22,125) XKEP(I),YYEP(I),XXIP(I),YYIP(I)
C 125 FORMAT(4F10.5)
  WRITE(22,126) (XNAG(I),YNAG1(I),YNAG2(I),I=1,101)
126 FORMAT(3F10.5)
C *****
C WRITING HEADINGS FOR PLOTTED VALUES
C *****
  WRITE(20,116)
116 FORMAT(' THESE VALUES ARE THE PHYSICAL DIMENSIONS OF THE NOZZLE, '
  @' FOR EXIT AND INLET, USING ROTATED AXES',/, ' XE(M) YE(
  @M) XI(M) YI(M)')

```

```

DO 120 I=1,51
120 WRITE(20,118) I,XXEP(I),YYEP(I),XXIP(I),YYIP(I)
WRITE(20,119)
119 FORMAT(/,' THESE VALUES ARE THE PHYSICAL DIMENSIONS OF THE NON-ROT
ATED AXES,','/,',' WHERE Y = A*X**3, FOR EXIT AND INLET.','.','/','
@XE(IN) YE(IN) XI(IN) YI(IN)')
118 FORMAT(I5,4F10.5)
DO 190 I=1,51
190 WRITE(20,118) I,XXE(I),YYE(I),XXI(I),YYI(I)
DO 130 I=1,51
130 WRITE(20,118) I,XE(I),YE(I),XI(I),YI(I)
WRITE(20,121)
121 FORMAT(/,' THESE VALUES ARE THE GRAPH COORDINATES FOR THE ROTATED
AXES,','/',' FOR EXIT AND INLET.','.','/',' XEP(IN) YEP(IN) XIP(IN
@) YIP(IN)')
C *****
C SCALING X AND Y VALUES
C *****
DO 30 I=1,51
XXEP(I)=SCALE*(XXEP(I))
YYEP(I)=SCALE*(YYEP(I))
XXIP(I)=SCALE*(XXIP(I))
YYIP(I)=SCALE*(YYIP(I))
C *****
C WRITING DATA TO BE PLOTTED
C *****
30 WRITE(20,118) I,XXEP(I),YYEP(I),XXIP(I),YYIP(I)
STOP
END
SUBROUTINE FUNCT(X,A,DXDY)
C *****
C THIS SUBROUTINE IS FOR CALCULATING THE VALUES FOR USE IN THE
C RUNGE-KUTTA METHOD.
C *****
DXDY=(1.0+9.0*A*A*X*X*X*X)*0.5
RETURN
END

```

Appendix B. FANPER1 FORTRAN

```
C *****
C ***** PERFORATED PLATE CALIBRATION *****
C *****
C THIS PROGRAM CALCULATES THE VELOCITY GIVEN THE TEMPERATURES *
C AND VELOCITY PRESSURE. THIS IS CONVERTED TO A FLOWRATE AND COMPARED *
C TO PRESSURE DROP ACROSS THE PLATE. THE PRESSURE DROP TO CONVERTED *
C TO NOMINAL PRESSURE TO PROPERLY COMPARE DIFFERENT TESTS. *
C CALCULATIONS ARE DONE IN ENGLISH UNITS, AND CONVERTED TO METRIC *
C UNITS FOR PRINTING. *
C *****
C VARIABLES:
C BP BAROMETRIC PRESSURE
C R GAS CONSTANT FOR AIR = 53.35
C VP VELOCITY PRESSURE (DIMENSIONED)
C RHO DENSITY OF ATMOSPHERIC AIR
C BPN NOMINAL BAROMETRIC PRESSURE, =29.921 IN HG.
C TDBN NOMINAL DRY BULB TEMPERATURE, = 68 DEG F.
C TMBN NOMINAL WET BULB TEMPERATURE, = 55 DEG F.
C AREA CROSS-SECTIONAL OF NOZZLE OUTLET
C RHON DENSITY OF AIR AT NOMINAL ATMOSPHERIC CONDITIONS
C SP MEASURED PRESSURE DROP (DIMENSIONED)
C SPC CONVERTED PRESSURE (DIMENSIONED)
C JR READ FORMAT NUMBER (11,12)
C JN WRITE FORMAT NUMBER (21,22)
C JMSAS WRITE FILE FOR SAS INPUT DATA (MEASURED VALUES)
C JMSASC WRITE FILE FOR SAS INPUT DATA (CONVERTED VALUES)
C CP PRESSURE COEFFICIENT
C RE REYNOLDS NUMBER
C XM MACH NUMBER
C *****
REAL TDB(100,2), TMB(100,2), SP(100,2), VP(100,2),RPM(100,2)
REAL BP(100,2), Q(100,2), SPC(100,2), A(2), B(2), AC(2), BC(2)
REAL RE(100,2), CP(100,2), XM(100,2), CPEQ(100,2), CPCONV(100,2)
INTEGER N(2)
DATA A/-0.01375288,-0.00475225/
DATA AC/-0.01358018,-0.00488709/
DATA B/0.00157970,0.00165048/
DATA BC/0.00169191,0.00168978/
C *****
C ** ASSIGNING DEFAULT VALUES FOR PLOTTING
C *****
DO 105 I=1,58
DO 106 J=1,2
RE(I,J)=-1000.0
CP(I,J)=-1000.0
106 XM(I,J)=-1000.0
```

```

105 CONTINUE
    DO 150 J=1,2
        JR=10+J
        DO 100 I=1,1000
            READ(JR,101) SP(I,J),RPM(I,J),VP(I,J),TDB(I,J),TMB(I,J),BP(I,J)
101 FORMAT(F5.3,F7.1,F6.3,F6.2,F6.2,F6.2)
C *****
C **   CORRECTING VELOCITY PRESSURE FOR MICROMANOMETER
C *****
        VP(I,J)=2.0*VP(I,J)
C *****
C **   TERMINATING "READ" STATEMENT AT END OF DATA SET
C *****
        IF(SP(I,J).LE.0.0) GOTO 110
100 CONTINUE
110 N(J)=I-1
150 CONTINUE
C *****
C **   CALCULATING NOMINAL AIR DENSITY
C *****
        R=53.35
        BPN=29.921
        TDBN=68.0
        TMBN=55.0
        PEN=2.96*TMBN*TMBN/10000.0-1.59*TMBN/100.0+0.41
        PPN=PEN-BPN*((TDBN-TMBN)/2700.0)
        RHON=70.73*(BPN-0.378*PPN)/R/(TDBN+459.7)
C *****
C **   CALCULATING ACTUAL AIR DENSITY AND FLOWRATE
C *****
        DO 250 J=1,2
            DO 200 I=1,N(J)
                TDB(I,J)=THERM(TDB(I,J))
200 TMB(I,J)=THERM(TMB(I,J))
            DO 300 I=1,N(J)
                PE=2.96*TMB(I,J)*TMB(I,J)/10000.0-1.59*TMB(I,J)/100.0+0.41
                PP=PE-BP(I,J)*((TDB(I,J)-TMB(I,J))/2700.0)
                RHO=70.73*(BP(I,J)-0.378*PP)/R/(TDB(I,J)+459.7)
                V=1096.0*SQRT(VP(I,J)/RHO)
                AREA=0.886*0.883/0.0254/0.0254/144.0
                Q(I,J)=V*AREA/2118.8
C *****
C **   DETERMINING PRESSURE COEFFICIENT, REYNOLDS AND MACH NUMBERS
C *****
                CP(I,J)=SP(I,J)*5.1985/0.5/RHO*32.174*3600.0/V/V
                XMU=0.000001*(11.00+0.018*TDB(I,J))
                RE(I,J)=V/60.0/12.00*RHO/XMU
                XM(I,J)=V/60.0/SQRT(1.400*BP(I,J)*2116.4/29.921/RHO*32.174)
C *****
C **   CONVERTING CP TO PROVIDE A CONSTANT VALUE FOR OUTLIER CALCULATION
C *****
                CPEQ(I,J)=0.98260464*(SQRT(196.0-(RE(I,J)/9333.0-3.0)**2)-12.0)
                CPCONV(I,J)=2.0*CP(I,J)/CPEQ(I,J)
C *****
C **   CONVERTING MEASURED STATIC PRESSURE DROP TO NOMINAL VALUE
C *****
                SP(I,J)=SP(I,J)*248.8
                SPC(I,J)=SP(I,J)*RHON/RHO
C *****
C **   WRITING OUT DATA FOR SAS FILE (PRESSURE DROP AND FLOWRATE)
C *****
                V=V/60.0/3.28084
                RHO=RHO*16.018

```

```

        WRITE(30,161) Q(I,J),SP(I,J),RHO,V,RE(I,J)
161  FORMAT(F10.5,F10.3,F10.5,F10.5,F10.2)
        JMSAS=J+30
        WRITE(JMSAS,131) SP(I,J),Q(I,J)
        JMSASC=J+40
        WRITE(JMSASC,131) SPC(I,J),Q(I,J)
131  FORMAT(F10.3,F10.5)
C *****
C **    USING THE ESTIMATES OBTAINED FROM SAS (ABOVE)
C *****
C      PCAL=A(J)+B(J)*Q(I,J)**2
C      PCALC=AC(J)+BC(J)*Q(I,J)**2
C      JM=J+20
C      WRITE(JM,121) PCAL,PCALC,SP(I,J),SPC(I,J),Q(I,J)
C 121  FORMAT(4F10.5,F10.1)
300  CONTINUE
250  CONTINUE
C *****
C **    WRITING OUT DATA FOR PLOTTING (PRESSURE DROP AND FLOWRATE)
C *****
        WRITE(20,141) ((RE(I,J),CP(I,J),XM(I,J),J=1,2),I=1,58)
141  FORMAT(F10.2,2F10.5,F10.2,2F10.5)
        WRITE(30,507) ((RE(I,J),CP(I,J),I=1,58),J=1,2)
507  FORMAT(F10.2,F10.5)
        WRITE(22,151) ((SP(I,J),SPC(I,J),Q(I,J),I=1,58),J=1,2)
151  FORMAT(3F10.3)
C      WRITE(20,506) ((CP(I,J),CPEQ(I,J),CPCONV(I,J),I=1,58),J=1,2)
C 506  FORMAT(3F10.4)
        STOP
        END
C *****
C **    CONVERTING TEMPERATURE FROM KILO-OHMS TO DEGREES FAHRENHEIT
C *****
        FUNCTION THERM(T)
          A1=-1926.525+2788.188*T+208.8876*T**2
          IF (A1)300,300,301
300   A1=0.0
301   THM=14.01179*T+86.231552-SQRT(A1)
          THERM = 1.8*THM +32.0
        RETURN
        END

```

Appendix C. PERF FORTRAN

```
C *****
C ** THIS PROGRAM IS USED FOR THE CALIBRATION OF THE RESISTANCE PLATES.
C ** IT PRODUCES THE FLOWRATE-PRESSURE DROP CHARACTERISTICS FOR THE
C ** RESISTANCE PLATES.
C *****
  DIMENSION PD(100,30),SP(100,30),QF(100,30),FS(100,30)
  DIMENSION SPC(100,30),SPCC(100,30)
  DIMENSION SPCM(100,30),SPCCM(100,30)
  DIMENSION REYN(100,30), CP(100,30), XM(100,30), RHOCH(30)
  DIMENSION QFM(100,30), V(100,30), XMU(30), RHOAM(30), RHOBM(30)
  CHARACTER * 12 OPEN
  COMMON/EQZ/PDI,Y,D6,RHX,EN,B,TDBD
  INTEGER PCODE
  EXTERNAL CFACT
C *****
C READING IN NUMBER OF DATA SETS, NOZZLE INLET AND EXIT DIAMETERS,
C AND THE COLLAR NUMBER
C *****
  READ(9,1) NN,D4,D6,NC
  1 FORMAT(40X,I5,/,40X,F10.5,/,40X,F10.5,/,40X,I5,/)
  WRITE(12,124) NN
124 FORMAT(' NUMBER OF DATA SETS:',4X,I5)
  DO 102 JJ=1,NN
  READ(9,2) OPEN,TDBA,TMBA,RHOB,NP
  2 FORMAT(/,40X,A12,/,40X,F10.5,/,40X,F10.5,/,40X,F10.5,/,40X,I5,/)
  TDBA=THERM(TDBA)
  TMBA=THERM(TMBA)
  TDBD=TDBA
  DO 15 I=1,NP
  READ(9,3) FS(I,JJ),SP(I,JJ),PD(I,JJ),SPC(I,JJ)
  3 FORMAT(F10.2,3F10.5)
15 CONTINUE
  PI=3.141592654
  A6=PI*((D6/12)**2)/4.
  NCODE=1
  PCODE=0
  GAMMA=1.4
  PVR=0.
  PT1=0.
  PT3=0.
  IOCODE=0
  N=1

C*****
C*** DETERMINE THE SPECIFIC VOLUME OF THE AMBIENT AIR. ***
C*****
```

```

J=0
RH=THBA
C*****
C*** CONVERT BAROMETRIC PRESSURE FROM IN HG TO PSI ***
C*****
RHOB=RHOB*14.696/29.921
CALL PSYCH(TDBA,THBA,TDP,RH,H,N,PV,PSMB,PSDB,SPV,RHOB,J)
CALL PSYCH(68.0,55.0,TDPC,RHC,HC,MC,PVC,PSMBC,PSDBC,SPVC,14.696,0)

C*****
C*** CALCULATE THE DENSITY OF THE AMBIENT AIR. ***
C*****

RHOA = 1.0/SPV
RHOC = 1.0/SPVC

DO 10 I=1,NP

C*****
C*** CALCULATE THE DENSITY OF AIR IN THE DUCT OR CHAMBER. ***
C*****

RHX= RHOX(RHOA,TDBA,TDBD,SP(I,JJ),RHOB)

C*****
C*** CALCULATE ALPHA RATIO. ***
C*****

R=53.35
A= ALPHA(PD(I,JJ),TDBD,RHX,R)

C*****
C*** CALCULATE BETA RATIO. ***
C*****

B= BETA(D6,D4,NCODE)

C*****
C*** CALCULATE EXPANSION FACTOR. ***
C*****

Y= YFACT(GAMMA,A,B)

C*****
C*** CALCULATE ENERGY FACTOR. ***
C*****

EN=E(NCODE,PVR,N,PCODE)

C*****
C*** CALCULATE REYNOLDS NUMBER AND DISCHARGE COEFFICIENT. ***
C*****

C1=0.945860929
C2=C1+0.01
STEP=0.0005
PDI=PD(I,JJ)
CALL ZEROUT(C1,C2,STEP,CFACT)
C=(C1+C2)/2.0
VIS6=VISCO(TDBD)
RE=REY(C,D6,VIS6,Y,PD(I,JJ),RHX,EN,B)

```

```

C*****
C*** CALCULATE FLOW RATE FOR A DUCTED NOZZLE. ***
C*****

      IF(NCODE)20,20,25
      20 Q=QFOUR(C,A6,Y,PD(I,JJ),RHX,EN,B)
      GO TO 30

C*****
C*** CALCULATE THE FLOW RATE FOR A CHAMBER NOZZLE. ***
C*****

      25 Q = QFIVE(Y,PD(I,JJ),RHX,C,A6,N)

C*****
C*** CALCULATE THE FAN FLOW RATE. ***
C*****

      30 RHF = RHO(RHOA,PT1,PT3,RHOB,TDBA,IOCODE)
      QF(I,JJ) = QFAN(Q,RHX,RHF)
C*****
C*** CONVERT ACTUAL PRESSURE READINGS TO NOMINAL READINGS *****
C*****
      SPCC(I,JJ)=SPC(I,JJ)*RHOC/RHOA

C*****
C*** CONVERT VALUES TO METRIC *****
C*****
      QFM(I,JJ)=QF(I,JJ)/2118.8
      V(I,JJ)=QFM(I,JJ)/0.34/1.16
      SPCM(I,JJ)=SPC(I,JJ)*248.8
      SPCCM(I,JJ)=SPCC(I,JJ)*248.8
      RHOAM(JJ)=RHOA*16.018
      RHOCM(JJ)=RHOC*16.018
      RHOBM(JJ)=RHOB*101325.0/14.969

C*****
C*** CALCULATE VISCOSITY *****
C*****
      TDBAM=(TDBA-32.0)/1.8
      XMU(JJ)=0.000001*(17.23+0.048*TDBAM)

C*****
C*** CALCULATE REYNOLDS NUMBER, PRESSURE COEFFICIENT, MACH NUMBER *****
C*****
      REYN(I,JJ)=RHOAM(JJ)*V(I,JJ)*0.0015/XMU(JJ)
      CP(I,JJ)=SPCM(I,JJ)*2.0/RHOAM(JJ)/V(I,JJ)/V(I,JJ)
      XM(I,JJ)=V(I,JJ)/SQRT((RHOBM(JJ)+SPCM(I,JJ))*1.400/RHOAM(JJ))

C*****
C*** PRINT OUT THE NECESSARY OUTPUT *****
C*****
C
      WRITE(13,112) SPCM(I,JJ), RHOAM(JJ), V(I,JJ), REYN(I,JJ)
112 FORMAT(F10.3,F10.5,F10.5,F10.3)
      10 CONTINUE
      WRITE(20,4) NC
      4 FORMAT(10X,'FLOW DATA FOR COLLAR NO.',I5,/)
      WRITE(10,5) OPEN
      5 FORMAT(' PHYSICAL SETUP OF COLLAR:',A12,/)
      WRITE(10,7)
      7 FORMAT(20X,'NOZZLE',8X,'NOZZLE',8X,'COLLAR',/, ' FLOWRATE',
      26X,'PRESSURE PRESSURE DIFF. PRESSURE DIFF.',/)

```

```

      WRITE(10,11) (QF(I,JJ),SP(I,JJ),PD(I,JJ),SPC(I,JJ),I=1,NP)
11  FORMAT(F12.6,3F14.5)
      WRITE(12,123) NC, OPEN
123  FORMAT(' THESE DATA ARE FOR COLLAR',I2,' ',A12)
      WRITE(12,122) NP
122  FORMAT(' NUMBER OF DATA POINTS: ',I5)
      WRITE(12,121) (QFM(I,JJ),SPCCM(I,JJ),I=1,NP)
121  FORMAT(F10.5,F10.3)
      WRITE(10,8)
      8  FORMAT(///)
102  CONTINUE
C    WRITE(13,113) ((REYN(I,J),CP(I,J),XM(I,J),J=1,NN),I=1,NP)
C 113  FORMAT(F8.3,2F8.5,F8.3,2F8.5,F8.3,2F8.5)
      STOP
      END

```

```

C*****
C*** ALPHA RATIO CALCULATION *****
C*****
C***
C*** THIS FACTOR IS THE RATIO OF ABSOLUTE NOZZLE EXIT PRESSURE TO ***
C*** ABSOLUTE APPROACH PRESSURE. ***
C***
C*****
C***
C*** INPUT VARIABLES: ***
C*** 1. DELP = PRESSURE DIFFERENTIAL ACROSS THE NOZZLE, IN. WATER. ***
C*** 2. TDX = DRY-BULB TEMPERATURE IN PLANE -X, DEGREES FARENHEIT. ***
C*** PLANE-X IS PLANE-4 FOR DUCT APPROACH, OR PLANE-5 FOR ***
C*** CHAMBER APPROACH. ***
C*** 3. RHX = FAN AIR DENSITY,IB/CU.FT. ***
C*** 4. R = GAS CONSTANT, 53.35 (FT-LB)/(LB R) FOR AIR ***
C***
C*****
C***
C*** RETURNED VARIABLE: ***
C*** 1. ALPHA = DIMENSIONLESS. ***
C***
C*****

```

```

      FUNCTION ALPHA(DELP,TDX,RHX,R)
      F1=5.187*DELP
      F2= RHX*R*(TDX+459.7)
      ALPHA= 1 - F1/F2
      RETURN
      END

```

```

C*****
C*** DUCT OR CHAMBER AIR DENSITY *****
C*****
C***
C*** PURPOSE: ***
C*** CALCULATES THE DENSITY OF AIR AT PLANE-X. IF THE STATIC ***
C*** PRESSURE AT PLANE-X IS LESS THAN 4 IN. WATER, THEN RHX=RHOA. ***
C***
C*****
C***
C*** INPUT VARIABLES: ***
C*** 1. RHOA = DENSITY OF ATMOSPHERIC AIR, LB/CU. FT. ***
C*** 2. TDO = DRY-BULB TEMPERATURE OF ATMOSPHERIC AIR, DEGREES ***
C*** FARENHEIT. ***
C*** 3. TDX = DRY-BULB TEMPERATURE AT PLANE-X, DEGREES FARENHEIT. ***
C*** PLANE-X IS PLANE-4 FOR A DUCT APPROACH, OR PLANE-5 FOR A ***

```

```

C***    CHAMBER APPROACH.                               ***
C***    4. PSX = FAN STATIC PRESSURE, IN. WATER.       ***
C***    5. RHOB = BAROMETRIC PRESSURE, IN. MERCURY.    ***
C***                                           ***
C*****
C***
C***    RETURNED VARIABLE:                             ***
C***    1. RHOX = LB/CU.FT.                           ***
C***                                           ***
C*****

```

```

FUNCTION RHOX(RHOA,TDO,TDX,PSX,RHOB)
  F1= (TDO+459.7)/(TDX+459.7)
  F2= (PSX+13.63*RHOB)/(13.63*RHOB)
  RHOX= RHOA*F1*F2
  IF (PSX.LE.4.0)RHOX=RHOA
RETURN
END

```

```

C*****
C***    BETA RATIO *****
C***                                           ***
C*****
C***
C***    INPUT VARIABLES:                               ***
C***    1. D6 = DIAMETER OF NOZZLE DISCHARGE STATION,FT. ***
C***    2. D4 = DIAMETER OF DUCT PIEZOMETER STATION,FT. ***
C***    3. NCODE = NOZZLE CODE INDICATING DUCT APPROACH OR CHAMBER ***
C***    APPROACH.                                     ***
C***          A. NCODE = 0 : DUCT APPROACH            ***
C***          B. NCODE = 1 : CHAMBER APPROACH         ***
C***                                           ***
C*****
C***
C***    RETURNED VARIABLE:                             ***
C***    1. BETA = DIMENSIONLESS                       ***
C***                                           ***
C***
C*****

```

```

FUNCTION BETA(D6,D4,NCODE)
  IF (NCODE) 2,2,3
2  DX=D4
  BETA=D6/DX
  RETURN
3  BETA=0
RETURN
END

```

```

C*****
C***    ENERGY FACTOR *****
C***                                           ***
C***    DETERMINE THE VELOCITY PRESSURE UPSTREAM OF THE NOZZLE AT THE ***
C***    STANDARD TRAVERSE STATIONS. SUFFICIENT ACCURACY FOR THIS ***
C***    STANDARD CAN BE OBTAINED FOR SETUPS QUALIFYING UNDER THIS ***
C***    STANDARD BY SETTING E=1.0 FOR CHAMBER APPROACH, E=1.043 FOR ***
C***    DUCT APPROACH.                                 ***
C*****
C***
C***    INPUT VARIABLES:                               ***
C***    1. NCODE = NOZZLE CODE INDICATING DUCT APPROACH OR CHAMBER ***
C***    APPROACH.                                     ***
C***          A. NCODE = 0 : DUCT APPROACH            ***

```

```

C***      B. NCODE = 1 : CHAMBER APPROACH      ***
C***  2. PVR = AN ARRAY CONTAINING N VELOCITY PRESSURE READINGS FROM ***
C***      AN UPSTREAM TRAVERSE STATION.      ***
C***                                           ***
C*****
C***
C*** RETURNED VARIABLE:                       ***
C***  1. E = ENERGY FACTOR, DIMENSIONLESS   ***
C***                                           ***
C*****

```

```

      FUNCTION E(NCODE,PVR,N,PCODE)
C      DIMENSION PVR(N)
C      IF (PCODE) 1,1,2
C
C
CC      *****
CC      *** SUM UP MEASURED VELOCITY PRESSURE FACTORS. *****
CC      *****
C
C      PVR1=0.
C      PVR2 = 0.
C      DO 10 I = 1,N
C          PVR1 = PVR1 + PVR(I)**1.5
C          PVR2 = PVR2 + PVR(I)**0.5
C 10      CONTINUE
C      E = (PVR1/N)/(PVR2/N)**3
C      RETURN
C 1      IF (NCODE)3,3,4
C 3      E = 1.043
C      RETURN
C 4      E = 1.0
C      RETURN
C      END

```

```

C*****
C*** EXPANSION FACTOR *****
C***                                           ***
C*****
C*** INPUT VARIABLES:                       ***
C***  1. GAMMA = RATIO OF SPECIFIC HEATS, DIMENSIONLESS. ***
C***  2. ALPHA = RATIO OF ABSOLUTE NOZZLE EXIT PRESSURE TO ***
C***      ABSOLUTE NOZZLE APPROACH PRESSURE, DIMENSIONLESS. ***
C***  3. BETA = RATIO OF NOZZLE EXIT DIAMETER TO APPROACH DUCT ***
C***      DIAMETER, FEET. ***
C***                                           ***
C*****
C*** RETURNED VARIABLES :                   ***
C***  1. Y = EXPANSION FACTOR, DIMENSIONLESS. ***
C***                                           ***
C*****

```

```

      FUNCTION YFACT(GAMMA,ALPHA,BETA)
      F1 = GAMMA/(GAMMA-1.)
      F2 = ALPHA ** (2./GAMMA)
      F3 = 1. - ALPHA**((GAMMA-1.)/GAMMA)
      F4 = 1. - ALPHA
      F5 = (F1*F2*F3/F4)**0.5
      F1 = 1. - BETA**4
      F2 = 1. - (BETA**4) * (ALPHA** (2./GAMMA))
      F3 = (F1/F2)**0.5
      YFACT = F3*F5

```

RETURN
END

```
C*****  
C*** REYNOLDS NUMBER *****  
C*****  
C*** PURPOSE: ***  
C*** AN APPROXIMATION FOR THE REYNOLDS NUMBER IS DESCRIBED BY THIS ***  
C*** FUNCTION. ***  
C*****  
C*** INPUT VARIABLES: ***  
C*** 1. C = DISCHARGE COEFFICIENT, DIMENSIONLESS. ***  
C*** 2. D6 = DIAMETER OF THE DUCT AT STATION 6, FT. ***  
C*** 3. VIS6 = VISCOSITY OF THE AIR AT STATION 6, LB/(FT-S). ***  
C*** 4. Y = EXPANSION FACTOR, DIMENSIONLESS. ***  
C*** 5. PD = PRESSURE DROP ACROSS THE NOZZLE, IN. WATER. ***  
C*** 6. RHOX = DENSITY OF THE AIR AT STATION X, LB/CU.FT. ***  
C*** 7. E = ENERGY FACTOR, DIMENSIONLESS. ***  
C*** 8. BETA = BETA RATIO, DIMENSIONLESS. ***  
C*** ***  
C*****  
C*** RETURNED VARIABLE : ***  
C*** 1. REY = REYNOLDS NUMBER, DIMENSIONLESS. ***  
C*** ***  
C*****
```

```
FUNCTION REY(C,D6,VIS6,Y,PD,RHOX,E,BETA)  
  F1 = 1096./(60.*VIS6)  
  F2 = C*D6*Y  
  F3 = (PD*RHOX)/(1.-E*BETA**4)  
  REY = (F1*F2*F3**0.5)  
RETURN  
END
```

```
C  
FUNCTION CFACT(C)  
COMMON/EQZ/PD,Y,D6,RHX,EN,B,TDBD  
VIS6=VISCO(TDBD)  
RE= REY(C,D6,VIS6,Y,PD,RHX,EN,B)  
CNEW= 0.9986-7.006/(SQRT(RE))+134.6/RE  
CFACT = CNEW-C  
RETURN  
END
```

```
C*****  
C*** FLOW RATE FOR A DUCTED NOZZLE *****  
C*****  
C*** PURPOSE: ***  
C*** CALCULATES THE VOLUME FLOW RATE AT THE ENTRANCE OF A DUCTED ***  
C*** NOZZLE. ***  
C*** ***  
C*****  
C*** INPUT VARIABLES: ***  
C*** 1. C = DISCHARGE COEFFICIENT, DIMENSIONLESS. ***  
C*** 2. A6 = THROAT AREA AT STATION 6, SQ. FT. ***  
C*** 3. Y = EXPANSION FACTOR, DIMENSIONLESS. ***  
C*** 4. PD = PRESSURE DROP ACROSS NOZZLE, IN. WATER. ***  
C*** 5. RHO4 = AIR DENSITY AT STATION 4, LB/CU.FT. ***  
C*** 6. E ENERGY FACTOR, DIMENSIONLESS. ***  
C*** 7. BETA = BETA FACTOR, DIMENSIONLESS. ***  
C*** ***
```

```

C*****
C***
C*** RETURNED VARIABLE: ***
C*** 1. QFOUR = VOLUME FLOW RATE AT THE ENTRANCE OF THE DUCTED ***
C*** NOZZLE, CFM. ***
C*** ***
C*****

```

```

FUNCTION QFOUR(C,A6,Y,PD,RHO4,E,BETA)
  F1 = 1096 * C * A6 * Y
  F2 = (PD/RHO4)**0.5
  F3 = (1 - E * BETA**4)**0.5
  QFOUR = F1 * F2 / F3
RETURN
END

```

```

C*****
C*** FLOW RATE FOR A CHAMBER NOZZLE *****
C*****
C*** PURPOSE: ***
C*** 1. Y = EXPANSION COEFFICIENT, DIMENSIONLESS. ***
C*** 2. PD = PRESSURE DROP ACROSS NOZZLE, IN. WATER. ***
C*** 3. RHO5 = DENSITY OF AIR AT STATION 5, LB/ CU.FT. ***
C*** 4. C = AN ARRAY OF DISCHARGE COEFFICIENTS, DIMENSIONLESS. ***
C*** 5. A6 =THROAT AREA AT STATION 6 , SQ.FT. ***
C*** ***
C*****
C***
C*** RETURNED VARIABLE: ***
C*** 1. QFIVE = VOLUME FLOW RATE AT THE ENTRANCE OF NOZZLE(S) WITH ***
C*** A CHAMBER APPROACH, CFM. ***
C*** ***
C*****

```

```

FUNCTION QFIVE(Y,PD,RHO5,C,A6,N)
  DIMENSION C(N),A6(N)
  SUM = 0.
  DO 10 I=1,N
    SUM = SUM + C(I) * A6(I)
10 CONTINUE
  F1 = 1096 * Y
  F2 = (PD/RHO5)**0.5
  QFIVE = F1 * F2 * SUM
RETURN
END

```

```

C*****
C*** FAN AIR DENSITY *****
C*****
C*** PURPOSE: ***
C*** 1. RHOA = DENSITY OF ATMOSPHERIC AIR, LB/CU.FT. ***
C*** 2. PT1 = TOTAL PRESSURE AT THE FAN INLET, IN. WATER. ***
C*** 3. TT1 = TOTAL TEMPERATURE AT THE FAN INLET, DEGREES FARENHEIT.***
C*** 4. RHOB = BAROMETRIC PRESSURE, IN. MERCURY. ***
C*** 5. TDBA = AMBIENT DRY-BULB TEMPERATURE, DEGREES FARENHEIT. ***
C*** 6. IOCODE = DUCT OR CHAMBER SETUP CODE. ***
C*** A. IOCODE = 0 : PT1 = 0. AND TT1 = TDBA ***
C*** B. IOCODE = 1 : PT1 = PT3 AND TT1 = TDBA ***
C*****
C***
C*** RETURNED VARIABLE: ***
C*** 1. RHO = FAN AIR DENSITY, LB/CU.FT. ***

```

```
C***
C*****
```

```
FUNCTION RHO(RHOA,PT1,PT3,RHOB,TDBA,IOCODE)
  IF (IOCODE) 1,1,2
1  F1 = (PT1 + 13.63 * RHOB)/(13.63 * RHOB)
  TT1 = TDBA
  F2 = (TDBA + 459.7)/(TT1 + 459.7)
  RHO = RHOA * F1 * F2
  RETURN
2  F1 = ( PT3 * 13.63 * RHOB )/( 13.63 * RHOB )
  TT1 = TDBA
  F2 = (TDBA + 459.7)/(TT1 + 459.7)
  RHO = RHOA * F1 * F2
  RETURN
END
```

```
C*****
C*** FAN FLOW RATE *****
C*****
C*** PURPOSE: ***
C*** FLOW CALCULATION FROM THE EQUATIONS OF CONTINUITY. ***
C*** ***
C*****
C*** ***
C*** INPUT VARIABLES: ***
C*** 1. QX = FAN FLOW RATE AT STATION X, CFM. ***
C*** 2. RHOX = DENSITY OF AIR AT STATION X, LB/CU.FT. ***
C*** 3. RHO = DENSITY OF FAN AIR, LB/CU.FT. ***
C*** ***
C*****
C*** ***
C*** RETURNED VARIABLES: ***
C*** 1. QFAN = FAN FLOW RATE, CFM. ***
C*** ***
C*****
```

```
FUNCTION QFAN(QX,RHOX,RHO)
  QFAN = QX * RHOX / RHO
  RETURN
END
```

```
SUBROUTINE ZEROUT(A, B, EPS, FUNC)
C  UPDATE 8/17/76.
C  RANGE SELECTOR ADDED.
  REAL I, M
  IC = 0
  D = B - A
20 CONTINUE
  IF(IC.GE.50) GO TO 30
  FA = FUNC(A)
  FB = FUNC(B)
  FC = FA
  C = A
  IF(SIGN(1.,FB).NE.SIGN(1.,FC)) GO TO 1
  IC = IC + 1
  IF(ABS(FA).GT.ABS(FB)) GO TO 21
  B = A + (2*EPS)
  A = A - D
  GO TO 20
30 CONTINUE
  WRITE(9,100) IC,A,B,FA,FB
100 FORMAT(1X,'ZEROUT CANT FIND A RANGE IN',I2,' ITERATIONS, LIMITS
```

```

      $=' ,2F12.6,' FUNCTION VALUES = ',2F12.6)
      RETURN
21  CONTINUE
      A = B - (2*EPS)
      B = B + D
      GO TO 20
1  IF(ABS(FC) - ABS(FB)) 2, 3, 3
2  C = B
      B = A
      A = C
      FC = FB
      FB = FA
      FA = FC
3  IF(ABS(C-B)-2.*EPS) 12,12,4
4  M=(C+B)/2.0
      DIV=FB-FA
      IF(DIV.EQ.0.) GO TO 7
      CALL OVERFL(IREG)
      I=(B-A)*FB/DIV
      CALL OVERFL(IREG)
      IF(IREG.NE.2) GO TO 7
5  I = -I + B
      CHINT = (B - I) * (M - I)
      IF(CHINT) 8, 8, 7
7  I = M
8  IF(ABS(B-I) - EPS) 9, 10, 10
9  I = SIGN(1.,(C-B)) * EPS + B
10 A = B
      B = I
      FA = FB
      FB = FUNC(B)
      IF(SIGN(1.,FB) - SIGN(1.,FC)) 1, 11, 1
11 C = A
      FC = FA
      GO TO 1
12 A = (C + B)/2.0
      FA = FUNC(A)
      IF(SIGN(1.,FA).EQ.SIGN(1.,FB)) B=C
      RETURN
      END

      FUNCTION VISCO(T)
      REAL VISCO
      VISCO=(11.00+0.018*T)*1E-06
      RETURN
      END

      SUBROUTINE PSYCH(TDB,TWB,TDP,RH,ENTH11,HUAB8,PV,PSNB,PSDB,
      *SPVOL,PATM,J)
      C PSYCH IS BASED ON THE EQUATIONS PRESENTED BY
      C D. B. BROOKER,PROFESSOR
      C DEPARTMENT OF AGRICULTURAL ENGINEERING
      C MICHIGAN STATE UNIVERSITY
      C LECTURE NO.2, INSTITUTE FOR SIMULATION OF COOLING AND DRYING OF AG
      C PRODUCTS, NOVEMBER 2-4,1970
      DOUBLE PRECISION A(10)
      DATA A/.3515789D02,.24592588D02,.21182069D01,-.3414474D00,
      *.15741642D00,-.31329585D-01,.38658282D-02,-.24901784D-03,
      *.68401559D-05,0.0D00/
      C J=0,DATA INPUT MUST BE DRY + WET BULB TEMPERATURES.
      C J=1,DATA INPUT MUST BE DRY BULB + DEW POINT TEMPERATURES.
      C J=2,DATA INPUT MUST BE DRY BULB TEMPERATURE & DECIMAL RELATIVE HUMI
      C J=3,DATA INPUT MUST BE DRY BULB TEMPERATURE& ABSOLUTE HUMIDITY (HUA

```

```

00004420
00004430
00004440
00004450
00004460
00004470
00004480
00004500
00004530
00004540
00004550
00004560

```

```

      IF(J.EQ.0.0.AND.TDB.LT.TNB)WRITE(9,10)TDB,TNB
      IF(J.EQ.1.0.AND.TDP.GT.TDB)WRITE(9,11)TDB,TDP
      IF(J.EQ.2.0.AND.RH.GT.1.)WRITE(9,12)RH
10  FORMAT(' ','TEMPERATURES ARE INCONSISTENT WITH PSYCHROMETRIC CHART',00004630
      * TEMP. DRY BULB=',E15.7/' ','TEMP. NET BULB=',
      *E15.7,2X,'COMPUTATION TRIED')
      00004640
11  FORMAT(1H ,'TEMPERATURES ARE INCONSISTENT WITH PSYCHROMETRIC',
      *' CHART,DRY BULB TEMPERATURE = ',E15.7/1H ,'DEW POINT ',
      *'TEMPERATURE = ',E15.7,2X,'COMPUTATION TRIED')
      00004650
12  FORMAT(1H ,'DECIMAL RELATIVE HUMIDITY IS REQUIRED FOR PSYCH INPUT',00004690
      *RELATIVE HUMIDITY = ',E15.7,2X,'COMPUTATION TRIED')
      TDB=TDB+459.69
      00004710
      IF(J.EQ.0)TNB=TNB+459.69
      IF(J.EQ.1)TDP=TDP+459.69
C *****
C ATMOSPHERIC PRESSURE MUST BE FED IN SEPARATELY
C *****
C
      PATM=14.646
      PSDB=PS(TDB)
      00004740
      IF(J.LT.3) GO TO 16
      00004750
      PV=PATM*(HUAB8/(0.6219+HUAB8))
      00004760
      GO TO 21
      00004770
16  CONTINUE
      00004780
      IF (J-1) 19,101,201
      00004790
19  CONTINUE
      00004800
      HVAP=HFG(TNB)
      00004810
      PSNB=PS(TNB)
      00004820
      B7=0.2405*(PSNB-PATM)/(0.6219*HVAP)
      00004830
      PV=B7*(TDB-TNB)+PSNB
      00004840
      KOUNT=0
      00004850
      DELTA=1.
      00004860
18  X=PV
      00004870
      B7=.2405*(PSNB-PATM)*(1.+1.15577*PV/PATM)/(0.6219*HVAP)
      00004880
      PV=B7*(TDB-TNB)+PSNB
      00004890
      Y=PV
      00004900
      DEL=Y-X
      00004910
      IF(ABS(DEL).LT.0.1) GO TO 21
      00004920
      KOUNT=KOUNT+1
      00004930
      IF(KOUNT.GT.20) GO TO 21
      00004940
      IF(DEL) 17,21,20
      00004950
17  CONTINUE
      00004960
      IF(TDB-671.69) 121,122,122
      00004970
121 DELTA=DELTA/2.
      00004980
121 PV=PV-DELTA
      00004990
      GO TO 18
      00005000
20  CONTINUE
      00005010
      IF(TDB-671.69) 123,120,120
      00005020
123 DELTA=DELTA/2.
      00005030
120 PV=PV+DELTA
      00005040
      GO TO 18
      00005050
21  CONTINUE
      00005060
      SUM=0.
      00005070
      DO 30 I=1,9
      00005080
      SUM=A(I)*(ALOG(10*PV))**(I-1)+SUM
      00005090
30  CONTINUE
      00005100
      TDP=SUM+459.69
      00005110
      IF (J-1) 25,25,101
      00005120
25  CONTINUE
      00005130
      IF(J.EQ.2)GO TO 35
      00005140
      RH=PV/PSDB
      00005150
35  CONTINUE
      00005160
      HVAPDP=HFG(TDP)
      00005170
      IF(J.EQ.3) GO TO 36
      00005180
      00005190

```

```

      HUAB8=0.6219*PV/(PATH-PV)                                00005200
36  CONTINUE                                                  00005210
      ENTH11=0.2405*(TDB-459.69)+HUAB8*(TDP-491.69)+HVAPDP*HUAB8+0.448 00005220
      ***(TDB-TOP)*HUAB8                                       00005230
      SPVOL=53.35*TDB/(144.*(PATH-PV))                        00005240
      TDB=TDB-459.69                                          00005250
      THB=THB-459.69                                          00005260
      TDP=TDP-459.69                                          00005270
      GO TO 500                                                00005280
201 PV=RH*PSDB                                               00005290
      GO TO 21                                                 00005300
101 CONTINUE                                                  00005310
      DELTA=5.                                                 00005320
      IF (J-2) 106,105,105                                    00005330
106 CONTINUE                                                  00005340
      PV=PS(TDP)                                              00005350
105 CONTINUE                                                  00005360
      THB=TDP                                                 00005370
      KOUNT=0                                                  00005380
102 PSMB=PS(THB)                                             00005390
      HVAPMB=HFG(THB)                                         00005400
      B7=(0.2405*(PSMB-PATH)*(1.+0.15577*PV/(PATH)))/(0.62194*(HVAPMB)) 00005410
      DEL=PSMB-PV-B7*(THB-TDB)                                00005420
      X=ABS(DEL)                                               00005430
      KOUNT=KOUNT+1                                           00005440
      IF(KOUNT.GT.20) GO TO 104                                00005450
      IF(X.LT.0.001) GO TO 104                                00005460
      IF (DEL.GT.0.0) GO TO 103                                00005470
      THB=THB+DELTA                                           00005480
      GO TO 102                                                00005490
103 DELTA=DELTA/2.                                           00005500
      THB=THB-DELTA                                           00005510
      GO TO 102                                                00005520
104 CONTINUE                                                  00005530
      GO TO 25                                                 00005540
500 RETURN                                                    00005550
      END                                                       00005560
      FUNCTION HFG(T)                                          00005670
      IF(T-609.49) 1,2,2                                       00005680
1  CONTINUE                                                    00005690
      HFG=1075.8965-0.56983*(T-491.69)                       00005700
      GO TO 3                                                  00005710
2  CONTINUE                                                    00005720
      HFG=(1354673.214-.9125275587*T**2)**.5                00005730
3  CONTINUE                                                    00005740
      RETURN                                                    00005750
      END                                                       00005760
      FUNCTION PS(T)                                           00005570
      REAL*8 AA,BB,CC,DD,EE,FF,GG,RR,L2                      00005580
      DATA AA,BB,CC,DD,EE,FF,GG,RR/                          00005590
      *-.2740552583614256D05,.5418960763289505D02,-.4513703841126545 00005600
      *D-01,.2153211916363544D-04,-.4620266568199822D-08,.24161272098 00005610
      *74D01,.1215465167060546D-02,.3206182232D04/          00005620
      L2=(AA+BB*T+CC*T**2+DD*T**3+EE*T**4)/(FF*T-GG*T**2)    00005630
      PS=RR*DEXP(L2)                                           00005640
      RETURN                                                    00005650
      END                                                       00005660
      FUNCTION THERM(T)
      A1=-1926.525+2788.188*T+208.8876*T**2
      IF (A1)300,300,301
300  A1=0.
301  THM=14.01179*T+86.231552-SQRT(A1)
      THERM = 1.8*THM +32.

```

RETURN
END

Appendix D. FIELD FORTRAN

```
C *****
C THIS PROGRAM TAKES THE FIELD DATA FROM FILES "TEST1 DATA",
C "TEST2 DATA", ETC., CALCULATES THE TOTAL FLOW FROM BOTH THE
C PERFORATED PLATE AND THE RESISTANCE PLATES, WITH THE DIFFERENCE
C ASSUMED TO BE LEAKS.
C *****
C VARIABLES:
C FN      FAN NUMBER: 1, 2, 3, OR 4
C IFAN    = 0 SUPPLY FAN NOT CONNECTED
C         = 1 SUPPLY FAN CONNECTED
C A       CHARACTER VARIABLES FOR INDICATING IF THE SUPPLY FAN IS
C         CONNECTED
C NS      NUMBER OF DATA SETS IN THE DATA FILE
C TDB     DRY BULB TEMPERATURE
C TWB     WET BULB TEMPERATURE
C BP      BAROMETRIC PRESSURE
C PC      POWER CONSUMPTION (COUNTS)
C PAVG    AVERAGE POWER CONSUMPTION (W)
C CMS     RATE OF AIR DELIVERED PER WATT CONSUMED (CMS/W)
C NC      RESISTANCE PLATE/COLLAR NUMBER
C SP      FIELD STATIC PRESSURE DROP ACROSS RESISTANCE PLATE
C SPC     NOMINAL STATIC PRESSURE DROP ACROSS RESISTANCE PLATE
C PP      PRESSURE ACROSS PERFORATED PLATE
C COEFF, POWER CALIBRATION EQUATION FOR RESISTANCE PLATES
C         FLOWRATE = (COEFF) * (PRESSURE DROP) ** POWER
C PERCNT  PERCENTAGE OF TOTAL FLOW EXPECTED THROUGH EACH OPEN PORT
C DIST    DEVIATION FROM IDEAL DISTRIBUTION
C *****
C         DIMENSION TDB(10), TWB(10), BP(10), PC(10), NC(8), SP(8), PP(10)
C         DIMENSION COEFF(8), POWER(8), SPC(8), QP(8), A1(4), A2(4), A3(4)
C         DIMENSION QPP(12), PPC(12), DIST(12)
C         CHARACTER*4 A(6)
C         DATA COEFF/8.89736818,8.93103311,8.89655544,8.88607375,
C         @8.89829157,8.90915799,8.91194094,8.83722721/
C         DATA COEFF/8.84395632,8.89401234,8.84443226,8.87042217,
C         @8.86477835,8.89018623,8.91194094,8.83722721/
C         DATA POWER/0.56265125,0.57878644,0.58034214,0.57240255,
C         @0.57835229,0.58445595,0.56912708,0.58179422/
C         DATA POWER/0.58224733,0.59312914,0.57525538,0.57634379,
C         @0.57721153,0.58042228,0.56912718,0.58179454/
C *****
C METRIC CALIBRATION, BOTH CALIBRATIONS
C *****
C         DATA COEFF/0.15458401,0.14625929,0.15014193,0.14483758,
C         @0.14188633,0.13868738,0.15137566,0.13096234/
C         DATA COEFF/0.13152115,0.13021348,0.13674926,0.13952726,
```

```

    20.13807927,0.13914901,0.15137566,0.13096234/
C   DATA POWER/0.56266553,0.57880094,0.56630972,0.57242071,
C   20.57836814,0.58442054,0.56910403,0.58181686/
    DATA POWER/0.58226640,0.59312951,0.57529078,0.57635361,
    20.57723179,0.58042739,0.56910403,0.58181686/
C *****
C THIS NUMBERS ARE THE VALUES FOR THE CONSTANTS IN THE EQUATION
C   Q = A1 + A2*P + A3*P**2
C FOR THE 10 AND 15 HP AEROVENT FANS AND THE 7.5 AND 10 HP LONG FANS
C *****
    DATA A1/37.85657123,33.43747399,27.31282216,34.13886281/
    DATA A2/-5.35295538,-5.03528146,-3.21891456,-5.95277016/
    DATA A3/-0.82467563,-1.39133090,-0.63144979,-0.93868048/
C *****
C ** READING IN FAN NUMBER, IF CONNECTED, AND NUMBER OF DATA SETS **
C *****
    READ(10,101) NF, (A(I),I=1,6),IFAN,NS,NG
    101 FORMAT(40X,I5,/,6A4,16X,I5,/,40X,I5,/,40X,I5,/)
    WRITE(20,102) NF, (A(I),I=1,6),NS
    102 FORMAT(' THIS IS FOR FAN #',I1,' WITH THE ',6A4,/, ' CONSISTING OF'
    2,I2,' DATA SETS',/)
    DO 100 J=1,NS
    READ(10,151)
    151 FORMAT(/)
    WRITE(20,112)
    112 FORMAT(' COLLAR',7X,' PRESSURE DROP',20X,'PERCENT',5X,'PERCENT',
    2/, ' NUMBER',4X,'MEASURED',3X,'CONVERTED',
    24X,'FLOWRATE',6X,'TOTAL',5X,'DEVIATION',/,70('-'))
C *****
C ** READING IN TEMPERATURES, BAROMETRIC PRESSURE AND POWER CONSUMED **
C *****
    READ(10,111) TDB(J), TMB(J), BP(J), PC(J)
    111 FORMAT(40X,F10.3,/,40X,F10.3,/,40X,F10.2,/,40X,F10.1,/)
C *****
C ** READING IN COLLAR NUMBER AND ASSOCIATED PRESSURE DROP **
C *****
    READ(10,121) (NC(I),SP(I),I=1,NG)
    121 FORMAT(I5,8X,F10.3)
    DO 109 I=1,NG
    109 SP(I)=SP(I)*248.8
C *****
C ** READING IN PRESSURE DROP ACROSS PERFORATED PLATE **
C *****
    IF(IFAN.EQ.0) GOTO 104
    READ(10,141) PP(J)
    141 FORMAT(/,40X,F10.3)
    PP(J)=PP(J)*248.8
    GOTO 103
    104 READ(10,151)
C *****
C ** DETERMINING NOMINAL AIR VALUES, AND FIELD VALUES **
C *****
    103 CALL PSYC(1,20.0,12.778,VSA,101325.0)
    RHOC=1.0/VSA
    BP(J)=BP(J)*101325.0/29.921
    TDB(J)=THERM(TDB(J))
    TMB(J)=THERM(TMB(J))
    CALL PSYC(1,TDB(J),TMB(J),VSA,BP(J))
    RHOA=1.0/VSA
C *****
C** DETERMINING INDIVIDUAL AND TOTAL FLOWRATES USING SIMULATORS **
C** AFTER CONVERTING MEASURED PRESSURES TO STANDARD PRESSURES **
C *****

```

```

TOTQP=0.0
II=0
DO 200 I=1,NG
SPC(I)=SP(I)*RHOC/RHOA
IF(SPC(I).GT.25.0) II=II+1
PPC(J)=PP(J)*RHOC/RHOA
QP(I)=(COEFF(I))*SPC(I)**POWER(I)
TOTQP=TOTQP+QP(I)
200 CONTINUE
PERCNT=100.0/FLOAT(II)
DO 600 I=1,NG
QPP(I)=QP(I)/TOTQP*100.0
IF(SPC(I).LT.25.0) DIST(I)=0.0
IF(SPC(I).GT.25.0) DIST(I)=(QPP(I)-PERCNT)/PERCNT*100.0
600 CONTINUE
C*****
C** DETERMINING TOTAL FLOWRATE FROM PERFORATED PLATE USING  $\rho=KQ^{**2}$ 
C** TO ESTIMATE USING REYNOLDS NUMBER AND PRESSURE COEFFICIENT
C*****
WRITE(20,131) (NC(I),SP(I),SPC(I),QP(I),QPP(I),DIST(I),I=1,NG)
131 FORMAT(15,5X,F10.3,2X,F10.3,1X,F10.5,5X,F7.2,4X,F7.2)
WRITE(20,181)
181 FORMAT(36X,7(' '),6X,6(' '))
WRITE(20,191) TOTQP
191 FORMAT(28X,'TOTAL',F10.5,5X,' 100.00')
IF (IFAN.EQ.0) GOTO 105
TOTQ=SQRT((PPC(J))/1.9188)
C*****
C** DETERMINING TOTAL FLOWRATE FROM PERFORATED PLATE USING CP AND RE
C*****
XMU=0.000001*(17.23+0.048*TDB(J))
V1=TOTQ
113 V=V1
RE=V*0.0254*RHOA/XMU
CP=1.8308-RE*5.5625E-06+RE*RE*8.5454E-10-RE*RE*RE*1.6679E-14
V1=SQRT(2.0*PP(J)/RHOA/CP)
IF(ABS(V1-V).GT.0.005) GOTO 113
QCPRE=V*0.883*0.886
QLEAK=TOTQ-TOTQP
WRITE(20,201) TOTQ
201 FORMAT(' TOTAL FLOW FROM PERFORATED PLATE',F10.6)
WRITE(20,202) QCPRE
202 FORMAT(' TOTAL FLOW FROM DIMENSIONALLESS ',F10.6)
WRITE(20,211) QLEAK
211 FORMAT(' TOTAL LEAKAGE ',F10.6)
105 CONTINUE
C*****
C** DETERMINING TOTAL POWER CONSUMED AND AIR DELIVERED PER WATT **
C*****
PAVG=PC(J)*5.0*60.0/5.0*2.0
PAVGC=PAVG*RHOC/RHOA
CFM=TOTQP/PAVG
CFMC=TOTQP/PAVGC
WRITE(20,555) PAVG
555 FORMAT(/,' THE AVERAGE POWER CONSUMED DURING 5 MINUTE INTERVAL',
@F10.3, ' W')
WRITE(20,556) PAVG
556 FORMAT(43X,'CONVERTED',F10.3, ' W')
WRITE(20,557) CFM
557 FORMAT(/,' THE AVERAGE AMOUNT OF AIR DELIVERED DURING INTERVAL',
@F10.7, ' CMS/W')
WRITE(20,558) CFMC

```

```

558 FORMAT(43X,'CONVERTED',F10.7, ' CMS/W' )
C*****
C** ESTIMATING PRESSURE DROP ACROSS FAN BASED ON WEIGHTED FLOWRATE **
C*****
      N=0
      DO 300 I=1,NG
      IF(SPC(I).GT.0.021) N=N+1
300 CONTINUE
      TOTP=0.0
      TOTPW=0.0
      DO 400 I=1,NG
400 TOTPW=(SPC(I)*QP(I))/TOTQP+TOTPW
      QWGHT=(A1(NF)+A2(NF)*TOTPW/248.8+A3(NF)*TOTPW*TOTPW/61901.)/2.1188
      WRITE(20,241) TOTPW
241 FORMAT(/,' WEIGHTED AVERAGE BASED ON FLOWRATE',F10.3)
      WRITE(20,242) QWGHT
242 FORMAT(' EXPECTED AIRFLOW RATE           ',F10.5)
100 WRITE(20,151)
      STOP
      END
C*****
C** PSYC **
C*****
C
C*****
C** SUBROUTINE PSYC CALCULATES THE PSYCHROMETRIC PROPERTIES OF **
C** THE DRYING AIR BASED ON THE ASAE DATA SHEET D271.2 IN THE **
C** AGRICULTURAL ENGINEERING YEARBOOK. **
C*****
C** RECEIVES: **
C** **
C** 1. MODE = FLAG TO SIGNAL WHICH VALUES ARE TO BE EN- **
C** TERED. **
C** **
C** = 1 THEN DRY BULB AND WET BULB TEMPERATURES **
C** ARE TO BE INPUT. **
C** **
C** = 2 THEN DRY BULB TEMPERATURE AND HUMIDITY RATIO **
C** ARE TO BE INPUT. **
C** **
C** 2. P1 = ENTERING DRY BULB TEMPERATURE (C). **
C** **
C** 3. P2 = WET BULB TEMPERATURE (C) OR HUMIDITY RATIO **
C** DEPENDING ON THE MODE (MODE). **
C** **
C** RETURNS: **
C** **
C** POUT AN ARRAY CONSISTING OF: **
C** **
C** 1. RH = RELATIVE HUMIDITY (DEC). **
C** **
C** 2. TDP = DEW POINT TEMPERATURE (C). **
C** **
C** 3. TMB = WET BULB TEMPERATURE (C). **
C** **
C** 4. H = HUMIDITY RATIO (KG WATER/KG DRIED AIR) **
C** **
C** 5. HS = SATURATION PRESSURE (PA). **
C** **
C** 6. PV = PARTIAL VAPOR PRESSURE (PA). **
C** **
C** 7. PS = SATURATION PRESSURE (PA). **

```

```

C***
C***      8. SH = ENTHALPY (J/KG).
C***
C***      9. VSA = SPECIFIC VOLUME (CUBIC M/KG).
C***
C*****
C
C      SUBROUTINE PSYC (MODE,P1,P2,VSA,PATM)
C      LOGICAL ERROR
C      DIMENSION POUT(9)
C      DATA PATH/101325.0/
C      ERROR=.FALSE.
C      TE=P1
C      PS=PWS(TE)
C      HS=0.6219*PS/(PATM-PS)
C      GOTO(10,20),MODE
C
C*****
C**      MODE 1 TA,TMBA ---> RH,TDP,TMB,H,HS,PV,PS,SH,VSA
C*****
C
C 10 CONTINUE
C      TMBA=P2
C      TMB=TMBA
C      PSMB=PWS(TMBA)
C      PV=PVMDB(TE,TMBA,PSMB)
C      H=0.6219*PV/(PATM-PV)
C 14 PV=H*PATM/(H+0.6219)
C
C*****
C**      IF THE PARTIAL VAPOR PRESSURE IS LESS THAN ZERO AN ERROR
C**      MESSAGE IS GENERATED.
C*****
C
C      IF (PV.LE.0.0) GOTO 96
C      TDP=DEW(PV)-273.16
C 16 RH=PV/PS
C 17 SH=ENTHAL(H,TDP,TE)
C      VSA=287.0*(TE+273.16)/(PATM-PV)
C      GOTO (90,24,24,24),MODE
C
C*****
C**      MODE 2 TE,HE ---> RH,TDP,TMB,H,HS,PV,PS,SH,VSA
C*****
C
C*****
C**      IF MODE = 2 THEN P2 = H (HUMIDITY RATIO)
C*****
C**      5. H = HUMIDITY RATIO (DEC).
C**
C
C 20 CONTINUE
C      H=P2
C      GOTO 14
C
C*****
C**      AN ITERATIVE PROCEDURE IS USED TO CALCULATE THE NET BULB
C**      TEMPERATURE.
C*****
C
C 24 JN=0
C      TMB=(TE+2.0*TDP)/3.0
C 26 CONTINUE
C      PSMB=PWS(TMB)

```

```

C      B=BP(PSWB,PATM,PV,TWB)
C      TWB1=TE+(PSWB-PV)/B
C
C*****
C***      A DIFFERENCE OF LESS THAN 0.012 BETWEEN THE PREVIOUS NET      **
C***      BULB TEMPERATURE AND THE ONE BEING CALCULATED MUST BE OB-    **
C***      TAINED TO SATISFY THE CONVERGENCE CRITERIA.                    **
C*****
C
C      TMCV=ABS(TWB-TWB1)/TWB
C      IF(TMCV.LT.0.012) GOTO 28
C      TWB=(TWB1+2.0*TWB)/3.0
C*****
C***      IF THE NUMBER OF ITERATIONS IS GREATER THAN 10 AN ERROR      **
C***      MESSAGE IS GENERATED.                                          **
C*****
C
C      JN=JN+1
C      IF(JN.LT.10) GOTO 26
C      GOTO 96
C 28 TWB=TWB1
C      GOTO 90
C 96 CONTINUE
C      ERROR=.TRUE.
C 90 CONTINUE
C
C*****
C***      IF THE RELATIVE HUMIDITY IS GREATER THAN 1.00 IT IS          **
C***      SET EQUAL TO 0.999.                                           **
C*****
C
C      IF(RH.GE.0.999) RH=0.999
C      POUT(1)=RH
C      POUT(2)=TDP
C      POUT(3)=TWB
C      POUT(4)=H
C      POUT(5)=HS
C      POUT(6)=PV
C      POUT(7)=PS
C      POUT(8)=SH
C      POUT(9)=VSA
C      IF(ERROR) GOTO 98
C      RETURN
C
C*****
C***      ERROR MESSAGE IS GENERATED IF THE PARTIAL VAPOR PRESSURE    **
C***      IS LESS THAN 0 OR THE NUMBER OF ITERATIONS REQUIRED TO        **
C***      CALCULATE THE NET BULB TEMPERATURE IS GREATER THAN 10.      **
C*****
C
C 98 WRITE(MOUT,500) MODE,JN,P1,P2
C 500 FORMAT(1H0,'**ERROR**PSYC**',2X,'MODE=',I2,2X,'ITER. NO.=',I2,2X,
C      &'P1=',F8.4,2X,'P2=',F8.4)
C      WRITE(MOUT,501) TWB,TWB1,TMCV
C 501 FORMAT(2X,'TWB=',F6.2,2X,'TWB1=',F6.2,2X,'TMCV=',F8.4)
C      RETURN
C      END
C
C*****
C***      PVWBDB                                                              **
C*****
C
C*****

```

```

C*** PARTIAL VAPOR PRESSURE OF AIR IS CALCULATED (ASAE D271.2) **
C*****
C
C*****
C***
C***      1. HFGP = LATENT HEAT OF VAPORIZATION (J/KG).      **
C***
C***      2. TDB = DRY BULB TEMPERATURE (C).                  **
C***
C***      3. TMB = WET BULB TEMPERATURE (C).                  **
C***
C***      4. PSMB = SATURATION VAPOR PRESSURE (PA).           **
C***
C***      5. PVMBDB = PARTIAL VAPOR PRESSURE OF AIR (PA).     **
C***
C*****
C
FUNCTION PVMBDB(TDB,TMB,PSMB)
HFGP=2.502553E6-2.385764E3*TMB
ARG1=0.62194*HFGP*PSMB-1.006925E3*(PSMB-101325.0)*(TMB-TDB)
ARG2=0.62194*HFGP+156.8488*(PSMB-101325.0)*(TMB-TDB)/101325.
PVMBDB=ARG1/ARG2
RETURN
END

C
C*****
C***      PMS
C*****
C
C*****
C*** SATURATION VAPOR PRESSURE IS CALCULATED (ASAE D271.2) **
C*****
C
C*****
C***
C***      1. TC = DRY BULB AIR TEMPERATURE (C).              **
C***
C***      1. PMS = SATURATION VAPOR PRESSURE (PA).           **
C***
C*****
C
FUNCTION PMS(TC)
T=TC+273.16
ARG1=-27405.53+97.5413*T-0.146244*T**2
ARG2=0.12558E-3*T**3-0.48502E-7*T**4
ARG3=4.34903*T-0.39381E-2*T**2
PMS=22105650.*EXP((ARG1+ARG2)/ARG3)
RETURN
END
FUNCTION THERM(T)
A1=-1926.525+2788.188*T+208.8876*T**2
IF (A1)300,300,301
300 A1=0.
301 THERM=14.01179*T+86.231552-SQRT(A1)
RETURN
END

```

**The vita has been removed from
the scanned document**